EVALUATION OF FIRE-AFFECTED CONCRETE STRUCTURES BY NON-DESTRUCTIVE TESTING METHODS

by

UPAL MOHAMMAD TOWFIQUL QUADIR

Presented to the Faculty of the Graduate School of

The University of Texas at Arlington in Partial Fulfillment

of the Requirements

for the Degree of

DOCTOR OF PHILOSOPHY

THE UNIVERSITY OF TEXAS AT ARLINGTON

DECEMBER 2019

Acknowledgments

Firstly, I would like to thank the almighty for giving me the strength to complete this study. I would like to convey my sincere appreciation to my supervisor Dr. Nur Yazdani for his guidance and mentorship. I am deeply thankful that he trusted me all along the work and did not hesitate to provide me with any crucial support, e.g. necessary new laboratory equipment and facilities. I am grateful to my committee members Dr. Himan Hojat Jalali. Dr. Samantha Sabatino and Dr. Ali Koymen for their encouragement and help during my research. I would like to thank them for unhesitatingly agreeing to serve as my dissertation committee members.

I would also like to express my gratitude to the Department of Civil Engineering of UTA for the supports throughout my research.

I am thankful to my once senior groupmate and presently post-doctoral research scientist of our group, Dr. Eyosias Beneberu, for his constant help and guidance. I would also like to express my gratitude to my friends and groupmates Dr. Mina Riad, Dr. Tariq Aljaafreh, Ikram Efaz, Mezanur Rahman, Khadiza Jalal, Zaid Momani, Karzan Habib, Eyad Alsuhaibani, Mai Aljaberi, Prem Egade, Jessica Thomas, Enrique Tapia, Jose Leyva, Sean Natelli, Adams Siphan, Elio Salloum, Phuc Chau, Jacque

Bussey, Dennis Mbaca, Javier Zugarramurdi, Javier Garcia, Lorena Jacobo and Rachel Meredith for all the hard work and help during the experiment.

I am deeply grateful to my parents and my family for their support. My heartiest thanks go to my father, the man behind my dream to pursue the Ph.D., also my mother, for supporting whatever goal I pursue. Last but not least; I would like to express my special thanks to my wife Farhana T. Quadir for standing by my side and supporting me throughout this whole journey with patience and confidence.

November 12, 2019

Abstract

EVALUATION OF FIRE-AFFECTED CONCRETE STRUCTURES BY NON-DESTRUCTIVE TESTING METHODS

Upal Mohammad Towfiqul Quadir

The University of Texas at Arlington, 2019

Supervising Professor: Nur Yazdani

Fire hazard on concrete structures has been a significant concern around the world. After a fire hazard, the crucial part is the evaluation of the fire-affected concrete for strengthening or demolition. For evaluation of a fire-affected concrete structure, Non-destructive Testing (NDT) methods would certainly be a more viable option than the destructive testing methods. Until now, no specific code was developed for quantifiable evaluation of fire-affected concrete with NDT.

To develop the method for Non-destructive Evaluation (NDE) of fire-affected concrete, 8 small-sized (4 in x 4 in x 15 in) and 32 medium-sized (8 in x 8 in x 36 in) concrete beams were prepared and heat-treated in the high capacity lab furnace for variable durations following standard

curve. After that ground penetrating radar (GPR), impact echo (IE), ultrasound pulse, thermal or infrared camera, and Schmidt hammer was used to scan the heat-treated beams. The scanned data were used to produce a quantitative relationship between the scanned outcome and the parameters. The medium-sized beams were then tested for four point bending, the data for which was used to verify the relationship between the NDE data and residual strength in concrete. A Finite Element Model (FEM) was also developed in ABAQUS. For the computer modeling, heat transfer theory was used for heat application simulation. Afterward, four point bending was also simulated for residual strength. The developed numerical models were calibrated with the experimental data and can be used for verification or further parametric analysis.

Table of Contents

List of Figures

List if Tables

Chapter 1

INTRODUCTION

1.1 Background

Fire can be considered as one of the common hazards for almost all types of concrete structures. There are 484,548 structural fire incidents on average per year in the United States according to the fire incidents data of 2013-2017 published by the National Fire Protection Association (NFPA) (NFPA Website, 2019). Figure 1-1 represents a summary of the structural property loss due to fire.

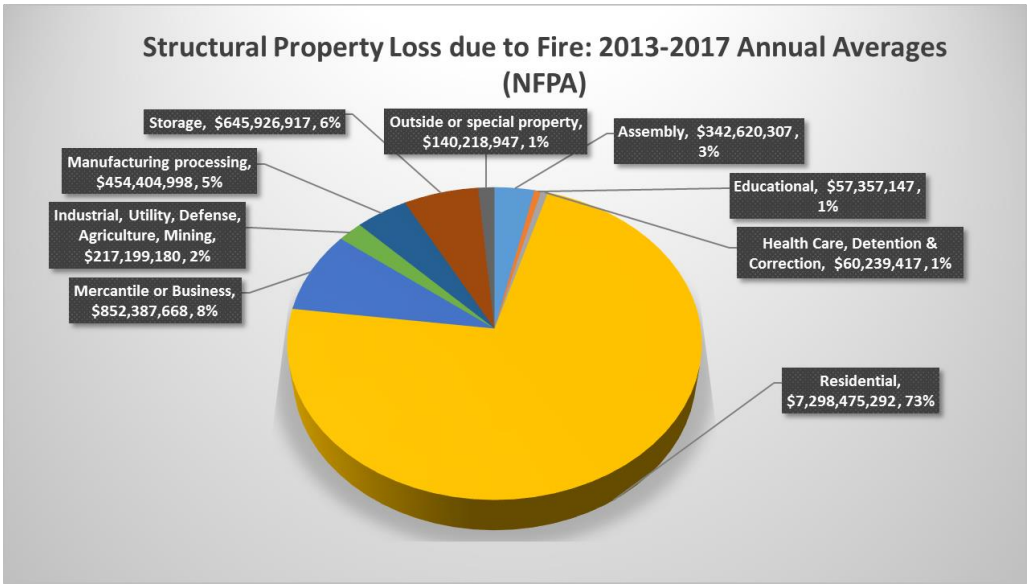

Figure 1-1 : Summary of annual averages of structural property loss due to fire according to NFPA.

Until now, no specific code was developed to evaluate fire-affected concrete. For evaluation of a fire-affected concrete structure, Non-destructive Testing (NDT) methods would certainly be a more viable option than the destructive testing (DT) methods for mainly two reasons. Firstly, NDT would be very less time consuming compared to DT. Secondly, NDT would not create any physical damage to the structure whereas DT would. In addition to the residual strength evaluation, the post-fire material composition and concrete reinforcement bonding appear to be a field yet to be thoroughly explored.

Previously, Infrared thermography/Thermal imaging was used as a Non-destructive Test (NDT) technique on different types of structures (Figure 1- 2) where it was considered highly cost-effective and immediate if used by a skilled practitioner (Titman, 2001). On the other hand, another study included three NDT techniques to assess fire-damaged concrete structures, which are Ultrasonic Pulse Velocity test (UPV) (based on the refraction of longitudinal waves), colorimetry, and the real-time monitoring of the drilling resistance. Two types of structures were chosen to conduct the study, precast RC industrial building and RC tunnel. The chosen NDT methods were reliable to assess the condition of the fire-affected structures (Colombo et al., 2007). In a separate study, Schmidt hammer test, Color

test, Ultrasonic pulse velocity test (UPV), Pull-off test, Core test, Thermogravimetric and Dilatometry test and Thermoluminescence test (TL) were used to assess the fire-damaged concrete. It was concluded that Schmidt hammer test and pull-off tests were not sensitive enough to detect small damage in concrete caused by fire, whereas TL tests were found to be more sensitive than other tests (Chew et al., 1993).

Since the last decade, Fiber Reinforced Polymer (FRP) materials offer a promising solution as reinforcing materials because for many years they have been used successfully in other industries such as the automobile and sports manufacturing industries and, more recently, in construction. Bond strengths developed by carbon fiber reinforced polymer and glass fiber-reinforced polymer bars appear to be very similar and just below what is expected from deformed steel bars under similar experimental conditions (Achillides et al., 2004). However, the post-fire condition and behavior of FRP rebar in a structure still needs to be investigated, especially by NDT methods.

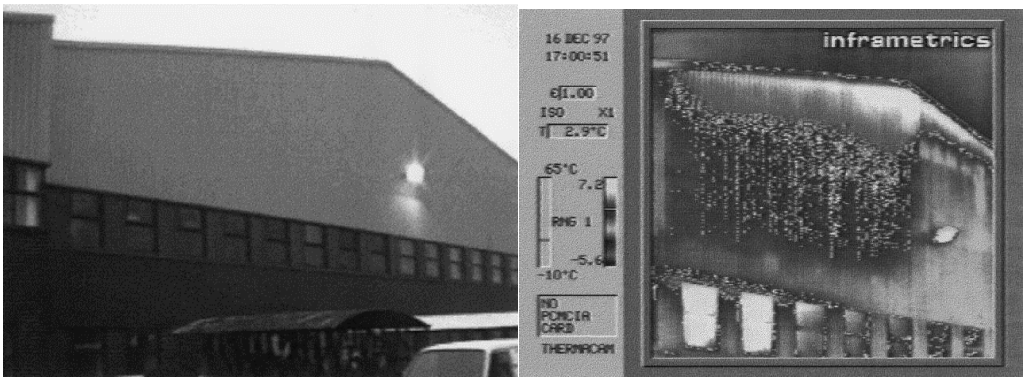

Figure 1- 2: Infrared Thermography on different types of structures (Titman, 2001).

Extensive research was done to assess the axial capacity of post-heated circular reinforced concrete columns repaired with Glass Fiber Reinforced Polymer (GFRP) and Carbon Fiber Reinforced Polymer (CFRP). Columns were tested under axial compression to determine their ultimate axial strength, stiffness, and ductility. From the results, it was evident that GFRP and CFRP repaired columns showed better performance in regards to load carrying capacity (Yaqub et al., 2011).

Research was conducted on the fire performance of GFRP and CFRP strengthened steel reinforced concrete T beams. The test results were achieved by the means of member deflections, strain in the steel reinforcement, and temperatures throughout the section. A numerical heat

transfer model was developed to predict the temperature variations throughout the cross section of a fire exposed FRP-strengthened and insulated T-beam (Williams et al., 2008). In addition, a study of numerical modeling was done on the development of an ABAQUS Fire Interface Simulator Toolkit (AFIST) by integration of a customized Fire Dynamics Simulator (FDS) with a customized ABAQUS structural analyzer through a two-way coupling. Simulation of multiple coupling interfaces, flame spread, thermal and mass diffusion were also introduced (Chen et al., 2011). Another study was conducted on degradation of shear modulus of Basalt Fiber Reinforced Polymer (BFRP) laminates due to high temperature (Hu et al., 2018).

However, until now, no specific study was done using NDT to evaluate the precise conditions of fire-affected concrete structures prepared with various types of concrete, fireproofing and reinforcement.

1.2 Problem Statement

Previous incidents show that lack of precise evaluation methods or codes led to the demolition of many fire-affected concrete structures. In November 2016, a bridge on Bardin Road over Texas 360, Arlington was demolished after an 18-wheeler carrying 1400 5-gallon propane tanks

caught on fire. The cost was estimated around half a million dollars (Figure 1- 3).

Figure 1- 3: Fire incident under a bridge in Bardin Road over Texas 360 (Star Telegram News, 2016).

In 2011, a bridge on the Los Angeles freeway was demolished after a fuel tanker caught on fire (Figure 1- 4).

Figure 1- 4: Fire incident under a bridge in the LA freeway (NBC news San Diego, 2011).

There are examples of fire damage beyond the range of repair. In March 2017, a bridge on I-85 in Atlanta collapsed after a massive fire started by a homeless man to a stuffed chair under the bridge (Figure 1- 5).

Figure 1- 5: Fire incident under a bridge on I-85 in Atlanta (Atlanta News, 2017).

Also recently, the Moulin Rouge building in Las Vegas was demolished after fire damage (Las Vegas Review Journal, 2017). Most of such demolishing occurs based on destructive tests and visual inspections rather than a reliable non-destructive on site test (Garlock et Al., 2012). This study was planned to diminish such knowledge gap due to the unavailability of a reliable NDT method for the evaluation of fire-affected concrete structures.

1.3 Objectives

Following are the objectives of the study:

- To develop a reliable method to evaluate fire-affected reinforced concrete (RC) structures using NDT.
- To validate and crosscheck the NDT evaluations by destructive lab tests and theoretical modeling.
- To compare and denote the differences in performance of fire-affected concrete structures prepared with different types of fireproofing and Steel or FRP bars with variable concrete strengths through NDT techniques.

1.4 Organization of the Dissertation

This dissertation is organized into seven chapters. The content of each chapter is described as following.

Chapter 2: Literature Review

The chapter presents the summary of experiments and numerical studies conducted previously related to the fire effect on structures e.g. buildings and bridges. A review of the overall evaluation and NDE is presented as well. The operation and previous studies with considered NDT equipment e.g. ground penetrating radar (GPR), impact echo (IE), ultrasound pulse, infrared camera, and rebound hammer are presented in this chapter. In addition, a review on the standard fire curves used for experiments is presented by the end of the chapter.

Chapter 3: Design of Experiments, Sample Construction and Heat Treatment

The considered design method was discussed and the designed experimental matrix is presented in this chapter. Afterward, the construction procedure of the samples was discussed. The code used for heat treatment is discussed in this chapter. Lastly, the heat treatment process was presented.

Chapter 4: Non-destructive Testing (NDT)

The detailed NDT procedure of the test samples is presented in this chapter. The test procedures for the equipment used for the NDT are presented separately along with their detailed data analysis. The developed equations from the experiments are also presented.

Chapter 5: Destructive Test

The four-point bending test procedure and data analysis are presented in this chapter. The developed equation for bending capacity from the test data is also presented in this chapter.

Chapter 6: Numerical Modeling

The procedure and outcome of the Finite Element Modeling (FEM) or numerical modeling are discussed in this chapter. The details and results

of heat transfer modeling and residual flexural capacity modeling are presented separately in this chapter.

Chapter 7: Discussion and Conclusion

The summary of findings and limitations are discussed in this chapter. The proposed procedure for NDE of a fire-affected concrete structure is presented in detail. Recommendations for future studies or continuation studies are discussed as well.

Chapter 2

LITERATURE REVIEW

2.1 Fire Hazard on Structures

Among all the other hazards, fire is one of the most severe. Fire has a devastating effect on almost all types of structures. A fire incident, if severe, can result in the total collapse of a structure like a bridge or building. For example, a voluntary survey of 18 highway departments mentioned that fire has caused more bridge collapse compared to the earthquake (Wright et al., 2013; Alos-Moya et al. 2014). However, more emphasis is given towards the research on the effects of other accidental events, such as earthquake, wind, flood and vessel collision on bridges, compared to fire hazards, even though fire hazards on structures can cause significant impact on economics and safety. According to National Fire Protection Association (NFPA), considering the number of fires reported to local fire departments in the United States and an annual average from 2013-2017, there have been a total 484,548 fire incidents having 2,828 civilian deaths and 13,031 civilian injuries. In relation to these incidents, not to mention that there was a total of $10,068,829,874 property loss (NFPA Website, 2019). Assessment of the extent and gravity of the damage done by fire on concrete structures is a crucial task in order to plan the rehabilitation or the demolition. Unfortunately, the fire resistance capacity of reinforced concrete

is very difficult to evaluate as concrete is a composite material consisting of components having different thermal properties. In addition to that, moisture and porosity have a great influence on the mechanical behavior of concrete as well. Also unlike concrete, steel reinforcements are very sensitive in case of effects of high temperatures created by fire.

Commonly bridge fire incidents take place by vehicles crashing and gasoline burning near the bridge. Such type of gasoline fires, known as hydrocarbon fires, are more severe than building fires and possess a faster heating rate and higher temperature peak. For these cases, the temperature rises to a very high range within the first few minutes. In some cases, this type of intense fire can cause severe threats to the structural members and can lead to bridge collapse (Garlock et al., 2012). Vehicles that are involved in the collision also create a threat to bridges due to the combustion of their contents, including the onboard hydrocarbon fuel and, increasingly common, hybrid batteries (Quiel et al., 2015). Other fire causes could include arson, accidental events, and wildfires. 1 in 10 (around 10%) of the bridges in the U.S. are deemed structurally obsolete. Bridges are considered structurally deficient if they are restricted to light vehicles, closed to traffic or in need of rehabilitation. Structural deficiency of a bridge means that there are elements of the bridge that require monitoring and/or repair. Such bridges need load restrictions, which can result in significant

increment of the driving time for large vehicles such as delivery trucks (ASCE Report Card 2017). However, each year, a significant number of bridges are damaged because of structural deterioration or extreme events e.g. fire, earthquakes, and accidents (FOX59, 2017).

Remarkable investigations were conducted on the effect of earthquake, wind, and flood on bridges as compared to hazards by fire. Fire hazards in bridges can cause significant losses in many aspects. The economic losses from bridge fire can have a direct repair or reconstruction cost, and indirect costs due to traffic congestions resulting in lengthy detours (Gong et al., 2014). In metropolitan areas, it can create a huge effect with associated social impacts. For example, the collapse of the MacArthur Maze Bridge in April 2007 in Oakland, CA, involved an overturned tanker truck fire on IH-80/880 underneath the I-580 expressway. The steel girders lost strength as the temperature reached 1110^{o} C and the bridge collapsed after 22 minutes of fire exposure. An estimated $6 million/day total economic impact was caused by this to the Bay area (Chung et al., 2008), and the cost of bridge repair and retrofitting was around $9 million and took months to complete (Astaneh-Asl et al., 2009). The 2017 collapse of a section of the IH-85 Bridge in Atlanta, GA, is another example of the devastating fire effect. Over 250,000 vehicles pass through that bridge on a daily basis (Trubey et al., 2017), and the incident caused

up to a 20% increase in the unit cost per mile for shipping of items and considerable delay to commuters. The taxpayers had to pay the cost of a staggering $16.6 million to rebuild the bridge (Wickert, 2017). Examples of severely damaged and repaired fire-damaged bridges include the SH-183 over MacArthur Blvd Bridge in Irving, TX (Sika Corporation, 2006).

2.2 Evaluation of Fire-affected Structures

Until now after a fire incident on a concrete structure, the most common practice is to evaluate the effected structure by visual inspection and destructive tests like collecting core samples and testing them in the lab for compressive strength. Sometimes fire-affected steel samples from a structure are collected to test in the lab for tensile strength as well. Previously, research was performed on the evaluation of fire-affected steel truss bridge by collecting affected and unaffected structural steel samples for tensile strength tests (Figure 2- 1).

Figure 2- 1: Fire-affected steel truss coal bridge evaluated based on tensile strength of structural steel (Wang et al., 2010).

Fire could reduce the strength of reinforced concrete structural members dramatically. Experimental and numerical research was done on reinforced concrete columns exposed to fire. For example, Bikhiet et al. studied the effect of cooling down a fire-exposed column. In this study, it was found that cooling down a fire treated column by jet water resulted in having 17% less reduction in failure load compared to the columns cooling gradually in room temperature (Bikhiet et al.,2014). Several studies were performed in the last few years on evaluation of post fire Reinforced Concrete (RC) structures. Research was performed presenting state of the art evaluation techniques on a fire-affected prestressed RC industrial warehouse structure. In this research load test, geometrical survey, Non-Destructive Tests (NDT) through sonic and ultrasonic tests, Destructive Tests, Microstructural and Colorimetric analysis (Figure 2- 2) was performed for evaluation of post fire RC structure (Stochino et al., 2017). This study presented valuable information regarding the recent practice of fire-effected structures' evaluation.

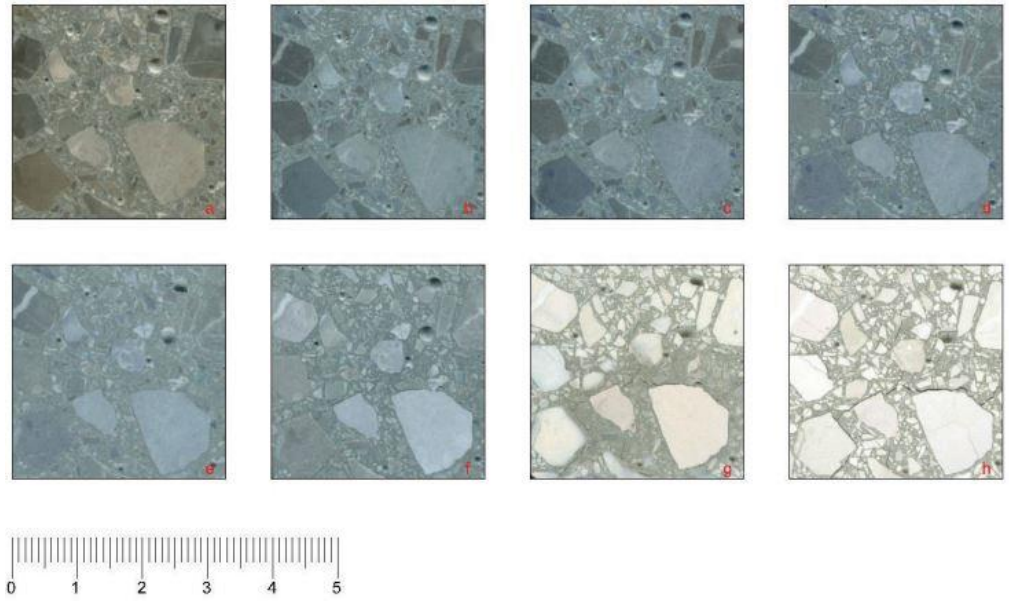

Figure 2- 2: Colorimetric analysis of concrete exposed to variable temperatures starting from room temperature (top left) to 800^{o} C (bottom right) respectively (Stochino et al., 2017).

Significant case studies were performed on the extent of the damage by fire on building and bridge structures. A study conducted by Pathak et al. on a fire-effected building presents a diagnostic technique involving a few on-site non-destructive methods such as ultrasound pulse velocity testing, colorimetry, a few laboratory based destructive test methods like core testing and X-ray diffraction analysis (Pathak et al., 2013).

2.3. Non-destructive Evaluation (NDE) of Fire-affected Structures

For a post fire structure, the requirement for a quick and reliable NDE method adopting various high sensitive Non-destructive Testing (NDT) equipment is undeniable. Previous research can be found on the use of Thermal imaging and Ultrasound for identifying and characterizing subsurface cracks in concrete that are not visible to eyes. In that study, it was found that Thermal/Infrared camera could detect subsurface cracks up to 11 mm depth (Figure 2- 3).

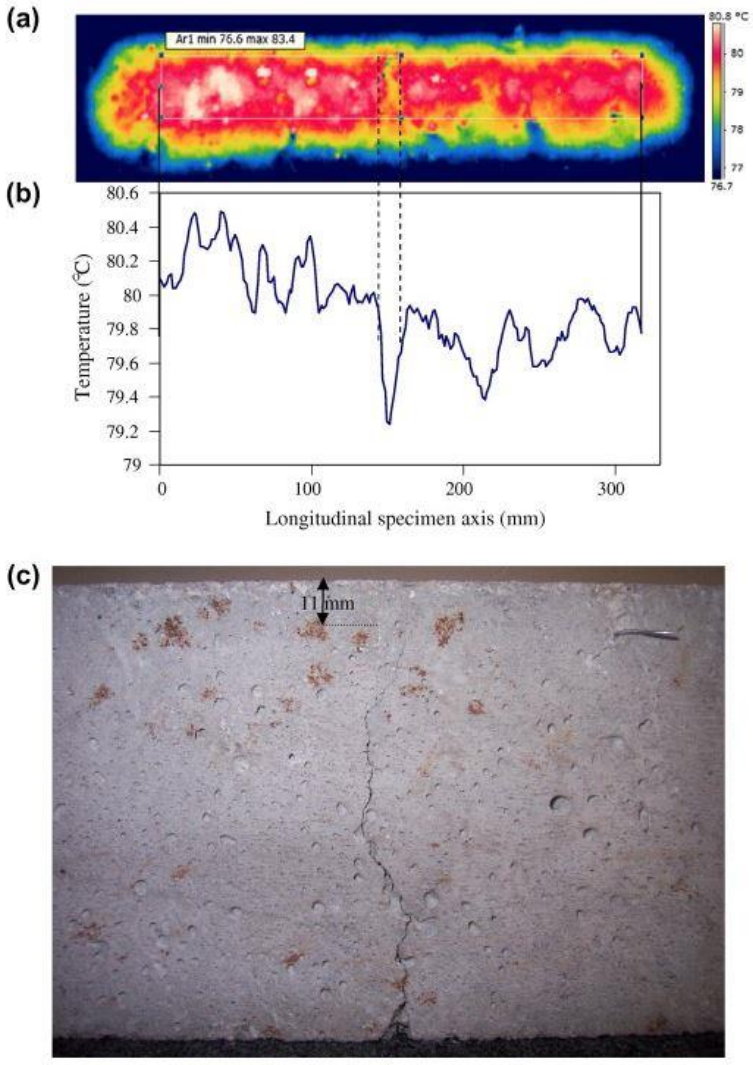

Figure 2- 3: (a) Thermal image of a specimen with 1 mm center deflection, (b) average temperature along the axis of specimen and (c) side view of the specimen showing the position of surface crack (Aggelis et al., 2010).

A few studies were done regarding the use of NDT methods to assess fire-affected concrete. Alcaíno et al. performed research on the evaluation of post-fire residual strength of reinforced concrete frame buildings based on NDT. In their work, they used Schmidt hammer and Ultrasound pulse as the NDT methods to develop a relationship between the strength ratio and the NDT ratio (Alcaíno et al., 2018). On the other hand, another research by Daungwilailuk et al. was performed to determine damaged concrete depth in reinforced concrete slab samples under different durations of fire exposure using a few NDT and destructive test techniques. The methods they used included Schmidt Hammer, Ultrasonic pulse and colorimetry. According to the study, a damaged concrete layer of 30-45 mm was observed for the slab samples exposed to fire for 60 and 90 minutes. The study also concludes that the higher strength concrete sample endures higher damage due to the same fire exposure compared to the comparatively lower strength concrete slab sample (Daungwilailuk et al., 2017). Another study conducted by Park et al. was found where the evaluation of fire-damaged concrete was performed using a nonlinear ultrasonic method. The study involved experimental analysis of residual properties of fire-damaged concrete, e.g. compressive strength, splitting tensile strength and static elastic modulus (Park et al., 2017). A few studies can be found on the use of NDE to determine concrete residual strength

after heat exposure. For example, Kirchhoff et al. performed research on the determination of residual strength in concrete cylinders after heat exposure up to 600^{o} C using ultrasound pulse velocity. As per the study, a downward trend in residual strength is observed with the increment of temperature.

2.3.1. Ground Penetrating Radar (GPR)

Ground Penetrating Radar (GPR) is a high-end NDT technique that uses radar pulses to image the subsurface and locate features underground. This technique adopts the technique of electromagnetic wave propagation through the media under investigation. The key components of a GPR consist of a wave generator, a single transducer composed of an emitting and receiving antenna, a signal processor and a data storage and display unit (Ekes, 2007). A tri-wheel cart-mounted GPR is shown in Figure 2- 4.

Figure 2- 4: Ground Penetrating Radar (GPR) on a Tri wheel cart setup.

As for the mechanism of GPR, the transmitter sends a signal into the ground and the transmitting signal is reflected from the target. Then the receiver antenna receives the reflected signal. The data received through the receiver is then processed and displayed. A typical GPR system methodology is shown in Figure 2- 5. GPR wave is reflected if there is a new material in the path of wave propagation. The reflection wave depends on the permittivity (ε), the magnetic permeability (μ) and the electrical

conductivity (σ) of the surface from where it is reflecting. Material consisting of high conductivity lowers the penetration of the GPR wave as it absorbs the radar signal. For most of the engineering materials, the magnetic permeability is very low. GPR signal is most sensitive to the permittivity of the medium.

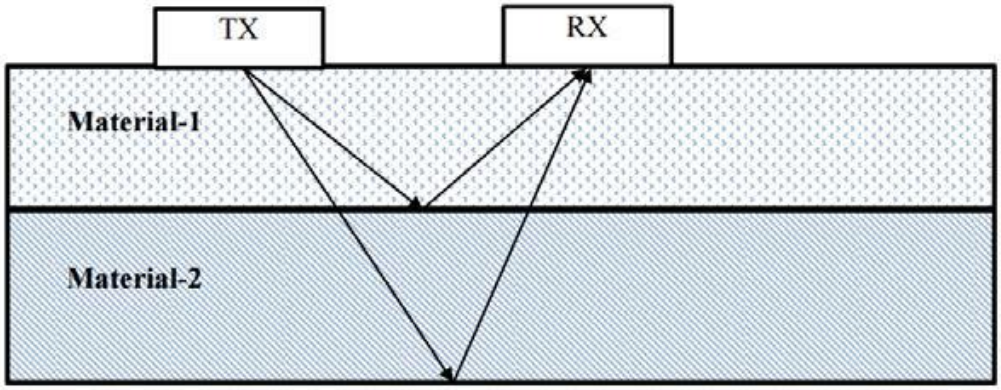

Figure 2- 5: Basic mechanism of the GPR system.

The receiver antenna records the reflected signal. GPR system records the amplitude, wavelength and travel time of the signal. This recorded information contains important information about the reflection surface or the media. The GPR scan output is not the real image of the subsurface. Rather it is a type of signature that depends on the size, shape, and dielectric constant of the target. GPR scan data collection and

presentation can be done in one to three dimensions known as A-scan, B-scan and C-scan as shown in Figure 2- 6.

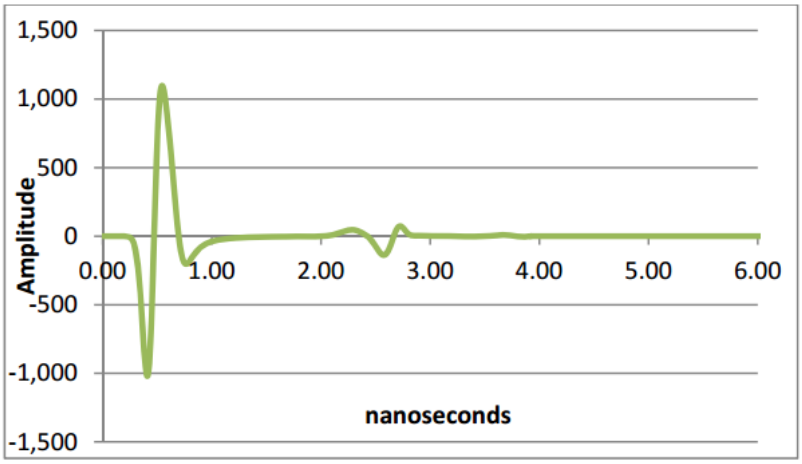

(a) A-scan

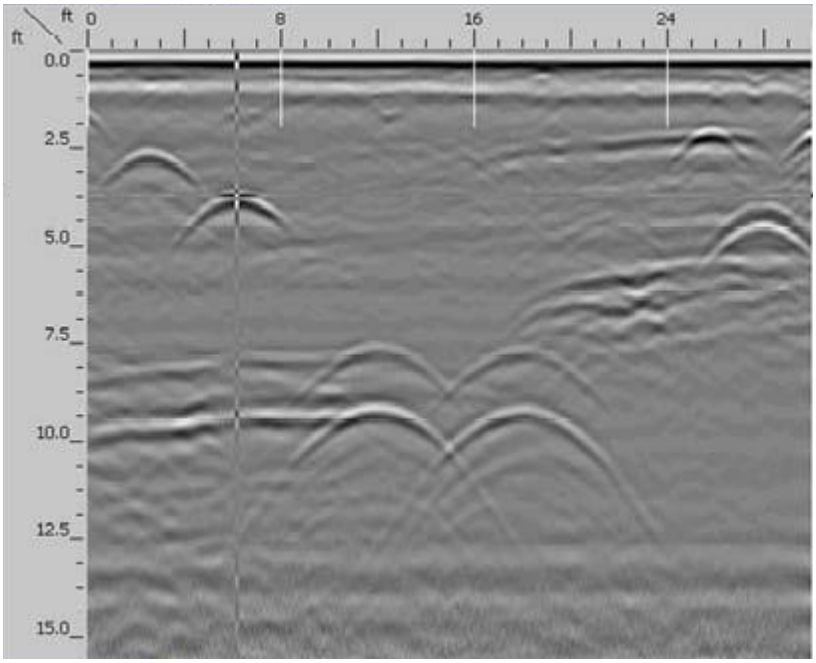

(b) B-scan

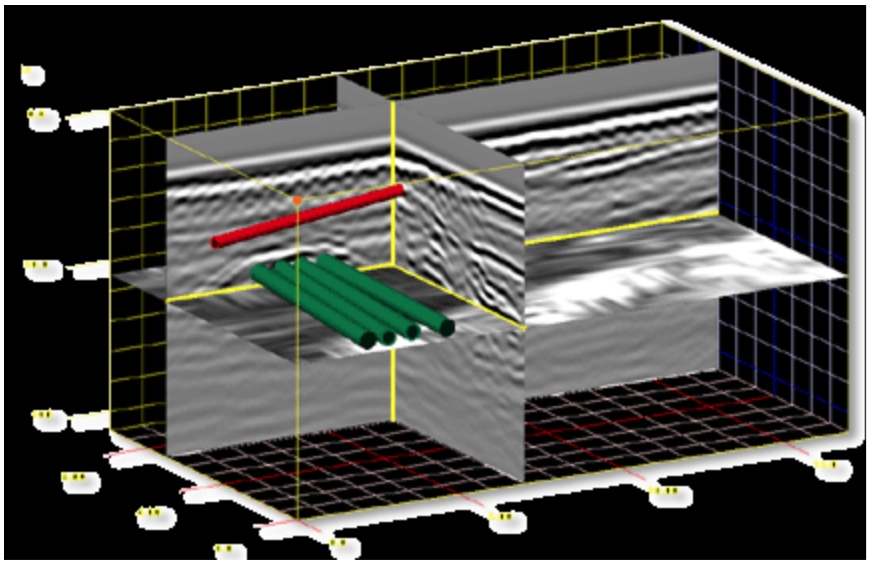

(c) C-scan

Figure 2- 6: Different versions and presentations of GPR scans.

Previously research was performed to determine defect and deterioration of concrete slab in a building after fire using GPR and visual inspection. In this research, a qualitative analysis was done to locate deterioration and cracks in a fire-affected concrete slab (Talaha et al., 2016).

2.3.2. Impact Echo

The impact echo (IE) system is used to determine the delamination condition and thickness of concrete structural members when voids,

honeycombs, and/or cracks are suspected. The device creates an impact at a spot on the surface and then records and analyzes the echo. Unlike the GPR, it is a spot scanning device, which is used to scan discrete data points in a pre-determined grid on the concrete deck surface. Figure 2- 7 shows the impact echo device that was used for the research.

Figure 2- 7: Olson Instruments impact echo (IE) device.

A key development leading to the success of the impact-echo method was the use of frequency analysis instead of time-domain analysis of the recorded waveforms (Carino et al., 1986). The principle of frequency analysis is illustrated in Figure 2- 8. The P-wave produced by the impact undergoes multiple reflections between the test surface and the reflecting interface. Each time the P-wave arrives at the test surface, it causes a characteristic displacement. Thus, the waveform has a periodic pattern that

depends on the round-trip travel distance of the P-wave. If the receiver is close to the impact point, the round trip travel distance is 2T, where T is the distance between the test surface and reflecting interface. As shown in Figure 1, the time interval between successive arrivals of the multiply reflected P-wave is the travel distance divided by the wave speed. The frequency, f, of the P-wave arrival is the inverse the time interval and is given by the approximate relationship:

$$f = \frac{C_{pp}}{2T} \qquad \text{---------[2-1]}$$

Where,

C_{pp} = the P-wave speed through the thickness of the plate,

T = the depth of the reflecting interface.

If the test object is a solid plate, the frequency calculated according to equation [2-1] is called the plate thickness frequency (Carino, 2001).

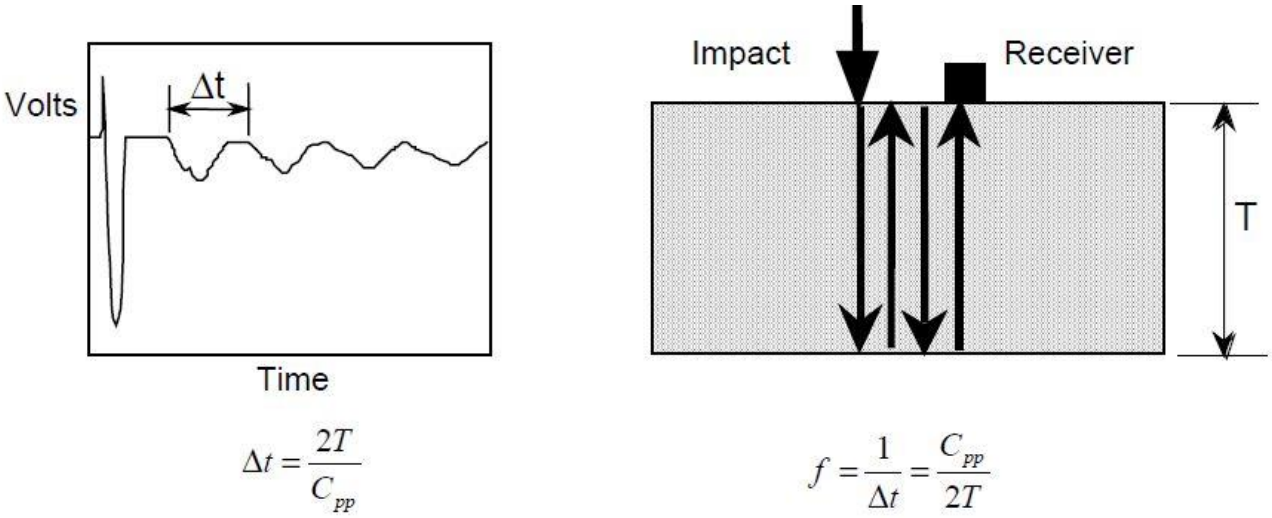

Figure 2- 8 Principle of frequency analysis in impact echo.

2.3.3. Ultrasound Pulse

Generally, Synthetic Aperture Radar (SAR) and Synthetic Aperture Focusing Technique (SAFT) formulations are applied for interpretation of multiple signals with sending and receiving transducers at the same location. These formulations are generalized for interpretation of signals with sending and receiving transducers located at different locations. The fundamental expression for SAR is generalized for each emitting and receiving transducer pair positioned at x_e' and x_r', respectively, and can be represented as shown in equation [2- 2]:

$$s(x_e', x_r', t) = \int_x \int_z f(x,z) * \delta\big(t^*(t, x_e', x_r', x, z)\big) dz dx$$

---------[2- 2]

Where $s(x_e', x_r', t)$ is the received impulse due to emitted impulse $\delta(t^*(t, x_e', x_r', x, z))$; $f(x, z)$ is the reflectivity function of the Region of Interest (ROI); and are the horizontal and vertical positions in the ROI, respectively; and t^* is defined by the following equation [2- 3]:

$$t^* = t - \frac{1}{c}\left(\sqrt{z^2 + (x - x_e)^2} + \sqrt{z^2 + (x - x_r)^2}\right)$$

----------[2- 3]

Figure 2- 9 shows a representation of potential contributing point sources for a single intensity value within $s(x_e', x_r', t)$ according to the fundamental SAR equation.

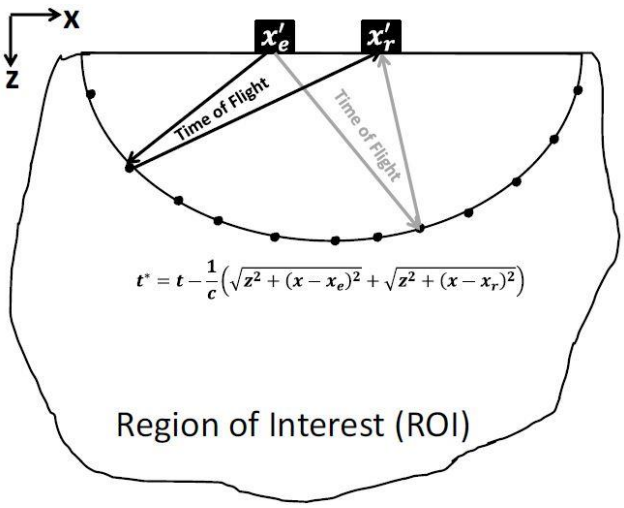

Figure 2- 9: Representation of potential contributing point sources at a constant time (Roundtrip) from the emitting/receiving transducer according to the fundamental expression (Clayton et al., 2013).

The synthetic aperture focusing technique can be used for the ultrasonic linear array used in this study in a similar manner to that described for single sending and receiving pairs. To allow for integration over the various transducer locations, $\int_{x'_e}^{\cdot} dx'_e \int_{x'_r}^{\cdot} \dots dx'_r$ the impulses received at the surface versus time can be expressed in terms of distances. This can be accomplished by assuming a constant shear wave velocity, $C_S = C_S^{Avg}$ determined from equation [2- 2]. If the signals are emitted within interval $[x'_{emin}, x'_{emax}]$, and received within interval $[x'_{rmin}, x'_{rmax}]$, the reconstructed image at each point $\hat{o}(x, z)$ can be obtained by integrating

over all possible transducer pair (impulse emit and receive) locations from the following equation [2- 4]:

$$\widehat{\boldsymbol{o}}(x,z) = \int_{x'_{emin}}^{x'_{emax}} dx'_e \int_{x'_{rmin}}^{x'_{rmax}} \mathrm{A}(x'_r, x'_e, x, z) * s\left(x'_r, x'_e, \frac{1}{c}\left(\sqrt{z^2 + (x - x'_e)^2} + \sqrt{z^2 + (x - x'_r)^2}\right)\right) dx'_r$$

-----[2- 4]

Here $\mathrm{A}(x'_r, x'_e, x, z)$ is the apodization factor that is typically a function of the distance traveled, incident angle, and/or divergence of the reflection point location with respect to the emitted/received signal. Figure 2- 10 shows the linear array representation.

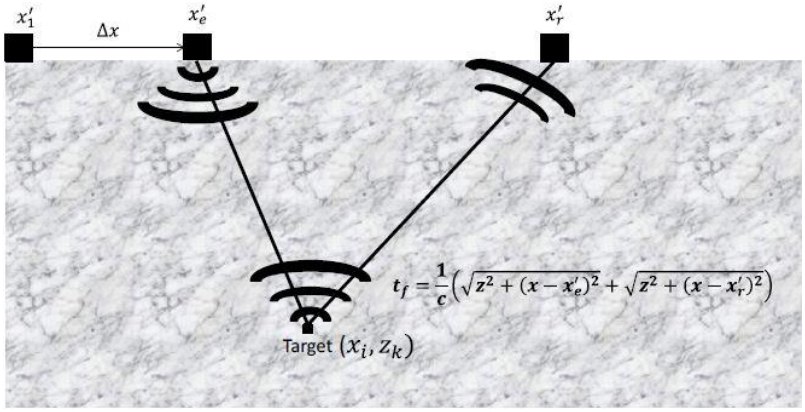

Figure 2- 10: Linear array representation (Clayton et al., 2013).

After applying the shift factor to account for system delay the reconstructed image is obtained at discrete points by summing over all

possible transducer pair locations using the following equation [2- 5] for the ultrasonic linear array:

$$\hat{o}_{i,k} = \sum_{e=1}^{T-1} \sum_{r=e+1}^{T} \mathrm{A}(x_r, x_e, x_i, z_k) \Psi_{e,r}(x_i, z_k)$$

---------[2-5]

Where,

$$\Psi_{e,r}(x_i, z_k) = s\left(x_r, x_e, \frac{1}{c}\left(\sqrt{{z_k}^2 + (x_i - x_e)^2} + \sqrt{{z_k}^2 + (x_i - x_r)^2}\right)\right)$$

----------[2-6]

Where $\hat{o}_{i,k}$ is the image reflectivity assigned to each position within the ROI, *T* is the number of transducer locations, *e* and *r* are the indexes for the emitting and receiving transducers, and *i* and *k* are the indexes for the horizontal and vertical positions of the ROI (Clayton et al., 2013).

2.3.4. Infrared/Thermal Camera

A thermal or infrared camera (Figure 2- 11) is a device that produces an image from infrared radiation. It is similar to a common camera, which produces an image from visible light. The use of thermal imaging is called Thermography. Though infrared radiation (IR) can not be detected by the human eye, an Infrared camera can convert the infrared radiation into an

image, which is visible, and that image represents thermal variations across an object or scene. IR covers a portion of the electromagnetic spectrum from approximately 900 to 14,000 nanometers (0.9–14 μm). All objects at temperatures above absolute zero emit IR, and the amount of radiation increases with temperature (FLIR, 2009).

Figure 2- 11: Infrared/Thermal Camera.

2.3.5. Rebound/Schmidt Hammer

In the 1950s, the first Schmidt hammer was invented and introduced into the market. Since that time, it has become the first and most widely used instrument for non-destructive estimation of concrete strength properties, asphalt, mortar, rock, and paper. In this test, the “Silver Schmidt

hammer” from “Proceq” is used as illustrated in Figure 2- 12. The silver Schmidt hammer principle is to measure the ratio between the rebound velocity and the impact velocity when the hammer hits the surface. The rebound is dependent on the hardness of the surface. The rebound value can be used to determine the bond strength between the concrete and the FRP. Schmidt hammer defines the ratio between the rebound velocity and the impact velocity as the quotient value “Q”. The Q value is used in this test to compare the surface hardness of each sample. The surface hardness of each sample to be correlated with the overall bending capacity. Studies mention that a rebound hammer can be used as a rough tool to calculate material homogeneity (Brenchich et al., 2013).

Figure 2- 12: Schmidt or rebound hammer.

2.3.6. Time-Temperature Curves for Experimental Use

An analysis was performed on the comparison between the fire curves of the NFPA 502 code and the ASTM E119-18ce1 code (NFPA 502, 2017) (ASTM E119-18ce1, 2018). The ASTM fire curve was followed for the research. The following table (Table 2- 1) shows the time vs temperature data, and the graphs (Figure 2- 13 and Figure 2- 14) show a comparison between three fire curves adopted from the mentioned codes.

Table 2- 1: Time-Temperature data for ASTM and NFPA curves

Time (min)	ASTM E119-18c Time-Temperature curve for buildings and materials		RWS Time-Temperature curve representing tunnel fires included in NFPA code (°C)		ISO 834 Cellulosic Time-Temperature curve for buildings and materials included in NFPA code (°C)	
	°C	°F	°C	°F	°C	°F
0	20	68	20	68	20	68
5	538	1000	1140	2084	349	660
10	704	1300	1200	2192	576	1069
30	843	1550	1300	2372	842	1548
60	927	1700	1350	2462	945	1733
120	1010	1850	1200	2192	1049	1920

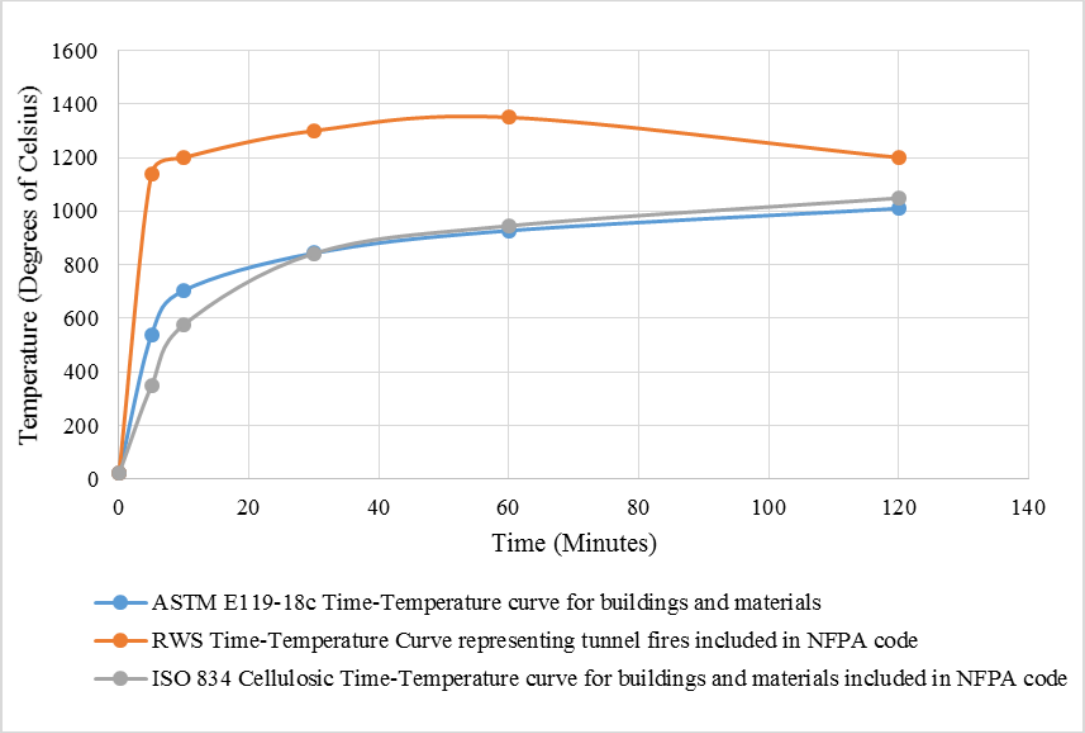

Figure 2- 13: Comparison between ASTM E119-18c and two curves included in the NFPA code (in ^{o}C).

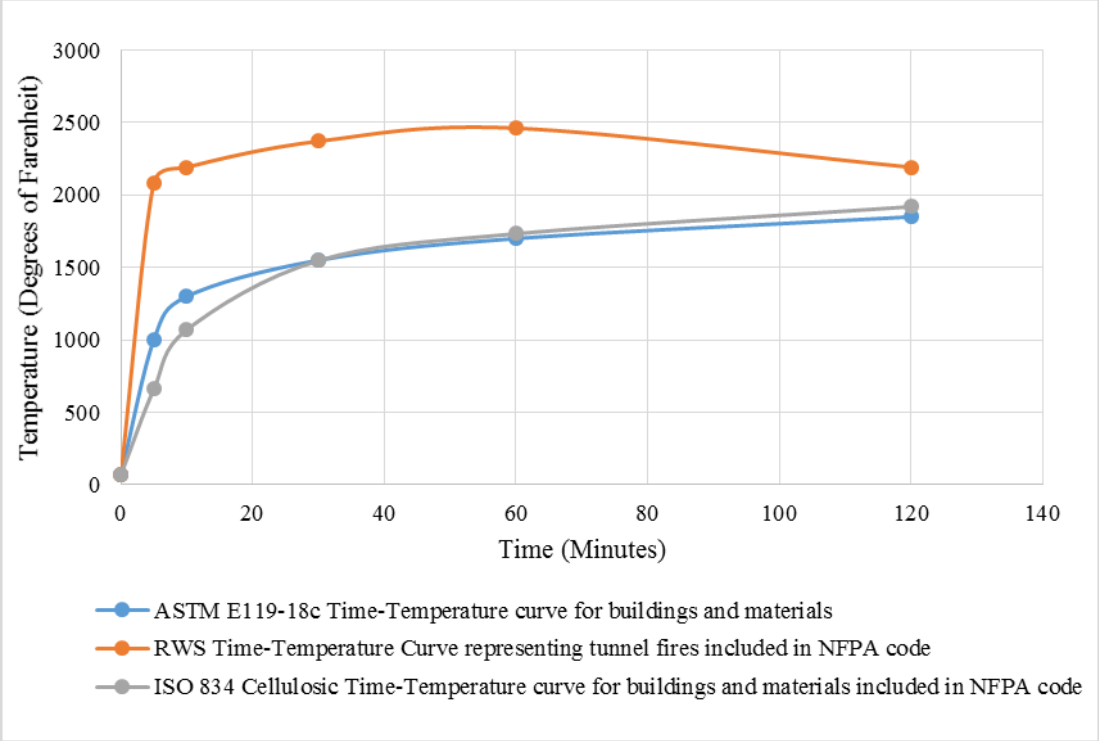

Figure 2- 14: Comparison between ASTM E119-18c and two curves included in NFPA code (in ^{o}F).

The summary of the comparative analysis between these curves is presented in the following table (Table 2- 2).

Table 2- 2: Comparative analysis between the fire curves.

Property	ASTM E119-18c Time-Temperature curve for buildings and materials	RWS Time-Temperature curve representing tunnels included in NFPA code	ISO 834 Cellulosic Time-Temperature curve for buildings and materials included in NFPA code
Publisher	American Standard for Testing Materials (ASTM).	RijksWaterStaat (RWS), Netherlands.	International Organization for Standardization (ISO).
Data Source	Buildings and materials.	Tunnels.	Buildings and materials.
Temperature Range in 120 mins	Varies from 20 ^{o}C (68 ^{o}F) to 1010 ^{o}C (1850 ^{o}F).	Varies from 20^{o} C (68 ^{o}F) to 1200^{o} C (2192 ^{o}F).	Varies from 20^{o} C (68 ^{o}F) to 1049^{o} C (1920 ^{o}F).
Curve property	Almost similar to the ISO curve.	Initially steeper than the other two curves resulting in overall	Almost similar to the ASTM curve.

		high-temperature values.	

Besides, the following few points relevant to bridges were found in the NFPA code:

- Chapter 6 is about Bridge and Elevated Highways. It is mentioned there that if the bridge length is less than 1000 ft., the provisions of that chapter shall not apply.
- It is also mentioned there that if a bridge is fully enclosed on both sides of the roadway and meet the requirements of Chapter 7 Section 7.2, then the provisions of Chapter 7 shall apply. On the other hand, where a bridge does not fully enclose the roadway on both sides, the decision to consider it as a road tunnel shall be made by the AHJ (Authority Having Jurisdiction) following an engineering analysis in accordance with Section 4.3.1.
- Provisions of Chapter 7 includes Section 7.3.2 which mentions to follow the RWS time-temperature curve for tunnels. It also mentions there that any other recognized standard time-temperature curve can be used if it is acceptable to AHJ following an engineering analysis as per Chapter 4.

Additionally, the code includes a graphical representation of various accepted time temperature curves. There the T (RWS) curve represents the mentioned RWS fire curve for tunnels and the T (Standard) curve represents the ISO fire curve that is similar to the ASTM curve.

Chapter 3

DESIGN OF EXPERIMENTS, SAMPLES CONSTRUCTION AND HEAT TREATMENT

This chapter describes the details of designing the experiment considering different parameters and deciding the sample size. It also includes information about the construction procedure of the samples and the heat treatment procedure after sample construction.

3.1. Design of Experiment

A pilot/preliminary study was planned to perform a qualitative analysis to justify if the chosen NDE methods can detect a significant difference in concrete before and after fire or heat exposure concerning the initially planned set of parameters. After the result analysis of the pilot/preliminary study, the main study was planned by finalizing the NDE methods and the parameters with larger sized samples. Statistical analysis was performed and the Half-fractional factorial design method was used for the design of the experiment for the main study considering the number of finalized parameters. The mentioned method is quite popular for experiments with multiple numbers of parameters as it depicts the number of test runs into half resulting in a less time consuming and less expensive

test plan with the same extended number of parameters compared to other methods of Design of Experiment (DOE).

3.1.1. Pilot/Preliminary Study

The preliminary study was mainly planned to get an initial idea about the test procedure and setup. This study helped to finalize the parameters, which were chosen initially. An initial experimental design matrix was prepared for the preliminary study, which is presented in Table 3- 1. The ASTM 4 inches X 4 inches X 15 inches (100 mm X 100 mm X 375 mm) beam size was chosen for the samples of the preliminary study. The experimental design consisted of three initial parameters having two levels for each. The first parameter was concrete strength and the two levels chosen were normal strength and high strength concrete. The strength considered for normal strength concrete was 3000 psi and for high strength, concrete was 6000 psi. The second parameter considered was the fireproofing layer on the concrete sample and the two levels considered for this parameter were presence or absence. The third parameter considered was steel reinforcing bar and the two levels for this parameter were presence or absence as well. Grade 40 #4 steel rebar was used for this parameter considering readily available in the market. The fourth parameter

was the duration of heat treatment. It was studied that a maximum temperature of around 1200^{o} C (2192^{o} F) is reached in a fire incident within the first 5 minutes and the time to extinguish the fire can vary from 30 minutes to up to 2 hours (Beneberu, 2016). Considering that, the two levels for the duration of the heat treatment parameter was chosen as ½ hour and 1 hour for preliminary study. Each of the combinations had one test sample planned for preparation. Table 3- 1 below shows the design matrix for the preliminary experiment.

Table 3- 1: Design of Experiment (Pilot/Preliminary study).

No of Combination	Concrete Strength	Fireproofing	Steel Reinforcement	Duration of Heat Treatment (hr)	No of Samples (4”x4”x15” ASTM size)
1	Normal	-	-	1/2	1
2	High	-	-	1/2	1
3	Normal	Present	-	1/2	1
4	Normal	-	Present	1/2	1
5	Normal	-	-	1	1
6	High	-	-	1	1
7	Normal	Present	-	1	1
8	Normal	-	Present	1	1
					Total= 8

3.1.2. Main Study

The main study was planned after the preliminary study showed promising outcomes. For the ease of more detailed assessment, a larger size sample with a size of 8 inches X 8 inches X 36 inches (200 mm X 200 mm X 900 mm) was chosen. For the main study, five parameters were fixed. Another type of reinforcement made of Basalt Fiber Reinforced Polymer (BFRP) was added as the new parameter considering the increasing demand for research in the field of Fiber Reinforced Polymer (FRP) rebar. As per the rule of the half-fraction factorial design method, two levels were chosen for each parameter.

The first parameter concrete strength had normal strength of 3500 psi and a high strength of 6000 psi as two levels. The strength of the high strength concrete was selected to be near the lower range is because the higher strength of concrete might result in a bursting effect inside the furnace which might hamper the proper functioning of the furnace.

The second parameter is 40-grade two #4 steel reinforcing bars per sample and its presence and absence are considered as two levels. The amount of presence of steel rebar can be quantified by the reinforcement ratio ρ having a value of 0.00625. The absence of steel rebar simply represents a value of zero for ρ.

The third parameter for the main study is the fireproofing layer and the levels for this parameter are also presence or absence. The Sikacrete 213f fireproofing mortar was used as the fireproofing for the main study samples. Sikacrete 213F is a phyllosilicate aggregate-based fireproofing mortar for concrete and reinforced concrete structures, manufactured by Sika. It is designed to provide more than 4 hours of fire resistance depending on the thickness of the application.

The fourth parameter is the BFRP reinforcing bar. For the FRP bar, there are usually two types, one is made of glass and the other one is made of carbon. In recent times, there is another type of FRP made of Basalt which gained popularity because of its ready availability in the market, lower cost than any other types of FRP, and higher capacity than conventional Glass Fiber Reinforced Polymer (GFRP) but slightly lower than Carbon Fiber Reinforced Polymer (CFRP). In addition, BFRP bars are available with a deformed shape similar to the conventional deformed steel rebar. Considering all these, two numbers of #3 BFRP rebar per sample was chosen as one of the parameters for the study. Presence and absence were the two levels considered for this parameter. The presence of two FRP rebars can be quantified by a reinforcement ratio ρ of 0.00344 whereas for absence the value of ρ is zero. The absence of rebar (steel and FRP) was

considered as the second level of the parameter to study the effect of the presence of rebar on the specific NDT method.

The duration of heat treatment was chosen as the fifth parameter. Considering the outcome from the preliminary study, as one hour of heat treatment proved to create enough major damage in concrete, half an hour and one hour of heat treatment was fixed as two levels for this parameter for the main study as well.

Four additional combinations were chosen considering control samples for cross-reference. These four combinations were planned to be kept heat untreated. Two samples were planned to be prepared for each combination. The experimental design matrix is shown in Table 3- 2.

Table 3- 2: Design of Experiment (Main study).

No of Combination	Concrete Strength	Reinforcement	Fireproofing	FRP Bar	Duration of Heat Treatment (hr)	No of Samples (8”x8”x 36” size)	Remarks
1	Normal	-	-	Present	-	2	Control
2	High	-	-	Present	-	2	Control
3	Normal	Present	-	-	-	2	Control
4	High	Present	-	-	-	2	Control
5	Normal	-	-	-	1	2	
6	High	-	-	-	1/2	2	
7	Normal	Present	-	-	1/2	2	
8	High	Present	-	-	1	2	
9	Normal	-	Present	-	1/2	2	
10	High	-	Present	-	1	2	
11	Normal	Present	Present	-	1	2	
12	High	Present	Present	-	1/2	2	
13	Normal	-	-	Present	1/2	2	
14	High	-	-	Present	1	2	
15	Normal	-	Present	Present	1	2	
16	High	-	Present	Present	1/2	2	
						Total=	

3.2. Samples Construction

3.2.1. Pilot/Preliminary Study

For this study, a simple rectangular short beam of 4” X 4” X 15” (100 mm X 100 mm X 375 mm), and American Standard for Testing Materials (ASTM) approved size is chosen. Eight of these beams were prepared considering fireproofing, variable concrete strength and rebar. First, the formworks were prepared at the lab and the rebars were placed (Figure 3-1). Curing compound was used on the beams after casting to seal the top layer so that there is an ample amount of moisture trapped inside the concrete for hydration (Figure 3- 2).

Figure 3- 1: Preparing preliminary study samples formwork and rebar placing.

Figure 3- 2: Preliminary study samples after hardening and having curing compound applied.

3.2.2. Main Study

For the main study, total 32 short scale rectangular beams of 8” X 8” X 30” (200 mm X 200 mm X 750 mm) (Figure 3- 3) were prepared considering two types of concrete (high strength and normal strength), No. 4 steel rebar, fireproofing, No. 3 BFRP rebar and duration of heat treatment. Two number of rebars were fixed for the samples in which rebars were supposed to be present. Firstly, the formworks were prepared in the laboratory using locally available woods and boards (Figure 3- 4). Then the formworks were sealed properly and the rebars were placed using glue on concrete blocks/dobby blocks to maintain proper cover (Figure 3- 5). Shear reinforcement was not considered as the shear force did not govern and also for the ease of NDT as there will be less disruption.

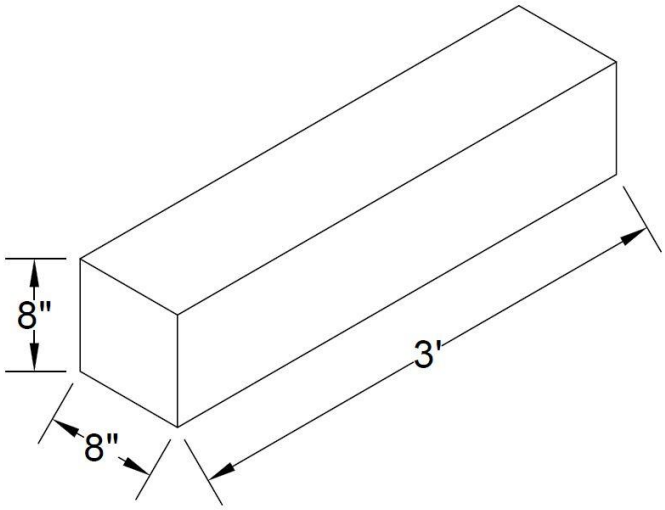

Figure 3- 3: Size of the concrete beam considered.

Figure 3- 4: Formwork preparation and laying for the main study.

Figure 3- 5: Rebar placing in the formwork for the main study.

After the rebars were done placing, the casting was done using ready mix concrete. Two types of concrete with strengths of 3500 psi and 6000 psi were cast. Around twelve cylinders were also poured for each strength of concrete (Figure 3- 6). Thermocouples were embedded in the samples before hardening so that the internal temperature can be measured when the samples will be exposed to heat. The curing compound was used for the main study beam and cylinder samples. The formworks were removed after the beams hardened (Figure 3- 7). Afterward, fireproofing was applied to the considered beams.

(a) Casting beam samples for the main study.

(b) Casting cylinder samples for the main study.

Figure 3- 6: Concrete pouring of main study samples.

Figure 3- 7: Hardened beams after removing formworks.

Afterward, Sikacrete 213F fireproofing mortar was applied on all the surfaces of the selected beams from the experimental design matrix. The mortar was applied by spraying (Figure 3- 8) as a 1 inch (25.4 mm) coating. The considered thickness did not require any wire mesh or reinforcement as per the product manual. Afterward, curing was done to ensure the bonding of the coating and to prevent cracks.

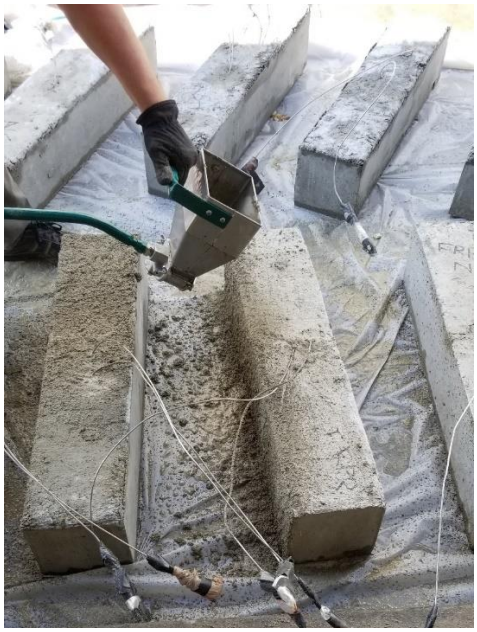

Figure 3- 8: Applying fireproofing mortar by spray or shotcrete.

3.3. Heat Treatment

3.3.1. Pilot/Preliminary Study

Two of the eight samples were applied with fireproofing. Afterward, the samples were treated with high temperature for 1 hour up to 927^{o} C (1700^{o} F) and ½ hour up to 843^{o}C (1550^{o}F) following the Temperature vs Time graph (Figure 3- 9 and Table 3- 3) from the standard for fire tests of building construction and materials (ASTM E119-18c, 2018) in the high capacity lab furnace (Figure 3- 10).

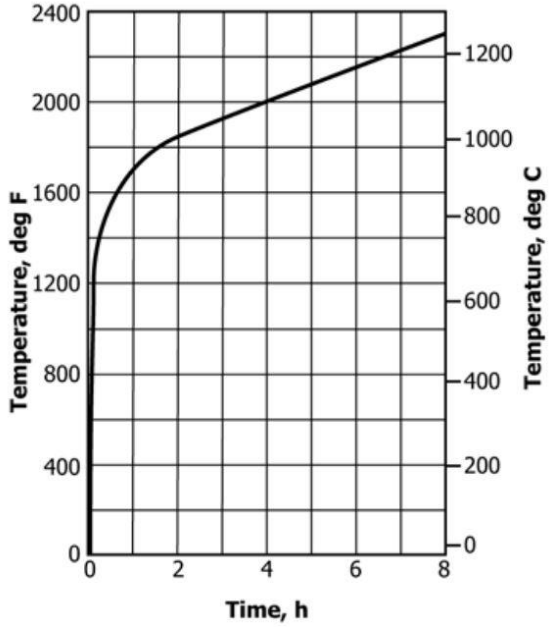

Figure 3- 9: Temperature vs Time curve (ASTM E119-18c, 2018).

Table 3- 3: Temperature vs Time values from ASTM E119-18c.

1000°F (538°C)	at 5 min
1300°F (704°C)	at 10 min
1550°F (843°C)	at 30 min
1700°F (927°C)	at 1 h
1850°F (1010°C)	at 2 h
2000°F (1093°C)	at 4 h
2300°F (1260°C)	at 8 h or over

(a) Furnace with a capacity of 2282^{o}F (1250^{o}C).

(b) Placing preliminary study samples in the furnace.

(c) Heat treating the samples.

Figure 3- 10: Heat treating samples in the lab furnace.

It appeared that 1 hour heat-treated samples endured significantly high damage than ½ hour heat-treated samples. The samples having fireproofing appeared to be damaged in the fireproofing layer only (Figure 3- 11). It was decided that, further study was needed to check if the damage due to heat exposure is only limited to the fireproofing layer or it propagates beyond that.

(a) ½ hour heat-treated sample

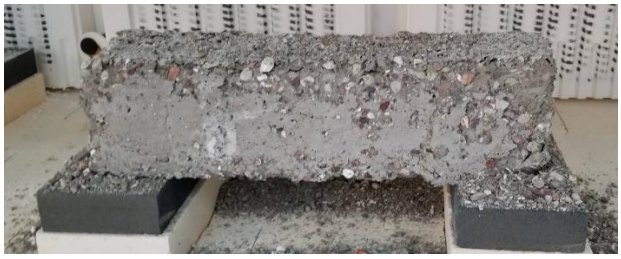

(b) 1 hour heat-treated sample

(c) Heat-treated sample having fireproofing mortar.

Figure 3- 11: Heat-treated preliminary study samples.

Afterward, NDT was performed on the heat-treated specimens. By analyzing the results, an initial idea was achieved on the most affected parameters and the most efficient NDT methods.

3.3.2. Main Study

32 short scale concrete beams of 8” X 8” X 36” (200 mm X 200 mm X 900 mm) size were prepared according to the experimental design mentioned earlier. 24 beams including the fireproofed beams were treated with high temperature for 1 hour and ½ hour according to the ASTM E119-18c graph in the laboratory furnace. This range was chosen because at a temperature higher than this, the concrete properties may deteriorate beyond the capacity of inspection. For the heat treatment, in addition to the two embedded thermocouples inside the samples at rebar level and at mid-level, at least two additional thermocouples were used on the top and bottom surfaces of the beam in the furnace (Figure 3- 12). All the thermocouples data were recorded through a data logger box during the heat treatment procedure. Afterward, NDT was performed on all the specimens.

(a) Placing the main study beam samples in the furnace for heat treatment.

(b) Placing external thermocouples.

(c) Heat treatment setup with data logger and computer.

Figure 3- 12: Heat treatment of samples in the lab furnace.

Chapter 4

NON-DESTRUCTIVE TESTING (NDT)

In this chapter, the procedure of the selected NDT methods, data analysis, and their results are discussed. The selected NDT methods are Schmidt hammer or rebound hammer, ground penetrating radar (GPR), ultrasound array tomography, impact echo (IE) and infrared camera or thermal camera. Each of the NDT methods was used to scan the samples having different parameters that affect the capacity such as the strength of concrete, duration of heat treatment, presence of steel rebar, presence of FRP rebar and the presence of fireproofing. For the quantitative data analysis of the main study, R, a coding-based open-source popular statistical analysis software was used for interrelationship and equations for the NDT methods. R Studio interface was used for coding, input, and output analysis of R (Figure 4- 1).

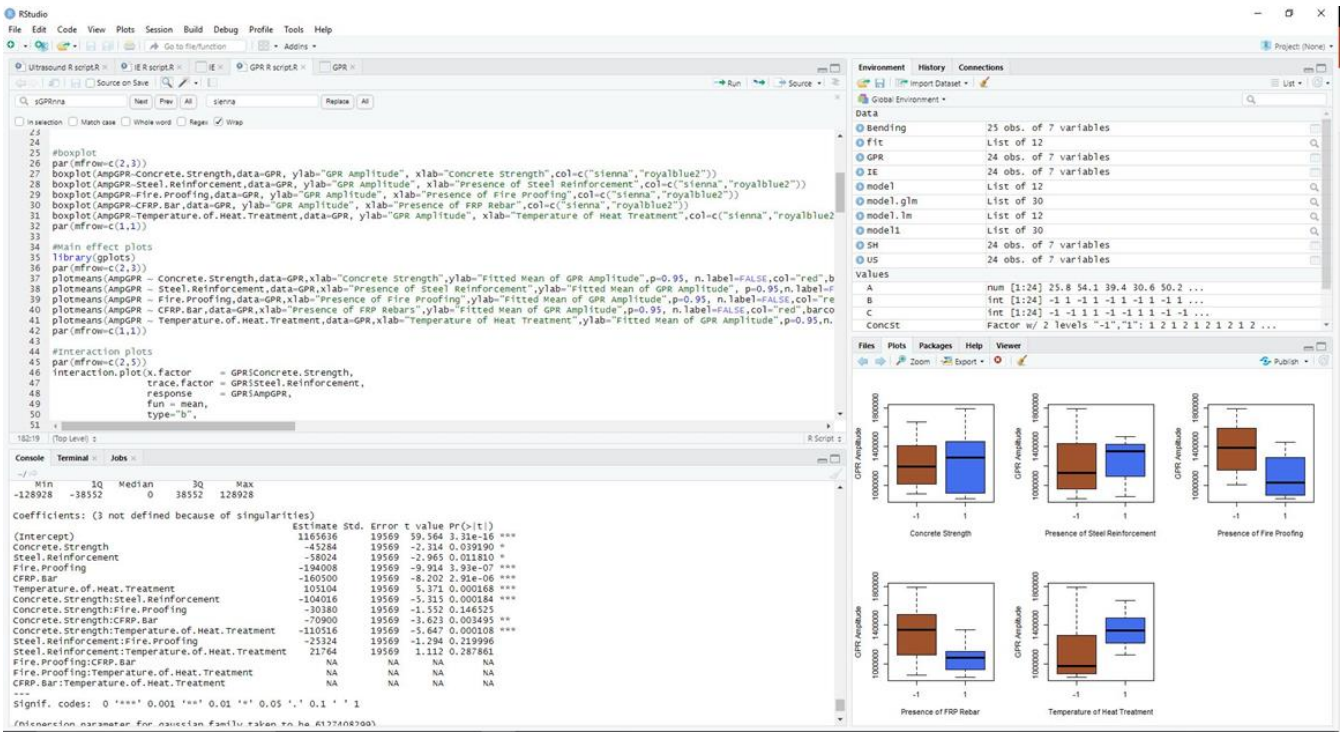

Figure 4- 1: R Studio interface used for data analysis.

4.1. Infrared/Thermal Camera

4.1.1. Pilot/Preliminary Study

FLIR E50 Infrared/thermal camera (Figure 4- 2) was used on the samples. However, the infrared camera needs heat dissipation for voids to be visible. As the samples from the preliminary study were unloaded right after heat treatment and set aside to cool down, after cooling down it did not show any voids inside the concrete in the infrared camera. That is why it was decided that for the main study, the samples would be scanned with

the infrared camera 15 minutes after the heat treatment when the samples still would not cool down fully. That way there will be a higher possibility of voids to be visible in the thermal images.

Figure 4- 2: FLIR E50 Infrared/thermal imaging camera.

4.1.2. Main Study

All the main study samples were scanned with the infrared/thermal camera after 15 minutes of the heat treatment in the furnace. As the position and size of failure modes such as voids and/or cracks cannot be controlled during the fire test, a quantitative analysis on Thermal Imaging data seemed irrelevant. Rather the data was planned to be used for qualitative analysis

combining with other modes of Non-destructive or Destructive test outcomes.

For the main study, the thermal imaging data were imported from the device and then analyzed. Figure 4- 3 below shows a typical Thermal Imaging outcome of a sample after one hour heat treatment where possible presence of voids and cracks is visible.

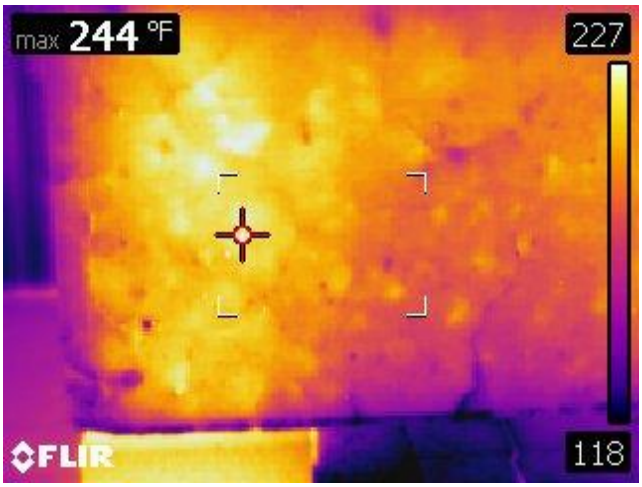

Figure 4- 3: Thermal Imaging of a one hour heat-treated sample.

The possible subsurface voids show a higher temperature in the thermal imaging as they tend to trap the heat. The cracks and surface voids show lower temperatures as their entrapped heat dissipates to the outer

environment. Figure 4- 4 shows a near-surface void visible only by the infrared camera in a heat-treated concrete sample.

Figure 4- 4: Infrared camera view vs bare eye view.

Now the infrared camera could successfully identify the locations of the most damaged area in a heat-affected sample after 15 minutes of heat exposure, whereas, the damage was not visible to bare eyes at that time. However, after 2 weeks of storage from the heat exposure, when the samples top surface crumbled apart, the same damaged areas seen in the thermal images became visible (Figure 4- 5). These examples indicate that the infrared camera can successfully perform a qualitative analysis to find

the most affected areas on a heat exposed concrete structural member, given that there is heat propagation in the member.

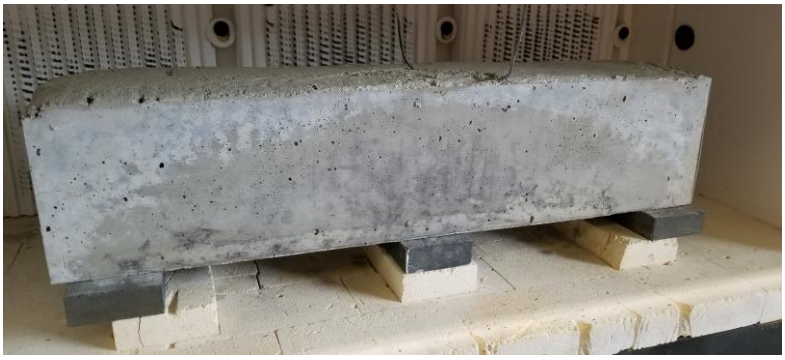	Normal strength concrete beam at 15 minutes after one hour heat exposure
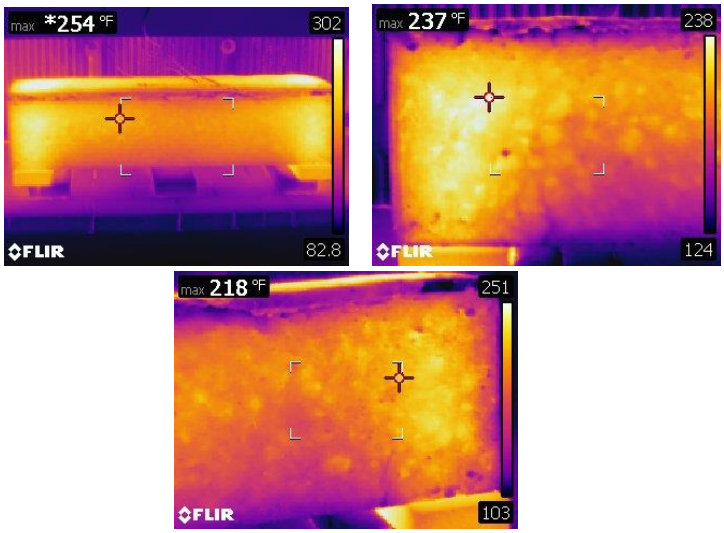	Thermal/Infrared Camera images of Normal strength concrete beam at 15 minutes after one hour heat exposure
	Normal strength concrete beam at 2 weeks after one hour heat exposure

Figure 4- 5: Qualitative analysis with the infrared camera.

4.2. Schmidt/Rebound Hammer

4.2.1. Pilot/Preliminary Study

This test was performed using a rebound hammer from Proceq (Figure 4- 6). Rebound hammer measures the ratio between the rebound velocity and the impact velocity also known as Q value. Q value represents the hardness of the concrete.

Figure 4- 6: Schmidt hammer or Rebound hammer.

Data was collected by having the hammer hit the top surface of the sample at a perpendicular orientation. Eight data were collected by the rebound hammer for each sample and the average Q values were determined. For normal strength concrete, it can be seen that the less

duration heat-treated and the fireproofed samples show higher values compared to other samples (Figure 4- 7). The Q values for the high strength concrete samples are presented in Figure 4- 8.

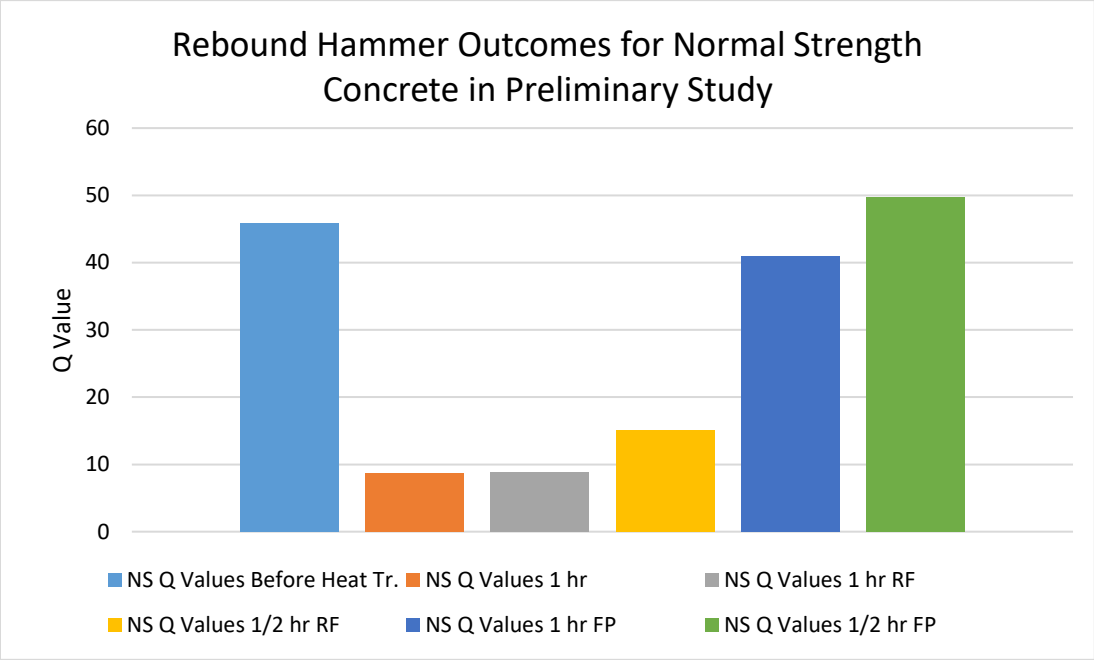

Figure 4- 7: Q values for normal strength concrete samples.

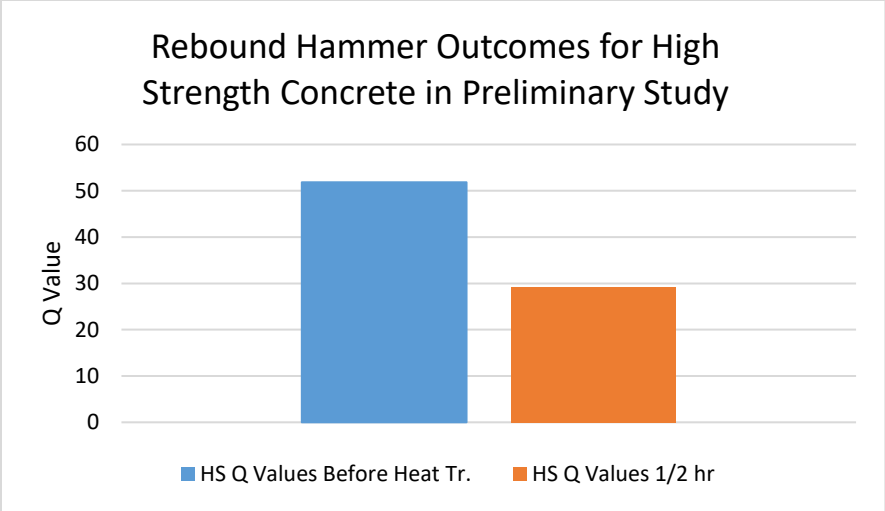

Figure 4- 8: Q values for high strength concrete samples.

4.2.2. Main Study

For the main study, twelve data were collected uniformly from the top surface of each sample as shown in Figure 4- 9. Before the data collection, the top surface of the main study samples was cleaned with a brush to remove any heat-damaged loose concrete debris. After that, data was collected from the top surface in two rows each having six points at equal distance.

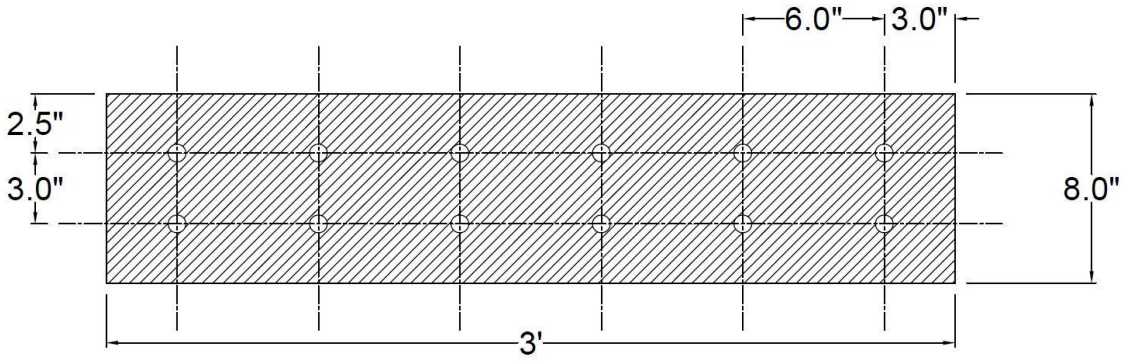

Figure 4- 9: Plan view of a sample showing test locations of Schmidt hammer.

After the data collection, the raw data of the Schmidt Hammer test was arranged and post-processed. Then it was formatted in a way it can be used as an input for the statistical analysis software R. Table 4- 1 shows a sample post-processed data set of Q values, which was used as an input file for R. Each color in Table 3 represents the average of Q value for one sample consisting individual treatment combination. Each treatment combination consists of a unique combination of factors and parameters.

Table 4- 1: Post processed data of Q values from Schmidt Hammer Test

Treatment Combination	Concrete Strength	Steel Reinforcement	Fire Proofing	CFRP Bar	Temperature of Heat Treatment	Q values
1	-1	-1	-1	1	-1	43.4
2	1	-1	-1	1	-1	51.9
3	-1	1	-1	-1	-1	44.2
4	1	1	-1	-1	-1	57.6
5	-1	-1	-1	-1	1	25.75
6	1	-1	-1	-1	0	54.15
7	-1	1	-1	-1	0	39.4
8	1	1	-1	-1	1	30.65
9	-1	-1	1	-1	0	50.2
10	1	-1	1	-1	1	41.55
11	-1	1	1	-1	1	40.6
12	1	1	1	-1	0	47.25
13	-1	-1	-1	1	0	42.25
14	1	-1	-1	1	1	32.55
15	-1	-1	1	1	1	39.9
16	1	-1	1	1	0	53.6
1	-1	-1	-1	1	-1	51.1
2	1	-1	-1	1	-1	49.6
3	-1	1	-1	-1	-1	42.05
4	1	1	-1	-1	-1	52.55
5	-1	-1	-1	-1	1	25.7
6	1	-1	-1	-1	0	53.56
7	-1	1	-1	-1	0	40.88
8	1	1	-1	-1	1	36.35
9	-1	-1	1	-1	0	47.45
10	1	-1	1	-1	1	46.8
11	-1	1	1	-1	1	45
12	1	1	1	-1	0	53.65
13	-1	-1	-1	1	0	41.05
14	1	-1	-1	1	1	34.05
15	-1	-1	1	1	1	39.9
16	1	-1	1	1	0	52.7

The R software codes were used to perform regression analysis on the post processed data of Q values. Figure 4- 10 shows the Residuals vs fitted values and the Normality Probability Plot (NPP) graph from R. The

distribution of the points in the Residuals vs fitted values graph implies that constant error variance is possible. In addition, the Normality Probability Plot (NPP) shows that the curve has a slightly shorter tail. The Shapiro-Wilk normality test result from R implies with 95% confidence that the distribution of the data is not significantly different from the normal distribution. Therefore, the data distribution did not need any further processing or modification.

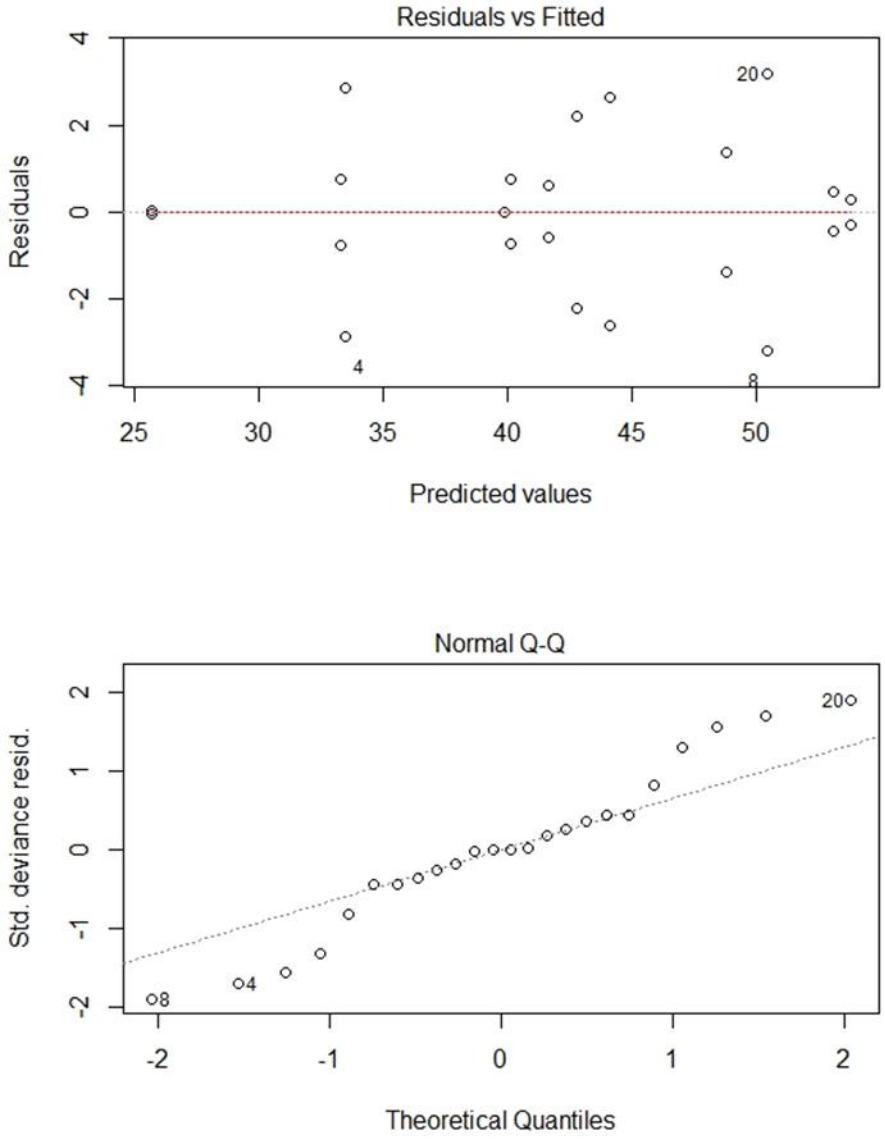

Figure 4- 10: Residuals vs fitted values, and Normality Probability Plot (NPP).

The Analysis of Variance (ANOVA) codes were applied for the data as well. Table 4- 2 shows the ANOVA output from R. Here the (***) means the highest probability of effect (around 100%), and (*) implies to the 95% probability of effect on Q value. It can be seen that the concrete strength, fireproofing and the temperature of heat treatment have very significant main effect on the Q values. The output also shows the probability of interaction effects of two factors on the Q value. According to the output, concrete strength and steel reinforcement, concrete strength and fireproofing, concrete strength and temperature of heat treatment show significant interaction effect on Q value.

Table 4- 2: Analysis of Variance (ANOVA) output for the Schmidt Hammer test.

	Df	Sum Sq	Mean Sq	F value	Pr(>F)	
Concrete.Strength	1	144.0	144.0	25.598	0.00028	***
Steel.Reinforcement	1	3.9	3.9	0.685	0.42397	
Fire.Proofing	1	435.7	435.7	77.474	1.40e-06	***
FRP.Bar	1	5.2	5.2	0.932	0.35329	
Duration.of.Heat.Treatment	1	785.9	785.9	139.745	5.71e-08	***
Concrete.Strength:Steel.Reinforcement	1	57.9	57.9	10.296	0.00751	**
Concrete.Strength:Fire.Proofing	1	73.4	73.4	13.044	0.00357	**
Concrete.Strength:FRP.Bar	1	86.3	86.3	15.346	0.00204	**
Concrete.Strength:Duration.of.Heat.Treatment	1	9.8	9.8	1.751	0.21044	
Steel.Reinforcement:Fire.Proofing	1	0.6	0.6	0.101	0.75568	
Steel.Reinforcement:Duration.of.Heat.Treatment	1	13.4	13.4	2.375	0.14921	
Residuals	12	67.5	5.6			

Signif. codes: 0 ‘***’ 0.001 ‘**’ 0.01 ‘*’ 0.05 ‘.’ 0.1 ‘ ’ 1

The box and whisker plots of Figure 4- 11 prepared by R shows the interquartile range, possible outliers, and means of the Q value data with

respect to each parameter. The two lines outside the boxes, also known as whiskers, extend to the highest and lowest values of observations. The horizontal lines inside the boxes represent the medians.

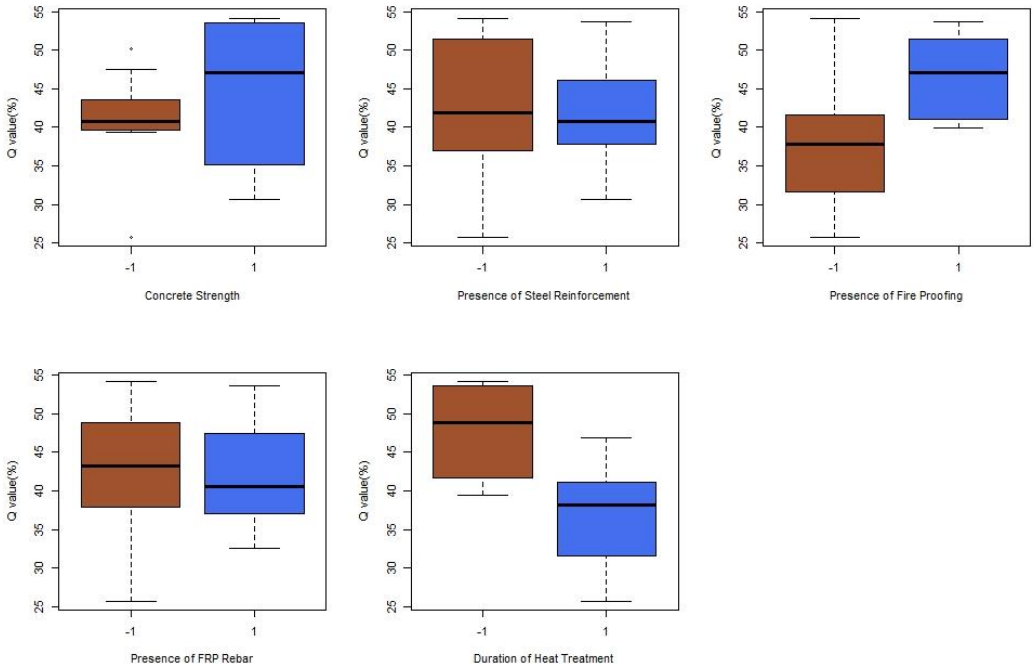

Figure 4- 11: Whisker Box Plot for Schmidt hammer test data.

Figure 4- 12 shows the main effect plots of the parameters. From the increasing slopes of the plots of concrete strength and the presence of fireproofing, it is evident that the Q value increases along with the increment of concrete strength and the presence of fireproofing separately. However,

the plot also shows that the Q value decreases along with the temperature of heat treatment.

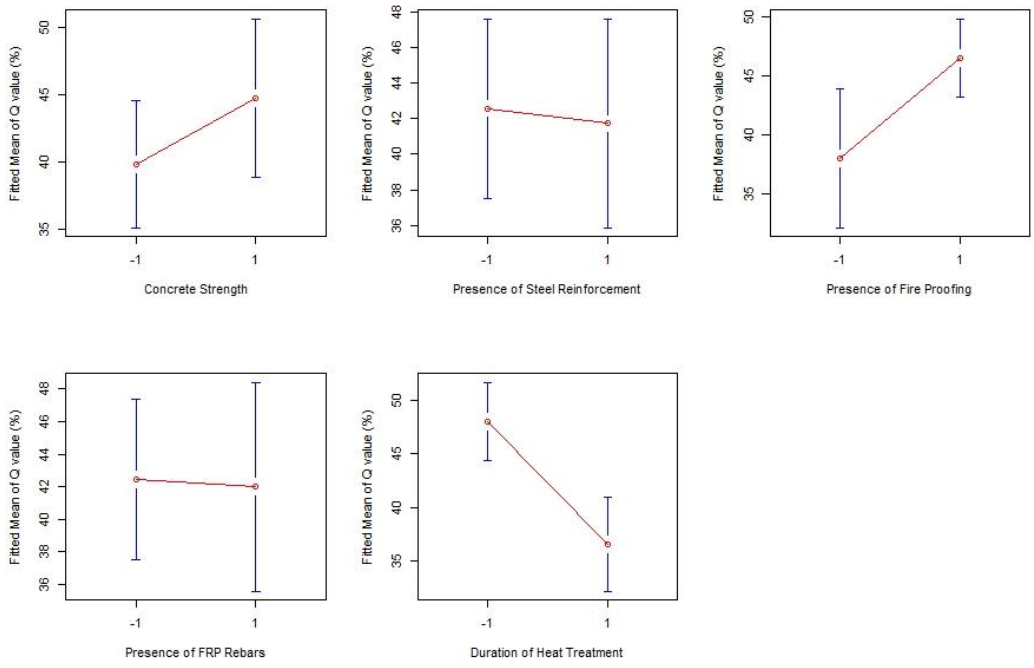

Figure 4- 12: Main effect plots for the Schmidt hammer test.

Figure 4- 13 shows the interaction plots of the parameters from R based on the Schmidt hammer test. In these plots, the crossing or un-parallel lines of a plot mean a higher probability of interaction effect. The graph shows no interaction effect of the concrete strength and fireproofing and almost no interaction effect of the FRP bar and the temperature of heat treatment. However, there is a slight interaction effect of concrete strength

and temperature of heat treatment. According to the graph, the interaction effect of the concrete strength along with the presence of steel rebar or the presence of FRP rebar is highly significant on the Q values.

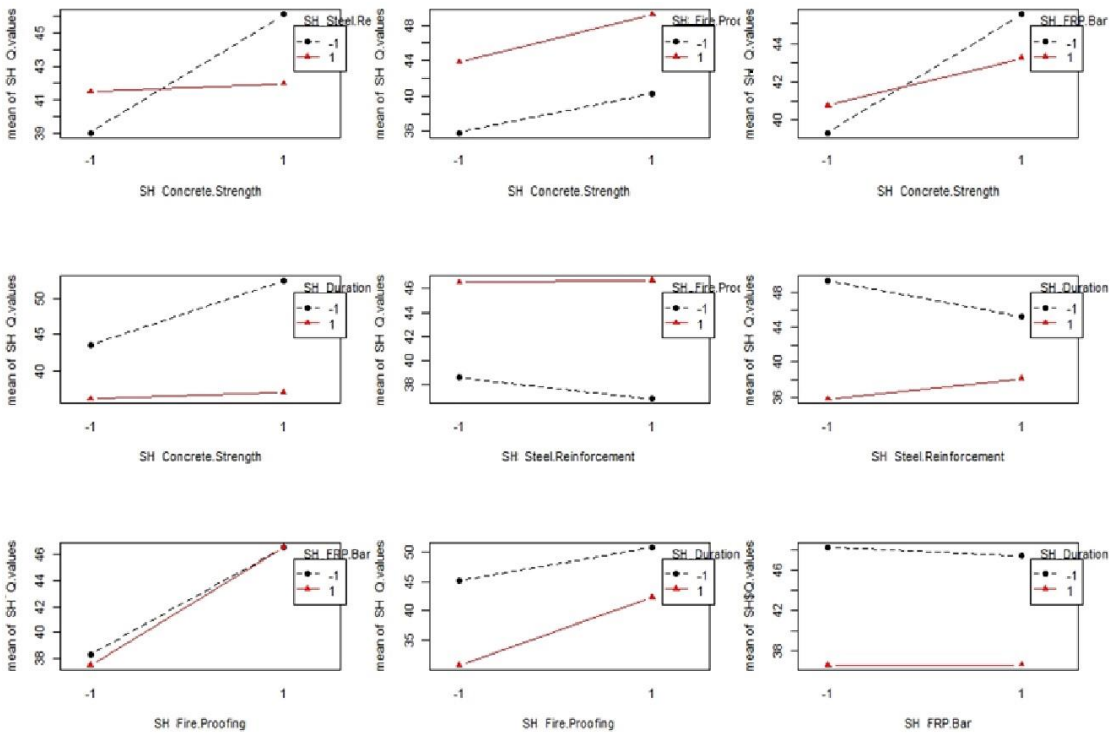

Figure 4- 13: Interaction plots for the Schmidt hammer test.

The following equation no [4-1] was achieved through the regression analysis by R. This equation was simplified by ignoring the low significant variables. :

$$Y = 41.861 + 4.129\ X_3 – 5.884\ X_5 – 2.809\ X_1\ X_2 - 1.398\ X_1\ X_3 – 2.322\ X_1\ X_4 + 0.914\ X_2\ X_5$$

------[4-1]

Here,

Y= Q Value

X_1= Concrete Strength

X_2= Steel Rebar

X_3= Fireproofing

X_4= FRP Rebar

X_5= Duration of heat exposure

Where, all the factors (X_1 through X_5) values can be either +1 or -1 indicating their highest range or lowest range respectively. For concrete strength, +1 and -1 represents 6000 psi and 3500 psi respectively. For the duration of heat exposure, +1 and -1 represents 1 hour (up to 927 degrees of Celsius) and ½ hour (up to 843 degrees of Celsius) respectively. For the rebar and fireproofing, they represent their presence or absence respectively. For steel rebar, the presence can be quantified by the

reinforcement ratio (ρ) value of 0.00625. For the absence of steel rebar, the reinforcement ratio is zero. Similarly, for the presence of FRP rebar, the reinforcement ratio is 0.00344, whereas the absence gives the value as zero. For any intermediate values of the factors representing numerical values at their two levels, the respective intermediate value between -1 and +1 can be used in this equation from interpolation.

The coefficient of determination, R^2 for this equation is found as 0.954 from the software R. This means that around 95.4% of the observed variation can be explained by the model's inputs.

4.3. Ultrasound Array Tomography

4.3.1. Pilot/Preliminary Study

The Proceq Pundit Ultrasonic Tomography device (Figure 4- 14), which was used for the NDT, is based on the ultrasonic multichannel pulse-echo technology using 8 channels. One channel transmits ultrasonic pulse and the echoes are received by the other seven channels. Each channel transmits in turn. A complete measurement consists of 56 A-scans (Figure 4- 15). These are used to compute and display a B-scan. This device produces a 50 kHz shear wave. For the preliminary study, the A and B scans by this device at midpoints were recorded.

Figure 4- 14: Proceq Pundit Ultrasonic Tomography device.

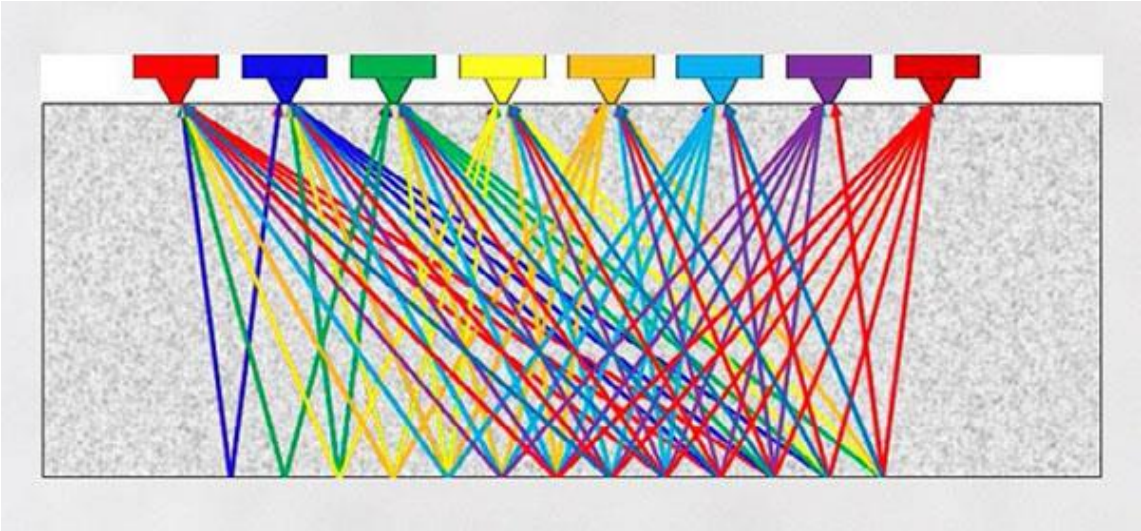

Figure 4- 15: A scans used to illustrate B scan in ultrasound array tomography.

Figure 4- 16 shows the B scan and A scan of a not heat-treated sample. The A scan (time vs amplitude) shows minimal absolute value of the amplitude at the mid-height of the sample. But, from Figure 4- 17, the B and A scan of a 1 hour heat-treated normal strength sample, it can be observed that the A scan shows higher absolute values in the mid-height range. This indicated that the ultrasonic pulse is capable to denote the difference in the concrete after heat exposure.

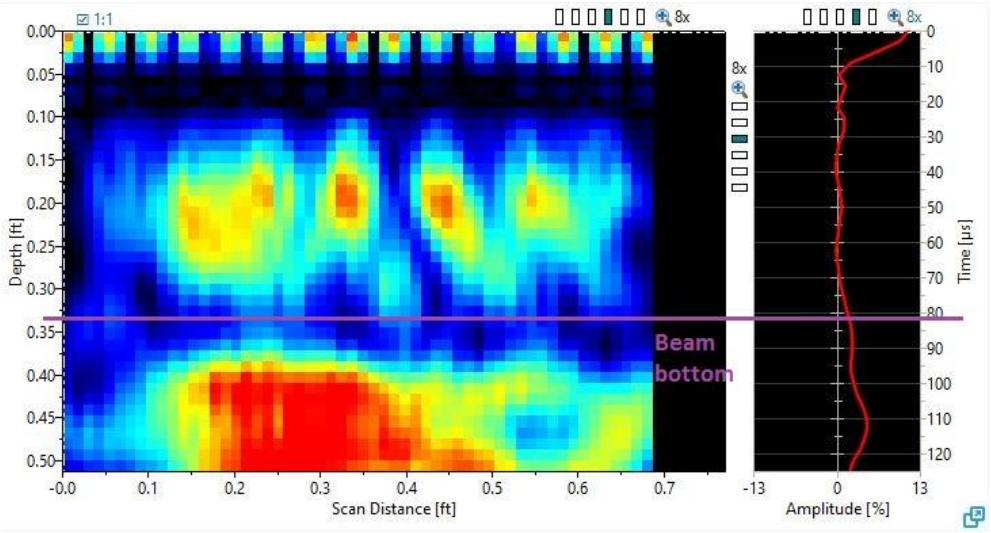

Figure 4- 16: Ultrasonic scan of not heat-treated sample.

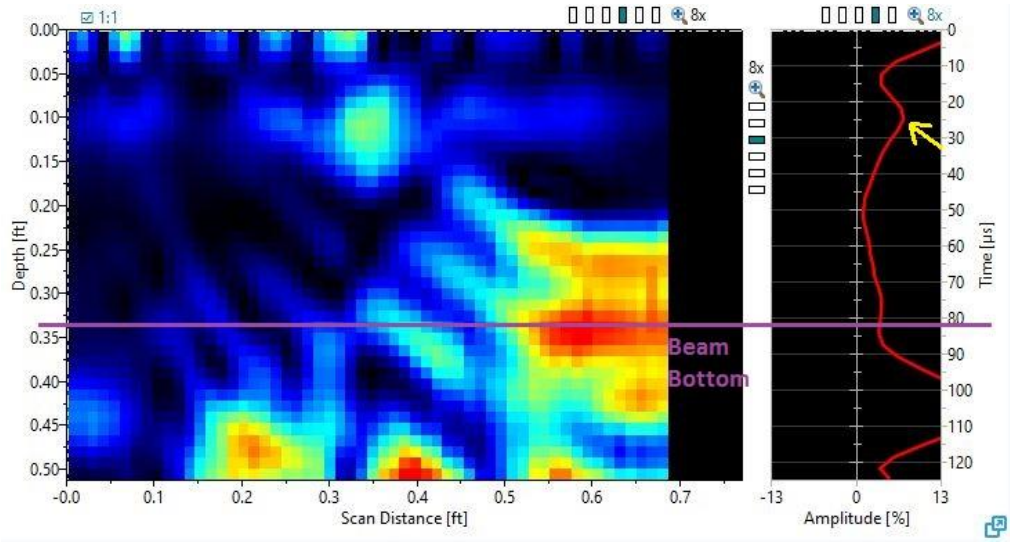

Figure 4- 17: Ultrasonic scan of the heat-treated sample.

4.3.2. Main Study

The main study samples were scanned using the ultrasonic array pulse-echo device. Two scans were done on the top surface of each sample as illustrated in Figure 4- 18. 30 dB probe gain was maintained to scan all the samples.

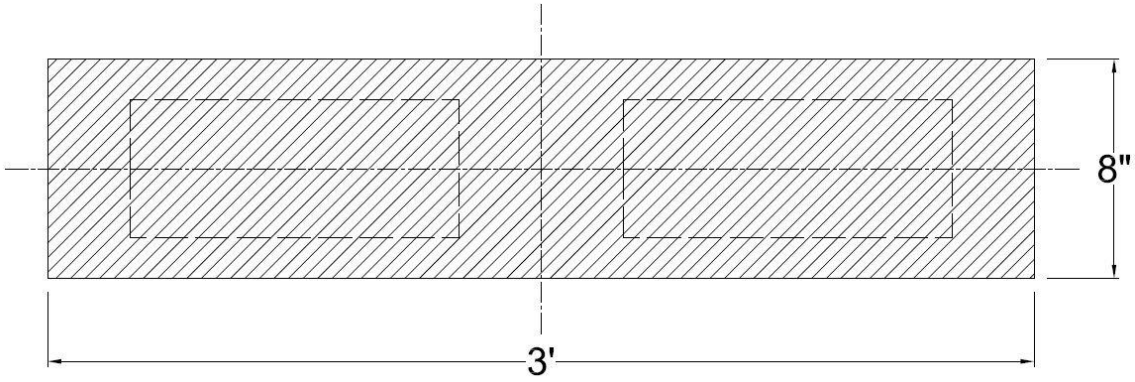

Figure 4- 18: Top view of main study beam sample indicating scan positions of ultrasound pulse array device.

Afterward, the raw data of the Ultrasound test was arranged and post-processed. Initially, four sets of data were chosen considering the furthest and nearest sensor/receiver probes of the instrument and maximum positive and minimum negative amplitudes. Then it was formatted in a way it can be used as an input for the statistical analysis software R. One of the four possible sets of data considering the pair of sensor probes 03<->04 in the middle and maximum positive values of amplitudes were finalized depending on the reliability.

Figure 4- 19 shows the Residuals vs fitted values and Normality Probability graphs for the initially selected ultrasound test data. The points in the Residual vs fitted values plot implies that non-constant error variance is possible due to ununiformed distribution. The Normality Probability Plot

shows that the normality might not be present. R^2 for the initial set of data came around 85.7%. However, the data distribution did not pass the Shapiro-Wilk normality test. This indicates the necessity of data transformation.

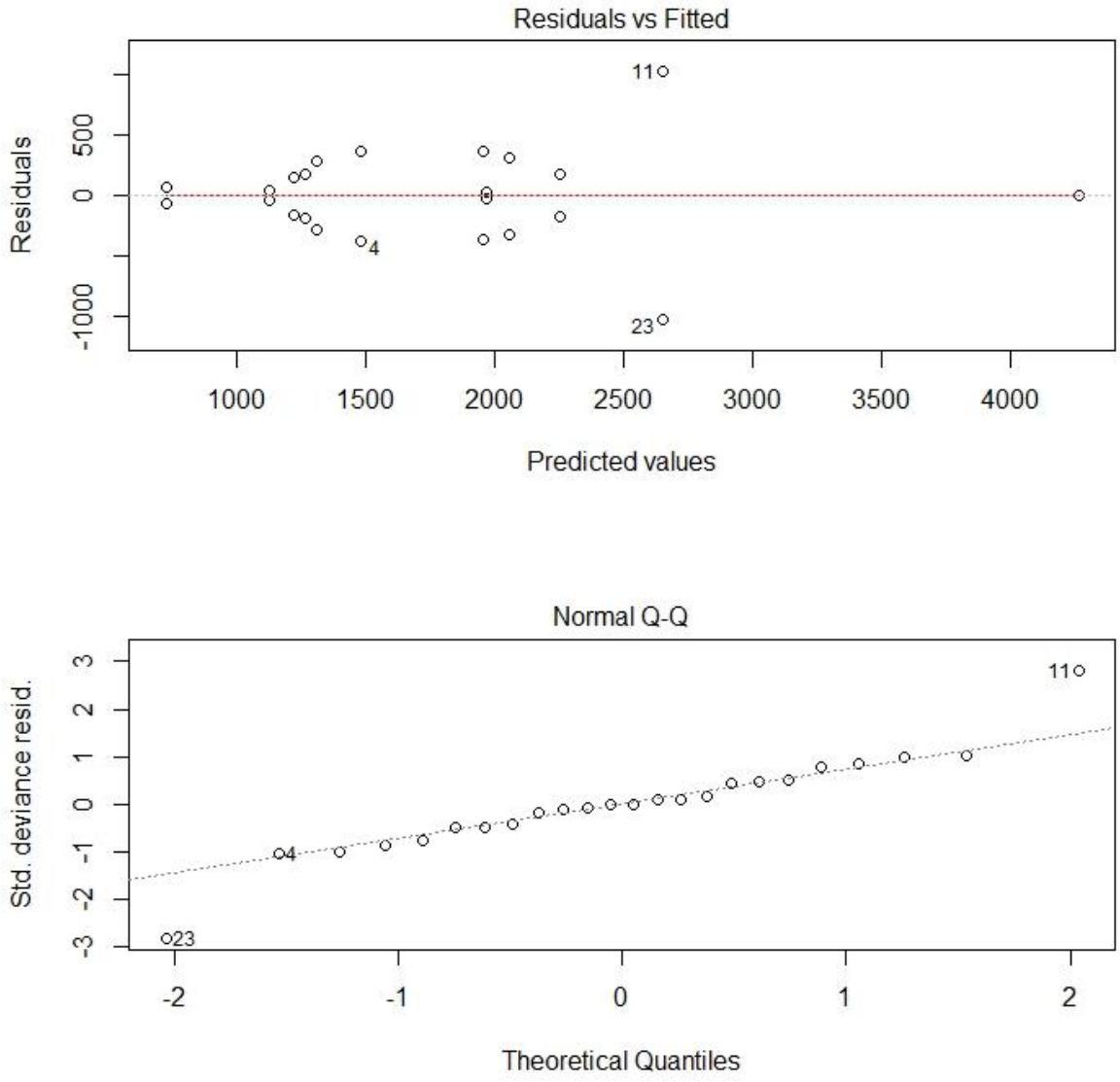

Figure 4- 19: Residual vs fitted values graph, and Normality Probability Plot (NPP).

For data transformation, the exponential Y method was chosen where all the response values were chosen as 10 based logarithmic

conversions of the initial amplitude values. The Residuals vs Fitted values and Normality Probability graphs for the transformed data are presented in Figure 4- 20. The graph shows significant improvement for Residuals vs fitted values as the plot distribution seems to be more uniform and the Normality Probability Plot seems more linear. The transformed data passes the Shapiro-Wilk Normality Test with a 95% confidence interval indicating the normal distribution.

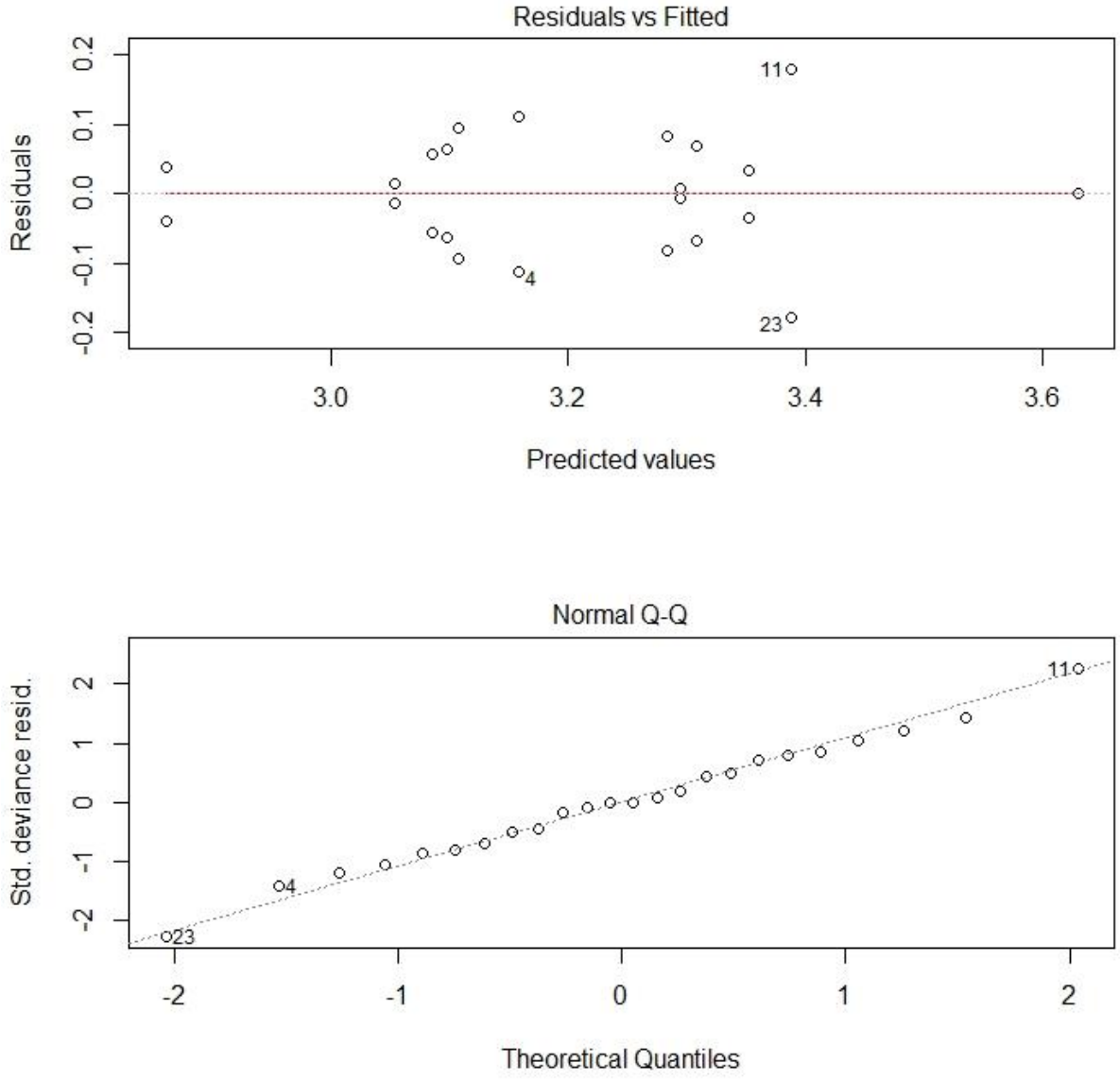

Figure 4- 20: Residual vs fitted values and Normality Probability Plot (NPP) after data transformation.

The Analysis of Variance (ANOVA) codes were applied for the transformed data in the R software. Table 4- 3 shows the ANOVA output from R. It can be seen that the concrete strength, steel reinforcement has a high probability of effect on the exponential versions of maximum amplitude values of the ultrasound test. It also shows that the temperature of heat treatment and fireproofing have a significant effect on the ultrasound test data. The output also shows the probability of combined factors' effects. The data shows that concrete strength and FRP bar, steel reinforcement and fireproofing have an interaction effect on the logarithmic values of maximum amplitudes.

Table 4- 3: R output of Analysis of Variance (ANOVA) of Ultrasound test data

	Df	Sum Sq	Mean Sq	F value	Pr(>F)	
Concrete.Strength	1	0.20180	0.20180	16.269	0.00166	**
Steel.Reinforcement	1	0.12304	0.12304	9.919	0.00838	**
Fire.Proofing	1	0.05459	0.05459	4.401	0.05776	.
FRP.Bar	1	0.00056	0.00056	0.046	0.83460	
Duration.of.Heat.Treatment	1	0.07857	0.07857	6.334	0.02707	*
Concrete.Strength:Steel.Reinforcement	1	0.00319	0.00319	0.257	0.62149	
Concrete.Strength:Fire.Proofing	1	0.01659	0.01659	1.337	0.27005	
Concrete.Strength:FRP.Bar	1	0.19535	0.19535	15.748	0.00186	**
Concrete.Strength:Duration.of.Heat.Treatment	1	0.01149	0.01149	0.927	0.35473	
Steel.Reinforcement:Fire.Proofing	1	0.17902	0.17902	14.432	0.00253	**
Steel.Reinforcement:Duration.of.Heat.Treatment	1	0.01247	0.01247	1.005	0.33582	
Residuals	12	0.14885	0.01240			

Signif. codes: 0 '***' 0.001 '**' 0.01 '*' 0.05 '.' 0.1 ' ' 1

Figure 4- 21 shows the box and whisker plots for the transformed data of the ultrasound test. The interquartile range, possible outliers, and

means of the logarithmic amplitude value data concerning each parameter are shown in the plot. The two lines outside the boxes, also known as whiskers, extend to the highest and lowest values of observations. The horizontal lines inside the boxes represent the medians.

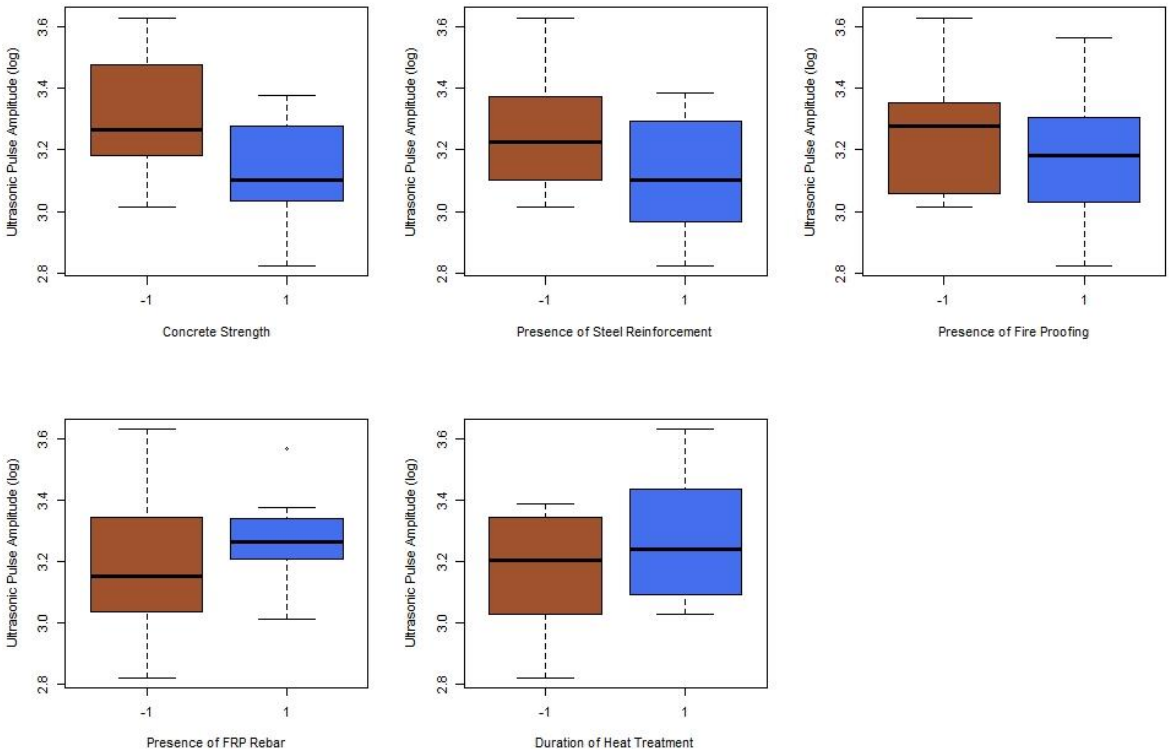

Figure 4- 21: Whisker Box plots for ultrasound test data.

Figure 4- 22 shows the main effects plots for the ultrasound test. It shows that almost all the plots have a slope, which means all the five factors

have a significant main effect on the log value of amplitude achieved from the ultrasound test.

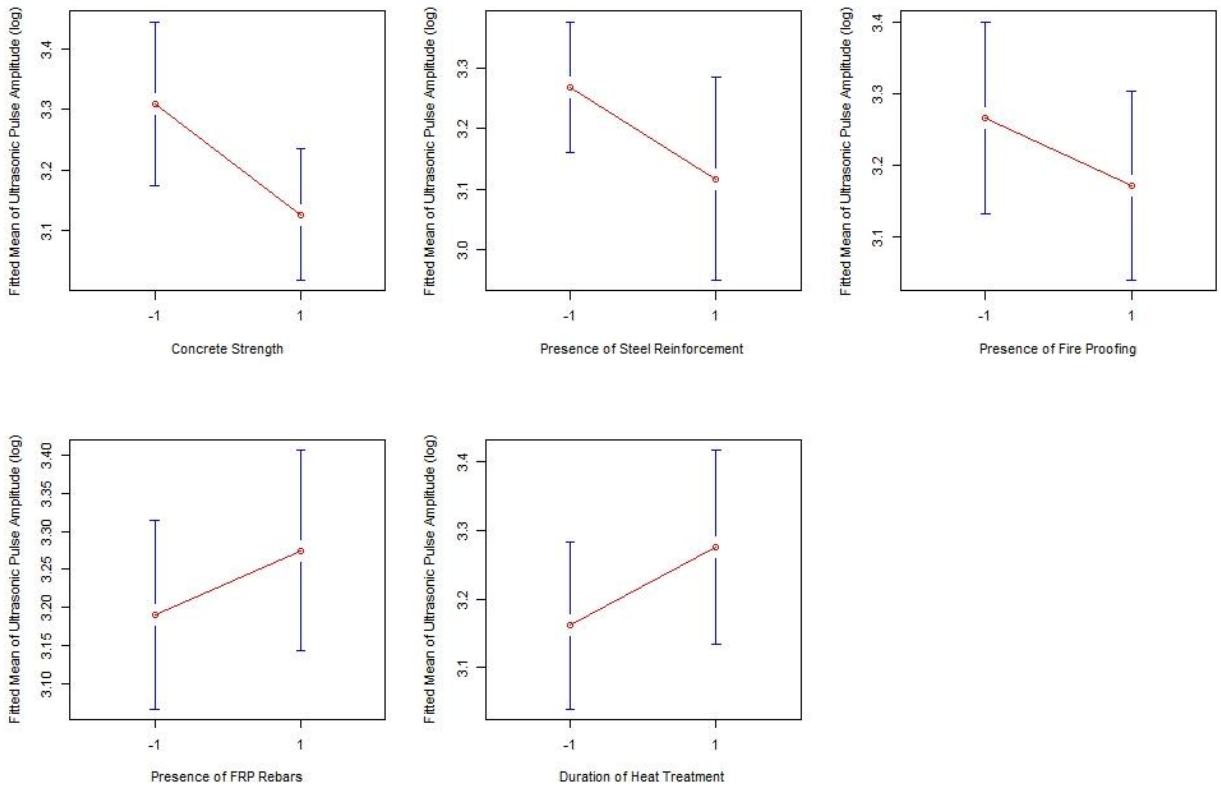

Figure 4- 22: Main effect plots for the ultrasound test.

Figure 4- 23 shows the interaction plots achieved from the R software for the ultrasonic test. The plots show significant interaction effect of concrete strength and FRP bar, fireproofing and FRP bar, steel reinforcement and fireproofing on the logarithmic value of amplitudes

achieved from the ultrasonic test. Steel reinforcement and temperature of heat treatment also have the probability of interaction effect on the ultrasonic test data.

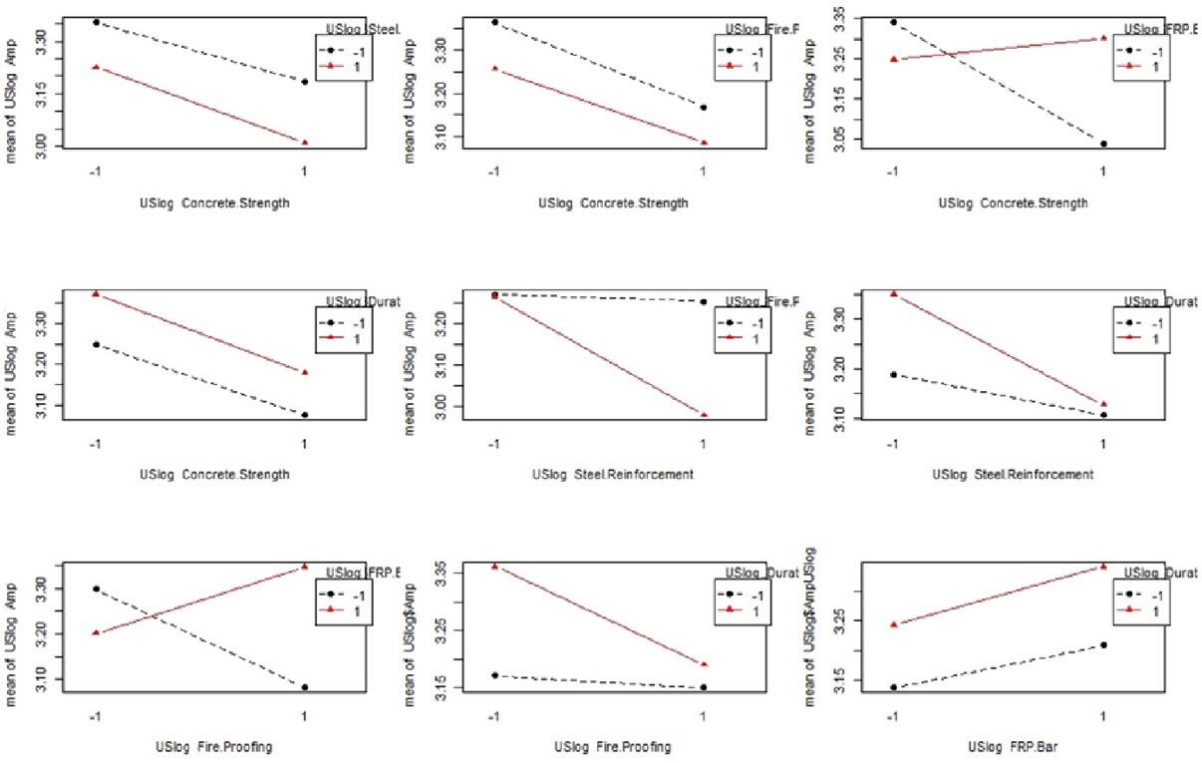

Figure 4- 23: Interaction plots for ultrasound test data.

Afterward, R code was used to perform regression analysis and achieve the equation for maximum amplitude relating with the factors for the ultrasound test data. Following simplified equation [4- 2] was derived:

$$Log(Y) = 3.196 – 0.041\ X_1 – 0.073\ X_2 – 0.108\ X_3 + 0.053\ X_5 + 0.043\ X_1\ X_2 + 0.11\ X_1\ X_4 - 0.076\ X_1\ X_5 – 0.106\ X_2\ X_3 – 0.028\ X_2\ X_5$$

----------[4- 2]

Here,

Y= Maximum amplitude from ultrasound pulse

X_1= Concrete Strength

X_2= Steel Rebar

X_3= Fireproofing

X_4= FRP Rebar

X_5= Duration of heat exposure

Where, all the factors (X_1 through X_5) values can be either +1 or -1 indicating their highest range or lowest range respectively. For concrete strength, +1 and -1 represents 6000 psi and 3500 psi respectively. For the duration of heat exposure, +1 and -1 represents 1 hour (up to 927 degrees of Celsius) and ½ hour (up to 843 degrees of Celsius) respectively. For the rebar and fireproofing, they represent their presence or absence

respectively. For steel rebar, the presence can be quantified by the reinforcement ratio (ρ) value of 0.00625. For the absence of steel rebar, the reinforcement ratio is zero. Similarly, for the presence of FRP rebar, the reinforcement ratio is 0.00344, whereas the absence gives the value as zero. For any intermediate values of the factors representing numerical values at their two levels, the respective intermediate value between -1 and +1 can be used in this equation from interpolation.

The coefficient of determination, R^2 for this equation was found as 85.2%.

4.4. Impact Echo (IE)

4.4.1. Pilot/Preliminary Study

The Olson Instruments impact echo (IE) system (Figure 4- 24) is designed to determine the condition and thickness of concrete structural members when voids, honeycombs, and/or cracks are suspected. IE device creates an impact on the surface and records the echo through its sensor. The recorded data is then analyzed and post processed for any possible cracks, honeycombs or delamination inside the concrete.

Figure 4- 24: Impact Echo (IE) device.

Federal Highway Administration (FHWA) has summarized the IE data analysis and conclusion in a very convenient way (FHWA, 2015). As per them, the condition of the concrete can be easily evaluated by the position of the peak of the frequency spectrum (amplitude vs. frequency plot) (Figure 4- 25).

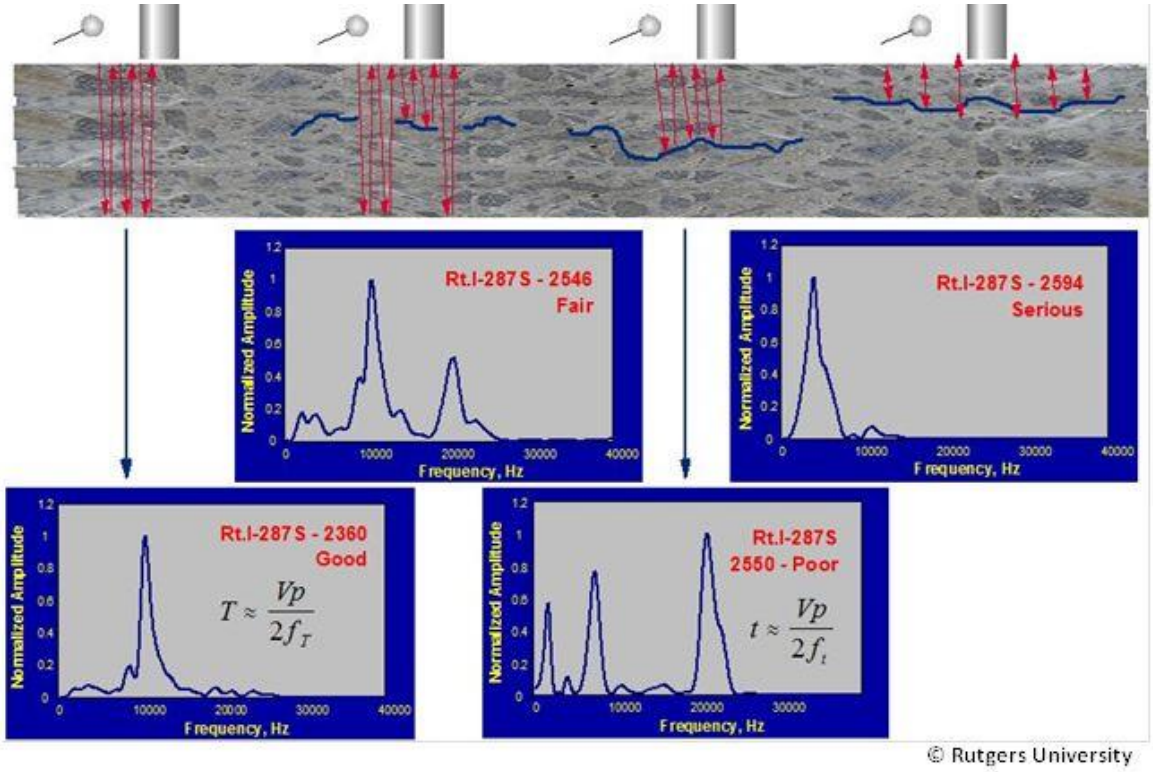

Figure 4- 25: IE frequency spectrum analysis theory in the FHWA website (FHWA, 2015).

The preliminary study samples were scanned with the IE device and the data were recorded. According to the post-processed data, in the frequency spectrum of one hour heat-treated normal strength concrete sample, it shows one peak at a lower frequency level along with a high thickness value than the sample's height of four inches (Figure 4- 26). This means a serious condition of the concrete and there are possible cracks, voids, and delamination inside. On the other hand, the spectrum of the 1

hour heat-treated fireproofed sample shows multiple peaks in the spectrum also indicating possible voids inside the sample (Figure 4- 27).

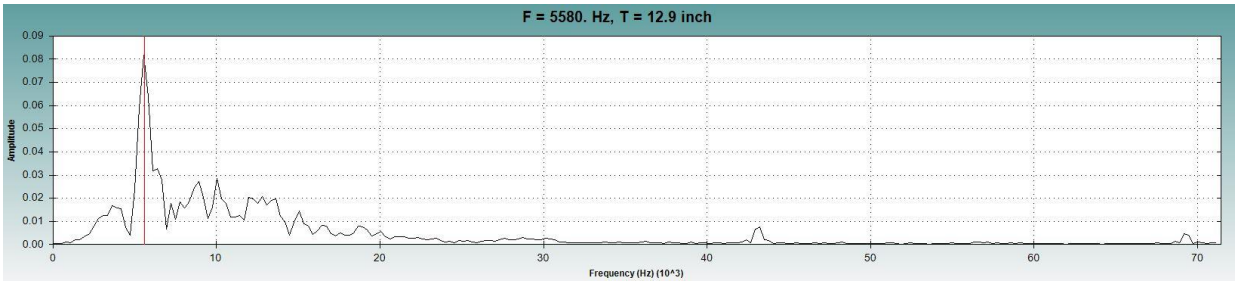

Figure 4- 26: IE frequency spectrum of one hour heat-treated normal strength concrete sample.

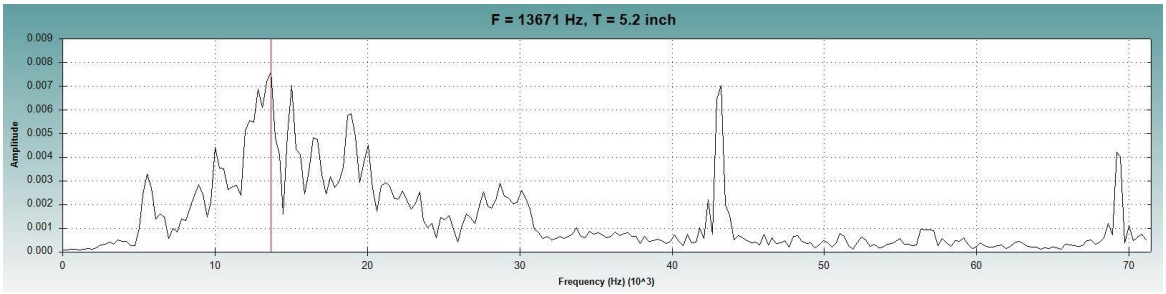

Figure 4- 27: IE frequency spectrum of one hour heat-treated fireproofed concrete sample.

4.4.2. Main Study

The main study samples were scanned using the impact echo device. Ten scans were done on the top surface of each sample as illustrated in Figure 4- 28.

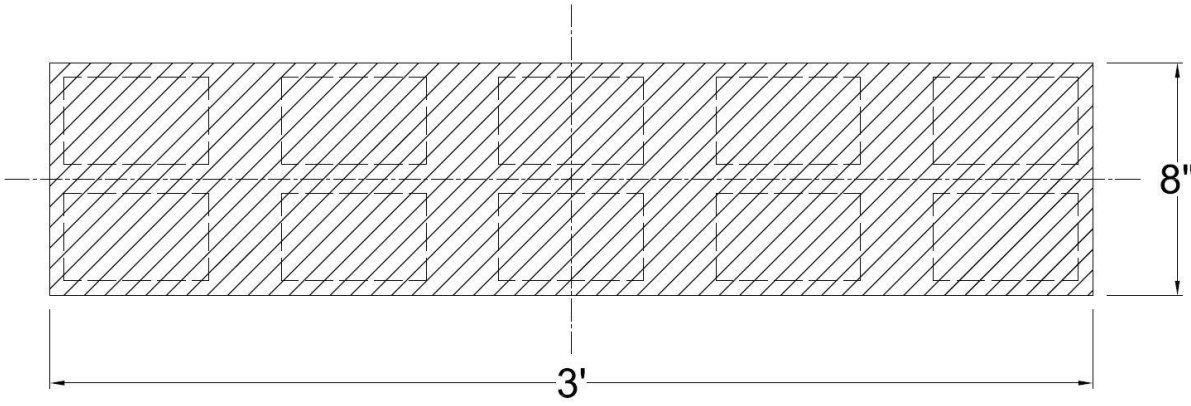

Figure 4- 28: Top view of main study beam sample indicating scan positions of impact echo device.

Afterward, the raw data of impact echo test was arranged and post-processed. Initially, two sets of data were chosen considering maximum and minimum peak frequencies. Then it was formatted in a way it can be used as an input for the software R. The maximum peak values of frequencies were finalized depending on the reliability.

Figure 4- 29 shows the Residuals vs fitted values and Normality Probability graphs for the initially selected impact echo test data. The distribution of the points implies that non-constant error variance might not be satisfied. For the Normality Probability Plot, the curve shows a slightly shorter tail. However, the R^2 for the initial set of data came around 67.6%

and the data set did not pass the Shapiro-Wilk test with a 95% confidence interval. This indicates the necessity of data transformation.

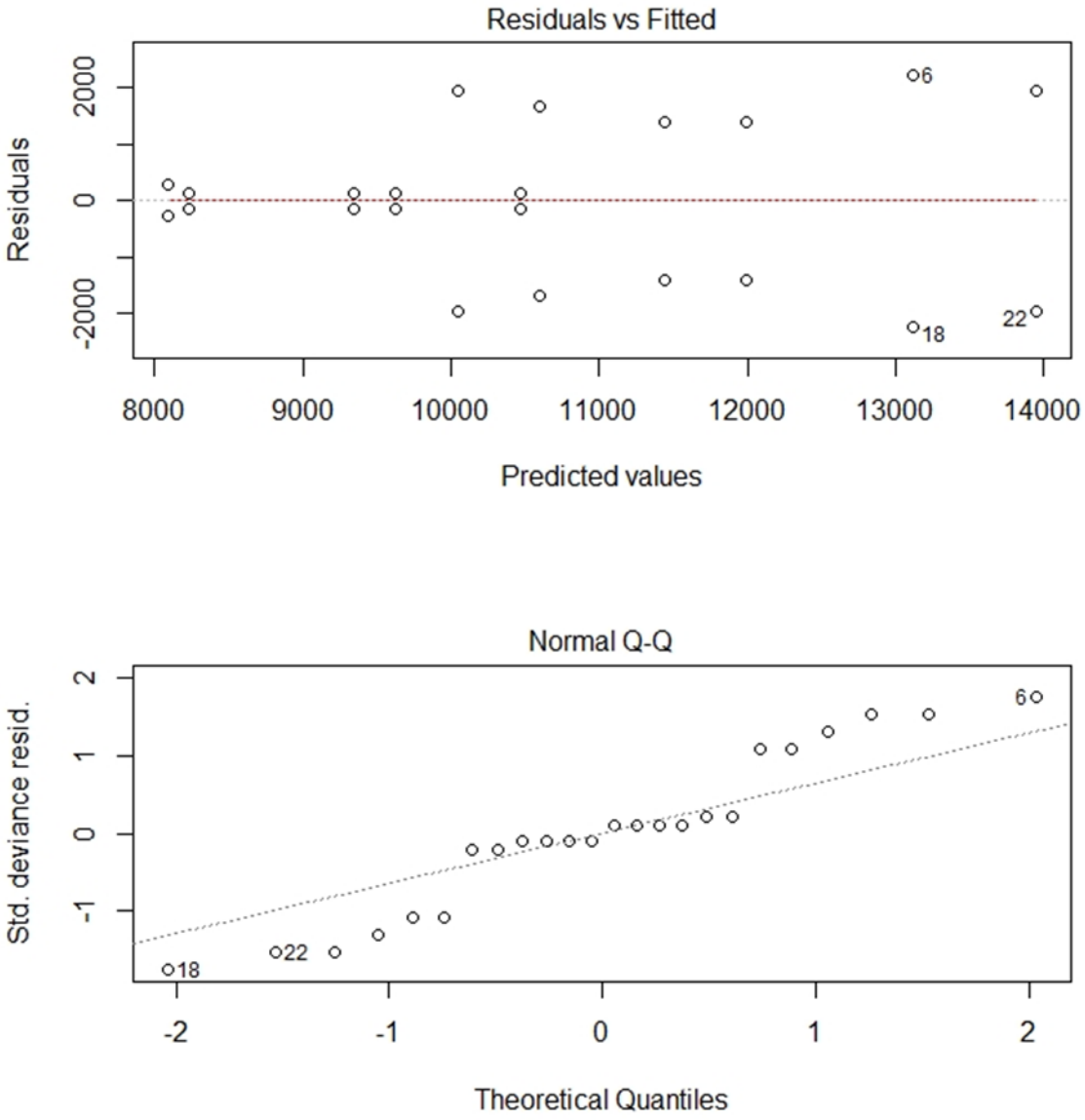

Figure 4- 29: Residual vs fitted values and Normality Probability Plot (NPP).

For data transformation, the exponential Y method was chosen where all the response values were chosen as 10 based logarithmic conversions of the initial amplitude values. The Residuals vs Fitted values and Normality Probability graphs for the transformed data are presented in Figure 4- 30. Though the graphs show very little changes, the transformed data passes the Shapiro-Wilk Normality Test with a 95% confidence interval indicating the normal distribution.

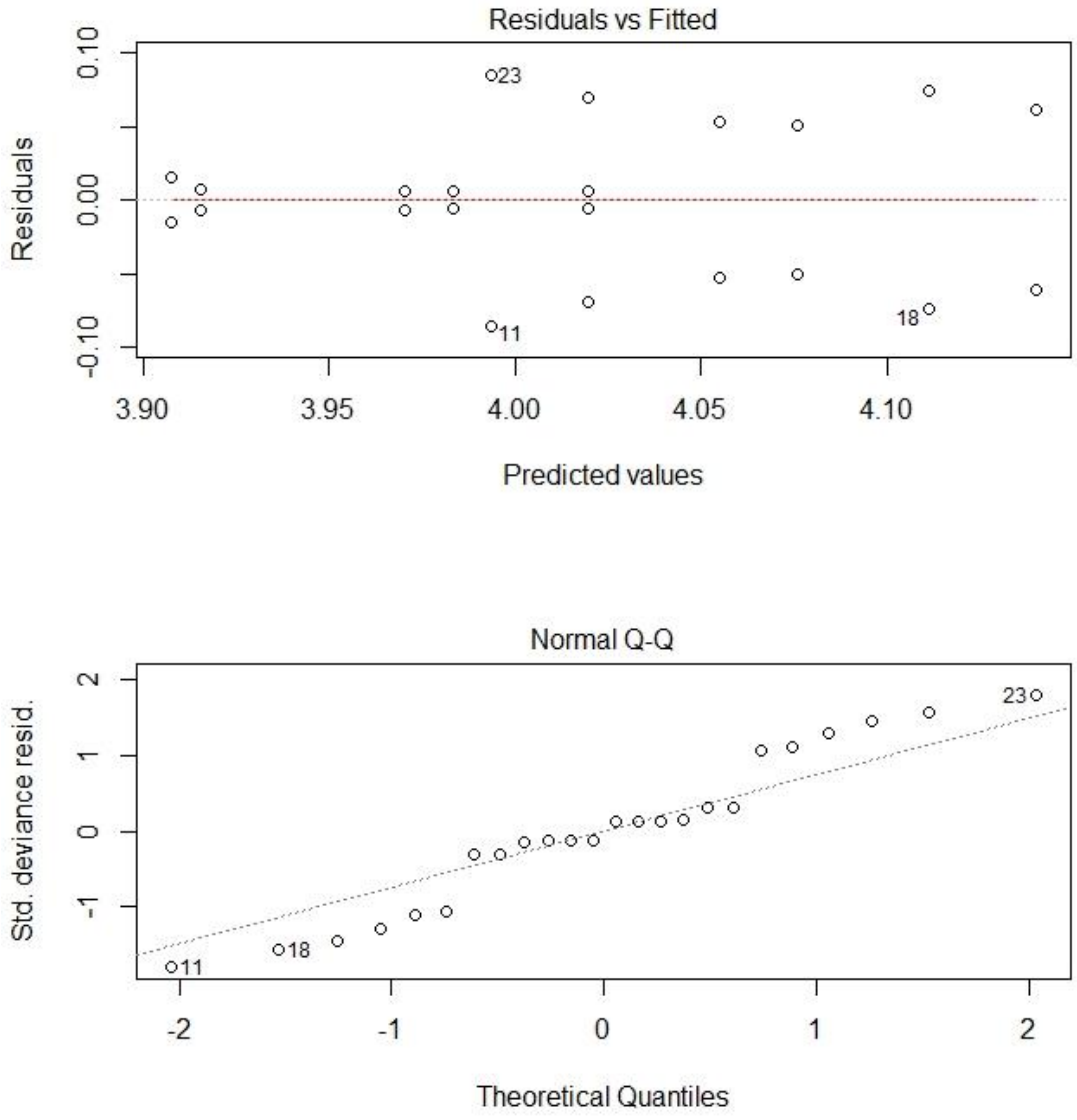

Figure 4- 30: Residual vs fitted values and Normality Probability Plot (NPP) after data transformation.

The Analysis of Variance (ANOVA) codes were applied for the transformed data in the R software. Table 4- 4 shows the ANOVA output

from R. It can be seen that the temperature of heat treatment has a very significant effect on the impact echo maximum peak frequency (Hz). The concrete strength also has a significant effect as well. The ANOVA table also shows very less interaction effects of paired factors on the impact echo data.

Table 4- 4: R output of Analysis of Variance (ANOVA) of impact echo test data.

	Df	Sum Sq	Mean Sq	F value	Pr(>F)	
Concrete.Strength	1	0.02238	0.02238	4.894	0.04710	*
Steel.Reinforcement	1	0.00048	0.00048	0.105	0.75130	
Fire.Proofing	1	0.00277	0.00277	0.606	0.45129	
FRP.Bar	1	0.00409	0.00409	0.895	0.36280	
Duration.of.Heat.Treatment	1	0.06382	0.06382	13.954	0.00285	**
Concrete.Strength:Steel.Reinforcement	1	0.00009	0.00009	0.020	0.89041	
Concrete.Strength:Fire.Proofing	1	0.00777	0.00777	1.698	0.21694	
Concrete.Strength:FRP.Bar	1	0.00142	0.00142	0.311	0.58733	
Concrete.Strength:Duration.of.Heat.Treatment	1	0.01346	0.01346	2.942	0.11200	
Steel.Reinforcement:Fire.Proofing	1	0.01326	0.01326	2.899	0.11436	
Steel.Reinforcement:Duration.of.Heat.Treatment	1	0.00287	0.00287	0.627	0.44377	
Residuals	12	0.05489	0.00457			

Signif. codes: 0 ‘***’ 0.001 ‘**’ 0.01 ‘*’ 0.05 ‘.’ 0.1 ‘ ’ 1

The box and whisker plots for the transformed data of the impact echo test are shown in Figure 4- 31. It shows the interquartile range, possible outliers, and means of the logarithmic peak frequency data concerning each parameter. The two lines outside the boxes, also known as whiskers, extend to the highest and lowest values of observations. The horizontal lines inside the boxes represent the medians.

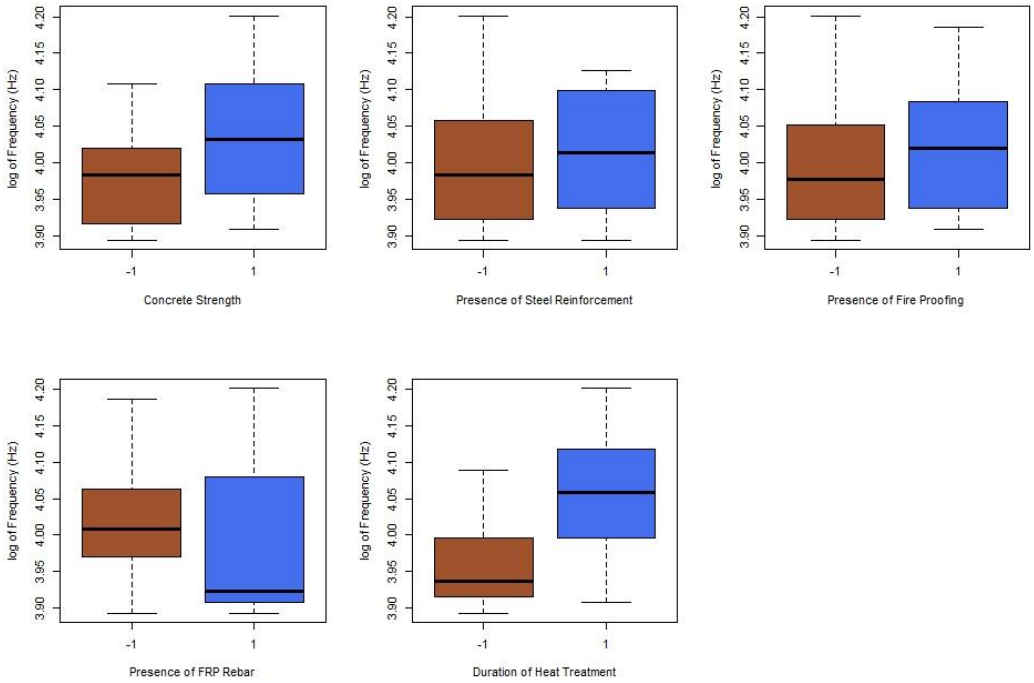

Figure 4- 31: Whisker Box plots of impact echo test data.

Figure 4- 32 shows the main effects plots for the impact echo test. It shows that concrete strength and temperature of heat treatment have significant main effect on the log of peak frequency (Hz) compared to the other three factors.

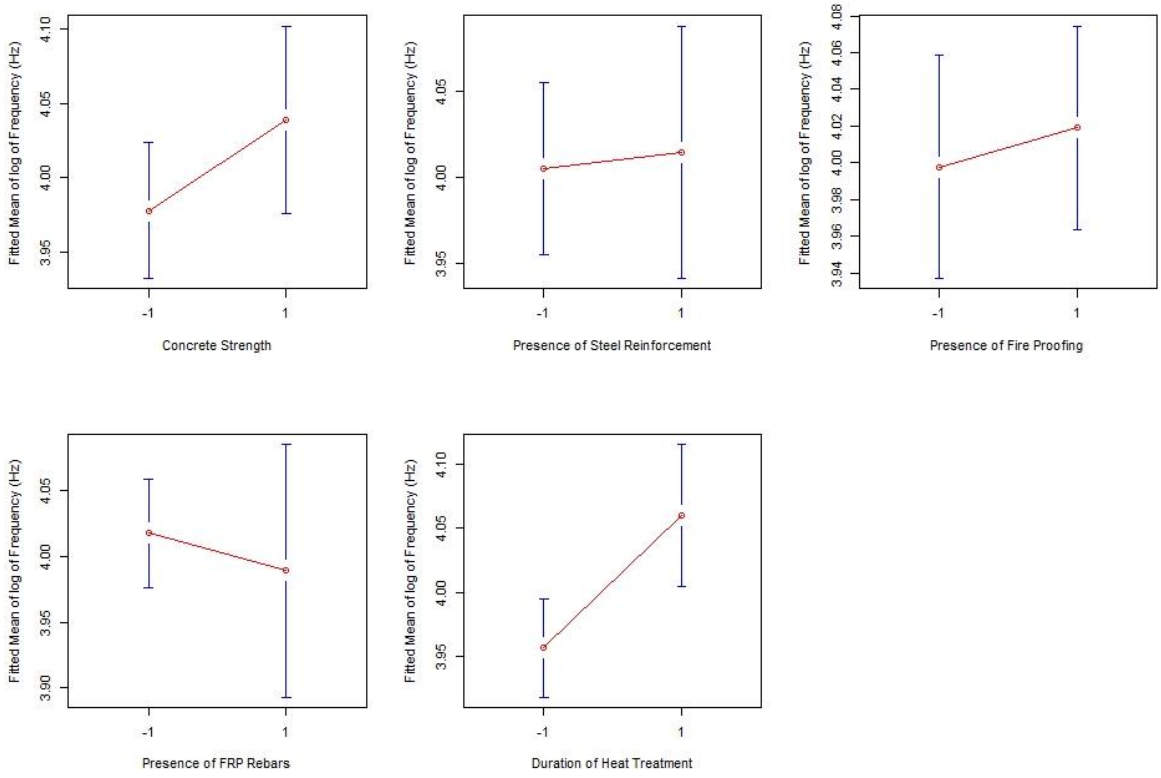

Figure 4- 32: Main effect plots for impact echo test data.

Figure 4- 33 shows the interaction plots achieved from the R software for the impact echo test. The plots show significant interaction effect of concrete strength and fireproofing, steel reinforcement and fireproofing, fireproofing and FRP bar on the logarithmic value of maximum peak frequency. The plot also shows possible interaction effect of concrete strength and steel rebar on the logarithmic value of peak frequency from the impact echo test.

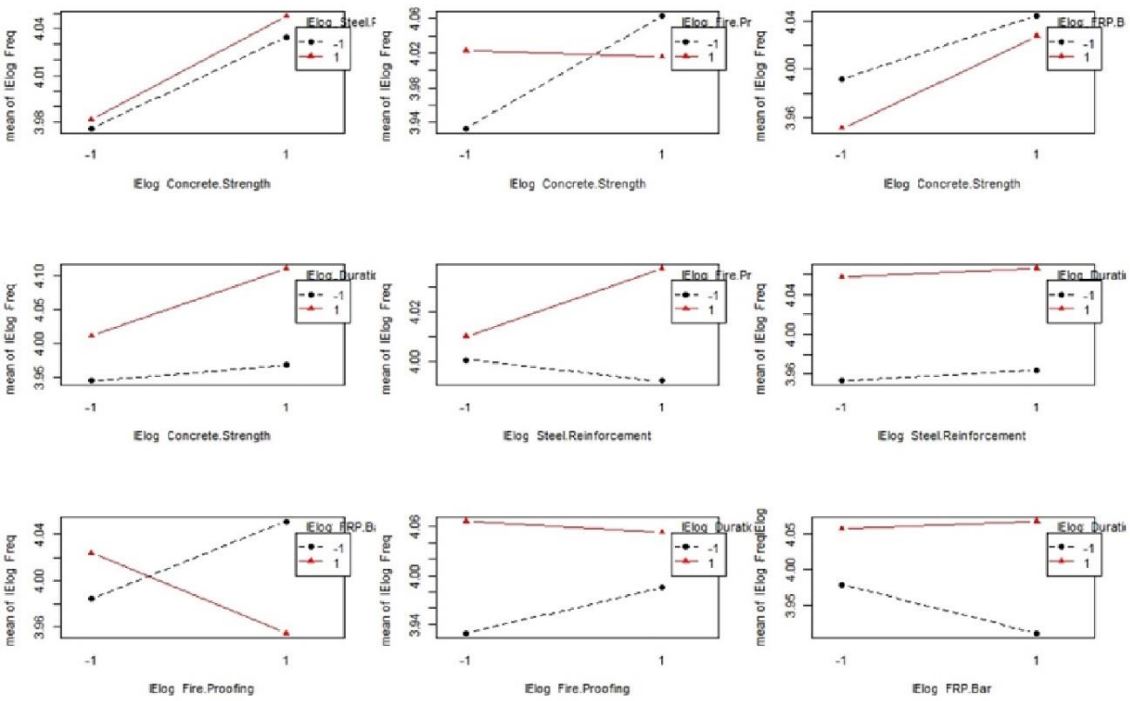

Figure 4- 33: Interaction plots for impact echo test data.

Afterward, R code was used to perform regression analysis and achieve the equation for maximum peak frequency relating to the factors for the impact echo data. Following simplified equation [4- 3] was derived:

$$Log(Y) = 4.002 + 0.036\ X_1 + 0.034\ X_3 - 0.016\ X_4 + 0.039\ X_5 - 0.026\ X_1\ X_3 + 0.04\ X_1\ X_5 + 0.029\ X_2\ X_3 - 0.013\ X_2\ X_5 \quad \text{--------- [4- 3]}$$

Here,

Y= Maximum peak frequency from impact echo (Hz)

X_1= Concrete Strength

X_2= Steel Rebar

X_3= Fireproofing

X_4= FRP Rebar

X_5= Duration of heat exposure

Where, all the factors (X_1 through X_5) values can be either +1 or -1 indicating their highest range or lowest range respectively. For concrete strength, +1 and -1 represents 6000 psi and 3500 psi respectively. For the duration of heat exposure, +1 and -1 represents 1 hour (up to 927 degrees of Celsius) and ½ hour (up to 843 degrees of Celsius) respectively. For the rebar and fireproofing, they represent their presence or absence respectively. For steel rebar, the presence can be quantified by the reinforcement ratio (ρ) value of 0.00625. For the absence of steel rebar, the reinforcement ratio is zero. Similarly, for the presence of FRP rebar, the reinforcement ratio is 0.00344, whereas the absence gives the value as zero. For any intermediate values of the factors representing numerical values at their two levels, the respective intermediate value between -1 and

+1 can be used in this equation from interpolation. The coefficient of determination, R^2 for this equation was found as 70%.

4.5. Ground Penetrating Radar (GPR)

4.5.1. Pilot/Preliminary Study

The test with GSSI SIR-30 Ground Penetrating Radar (GPR) was performed using a 2.6 GHz GPR antenna (Figure 4- 34). The 2.6 GHz antenna is able to scan concrete up to a depth of 10 inch with high resolution.

Figure 4- 34: GPR antenna 2.6 GHz (2600 MHz).

Each sample was scanned and the wave profile, the frequency and the amplitude of the wave was recorded. Figure 4- 35 shows the test setup.

Figure 4- 35: Test setup for GPR scanning.

The GPR scans of heat untreated beam and one hour heat-treated normal strength concrete beam are shown in Figure 4- 36. It is evident that the GPR scan of not heat-treated sample is showing lower positive amplitude in A-scan at the mid-height level of the beam (a) compared to the amplitude at the same height in the A-scan of the not heat-treated sample's GPR scan (b).

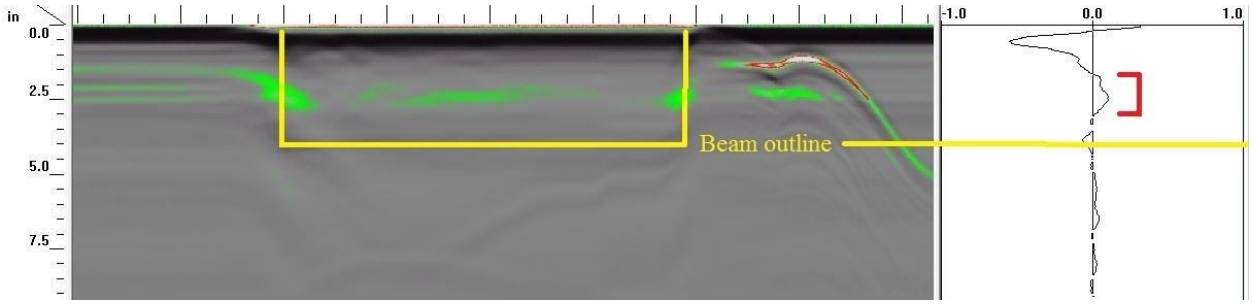

(a) GPR B Scan and A Scan of a not heat-treated sample.

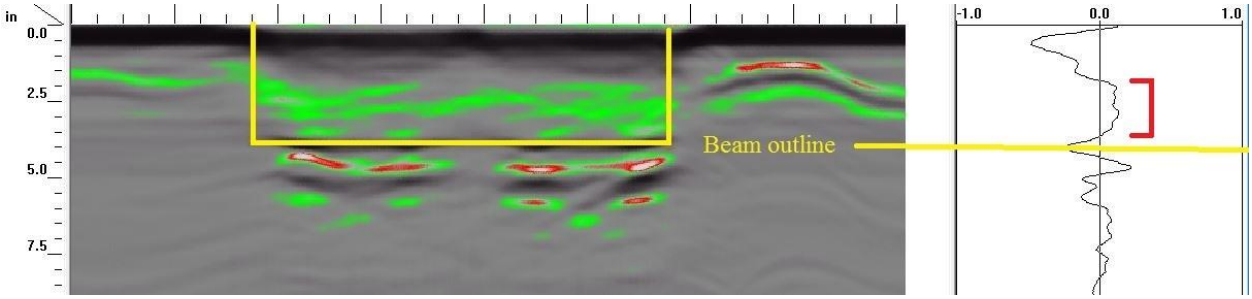

(b) GPR B Scan and A Scan of 1 hour heat-treated normal strength concrete sample.

Figure 4- 36: GPR scans of the preliminary study.

4.5.2. Main Study

The samples were scanned with a GSSI GPR hand scanner using 2.6 GHz antenna. Three scans were done on each beam as shown in Figure 4- 37. Scan 1 and 2 was done having the antenna oriented in the direction

of scanning. Scan 3 was done having the antenna oriented at 90^{o} to the direction of scanning.

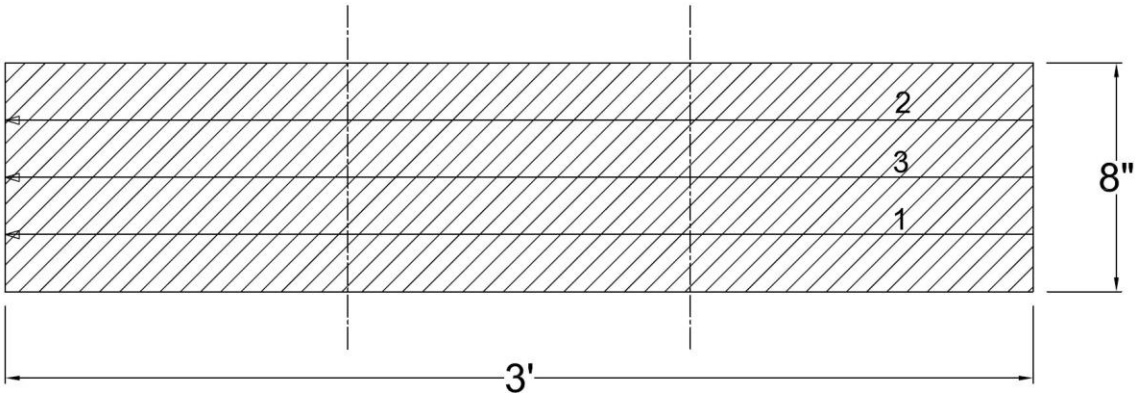

Figure 4- 37: Scan positions and direction for GPR scanning (plan view).

Afterward, some work procedure study was performed on the Direct Coupling Zone in the A scan profile of GPR. The first reflection of the GPR wave is called a direct wave or direct coupling. This direct wave indicates the top surface. Figure 4- 38 shows a GPR reflection signal with direct coupling at the top of it (Riad, 2017). The following statement is mentioned in the GSSI concrete inspection handbook. “The negative peak (a straight horizontal black line in the B-scan display) immediately below the surface is a part of the direct coupling. Some variations may be seen within the negative peak. They usually indicate changes in concrete properties within

the top inch of material, though their accurate interpretation is difficult" [GSSI Concrete Handbook, 2005].

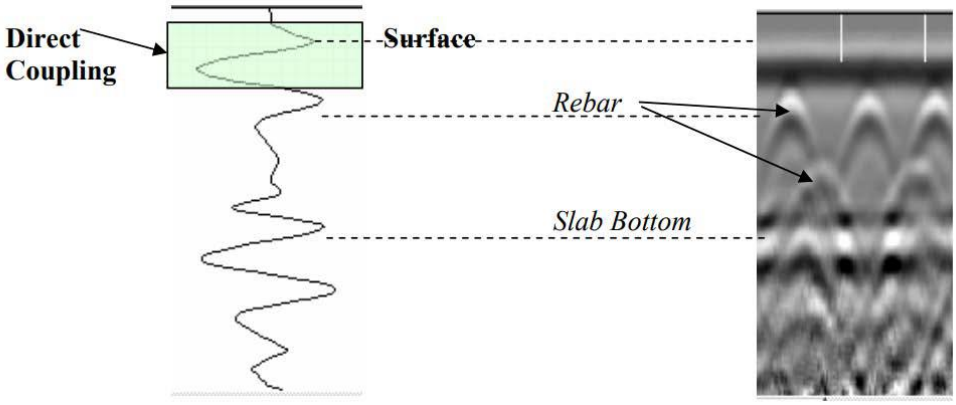

Figure 4- 38: Direct Coupling Zone in a GPR A scan (left) and B scan (right).

The GPR raw data were post-processed and summarized into an R acceptable .CSV format. The Data was processed in such a way that the Direct Coupling Zone peaks were avoided. The amplitude spectrum below the beam depth was discarded as well. As per the qualitative analysis by the infrared camera, the middle portion of the beam samples seemed to be most damaged. For that reason, GPR scan data from the mid-one-third span length was chosen for analysis. The maximum amplitude indicating the maximum possibility of failure in that region for each sample was selected.

Figure 4- 39 shows the Residuals vs fitted values and the Normality Probability Plot (NPP) graph from R. The distribution of the points in the Residuals vs Fitted values graph implies that constant error variance is possible. In addition, the Normality Probability Plot (NPP) shows that the curve is pretty much linear. The Shapiro-Wilk normality test result from R implies with 95% confidence that the distribution of the data passes normality. Therefore, the data distribution did not need any further modification.

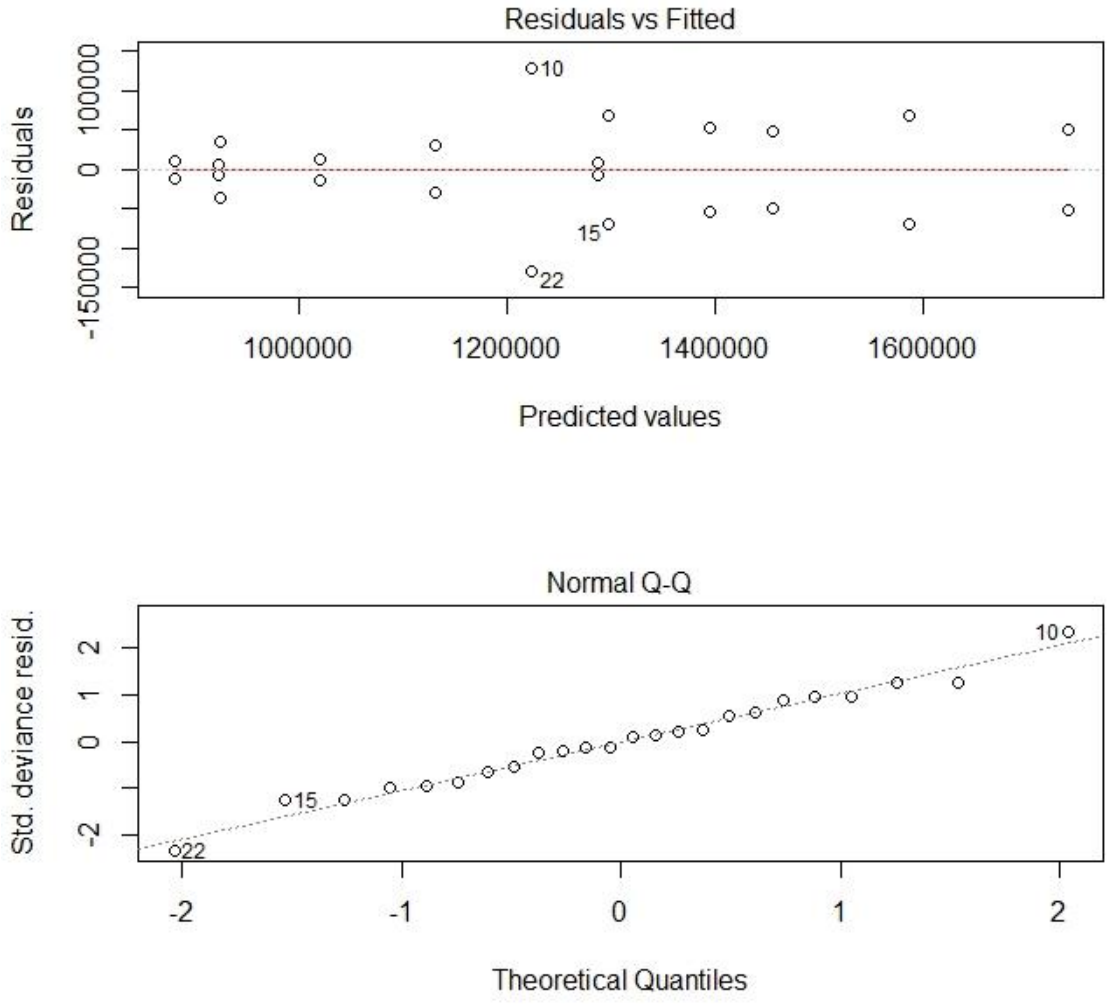

Figure 4- 39: Residuals vs fitted values and Normality Probability Plot for GPR test data.

The Analysis of Variance (ANOVA) codes were applied for the data as well. Table 4- 5 shows the ANOVA output from R. It can be seen that the fireproofing, FRP bar and the temperature of heat treatment have very

significant main effect on the GPR amplitudes. The output also shows the probability of interaction effects of two factors on the GPR amplitude. According to the output, concrete strength and temperature of heat treatment show a very high interaction effect on GPR amplitude. Concrete strength and presence of steel rebar, concrete strength, and presence of FRP rebar, and concrete strength and fireproofing have a significant interaction effect on GPR amplitude.

Table 4- 5: Analysis of Variance (ANOVA) output for the GPR test.

	Df	Sum Sq	Mean Sq	F value	Pr(>F)	
Concrete.Strength	1	4.069e+09	4.069e+09	0.664	0.43099	
Steel.Reinforcement	1	1.054e+10	1.054e+10	1.720	0.21424	
Fire.Proofing	1	5.309e+11	5.309e+11	86.640	7.73e-07	***
FRP.Bar	1	4.122e+11	4.122e+11	67.266	2.91e-06	***
Duration.of.Heat.Treatment	1	2.798e+11	2.798e+11	45.666	2.02e-05	***
Concrete.Strength:Steel.Reinforcement	1	1.003e+11	1.003e+11	16.368	0.00162	**
Concrete.Strength:Fire.Proofing	1	3.632e+10	3.632e+10	5.928	0.03146	*
Concrete.Strength:FRP.Bar	1	8.043e+10	8.043e+10	13.126	0.00350	**
Concrete.Strength:Duration.of.Heat.Treatment	1	2.043e+11	2.043e+11	33.338	8.83e-05	***
Steel.Reinforcement:Fire.Proofing	1	1.026e+10	1.026e+10	1.675	0.22000	
Steel.Reinforcement:Duration.of.Heat.Treatment	1	7.579e+09	7.579e+09	1.237	0.28786	
Residuals	12	7.353e+10	6.127e+09			

Signif. codes: 0 '***' 0.001 '**' 0.01 '*' 0.05 '.' 0.1 ' ' 1

The box and whisker plots of Figure 4- 40 prepared by R represents the interquartile range, possible outliers, and means of the GPR data concerning each parameter. The two lines outside the boxes, also known as whiskers, extend to the highest and lowest values of observations. The horizontal lines inside the boxes represent the medians.

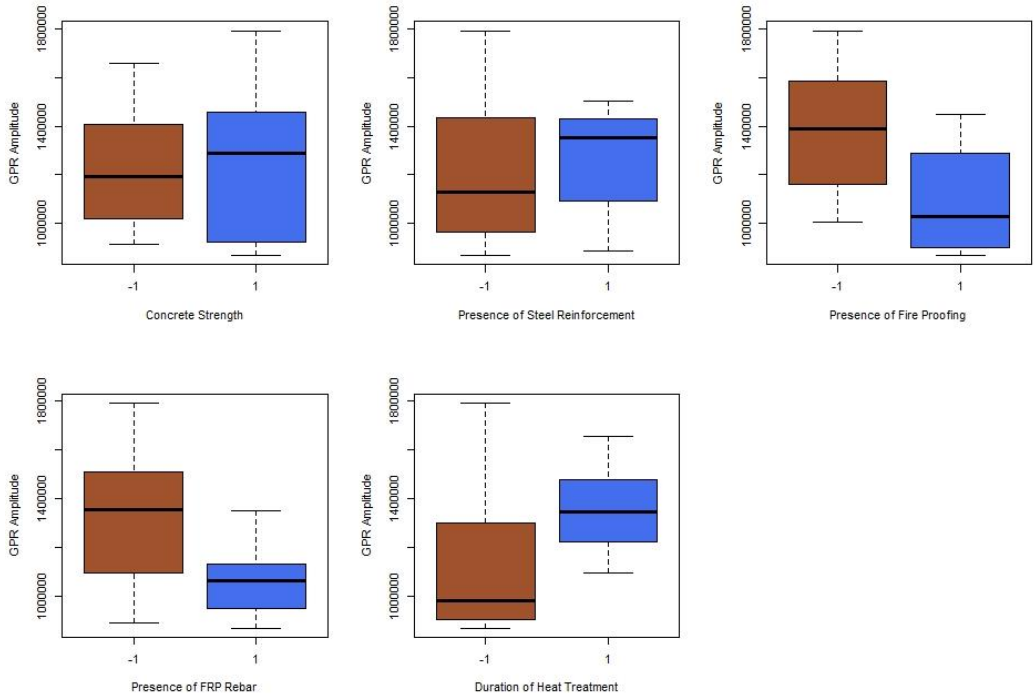

Figure 4- 40: Whisker Box plots for GPR test data.

Figure 4- 41 shows the main effect plots of the parameters. From the increasing or decreasing slopes of the plots of steel rebar, fireproofing, FRP rebar and presence of heat treatment it is evident that these factors have a significant main effect on the GPR amplitude.

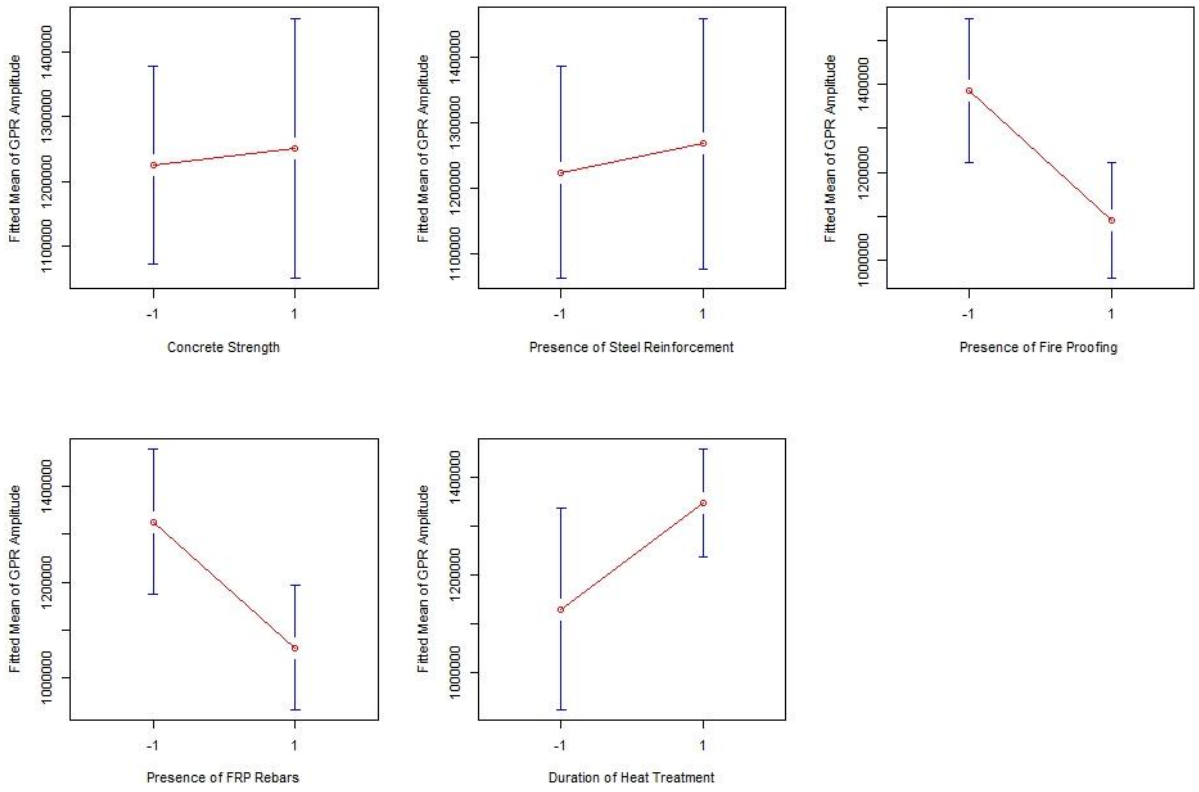

Figure 4- 41: Main effect plots for GPR test data.

Figure 4- 42 shows the interaction plots of the parameters from R based on the GPR test. According to the graph, the interaction effect of the concrete strength and the presence of steel rebar on the GPR amplitude is high. In addition to that, there seems to be a slight interaction effect of fireproofing and FRP bar and fireproofing and temperature of heat treatment on the GPR amplitude.

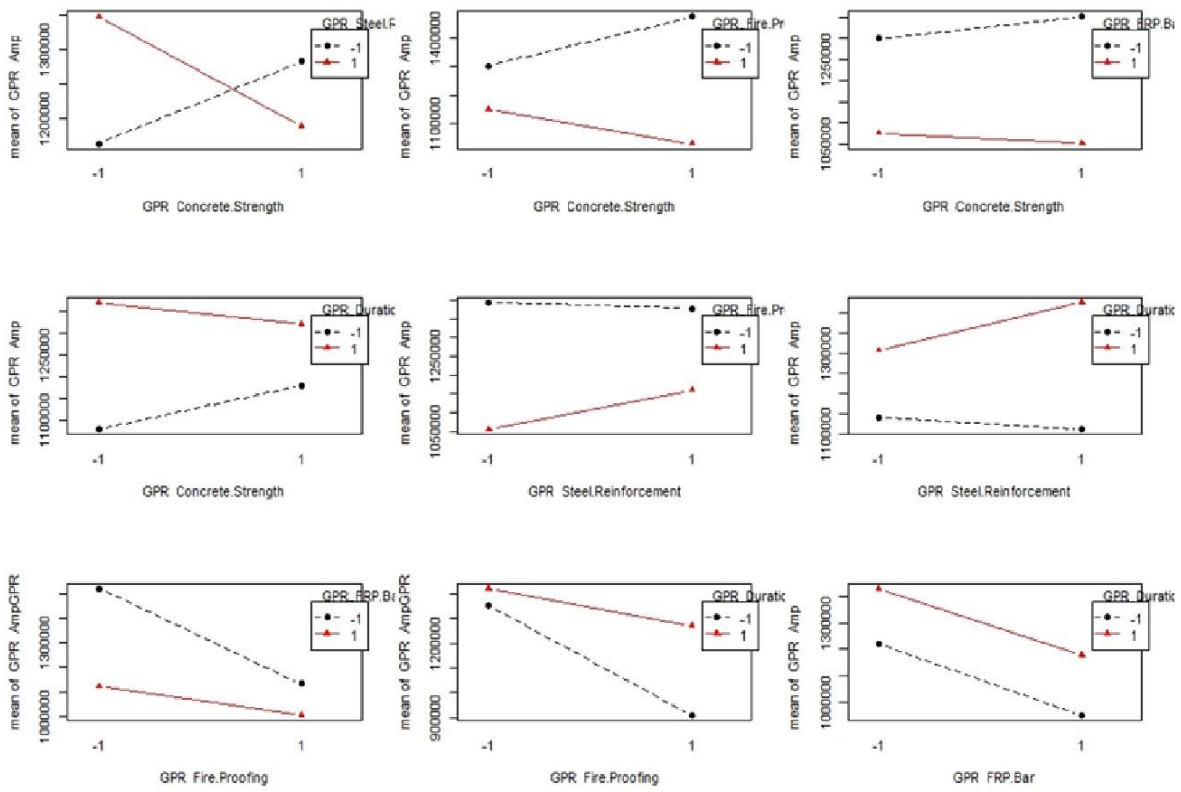

Figure 4- 42: Interaction plots for GPR test data.

The following simplified equation no [4- 4] was achieved through the regression analysis by the software R:

$$Y = 1165636 - 45284\,X_1 - 58024\,X_2 - 194008\,X_3 - 160500\,X_4 + 105104\,X_5 - 104016\,X_1X_2 - 30380\,X_1X_3 - 70900\,X_1X_4 - 110516\,X_1X_5$$

------ [4- 4]

Here,

Y= Maximum Amplitude from GPR

X_1= Concrete Strength

X_2= Steel Rebar

X_3= Fireproofing

X_4= FRP Rebar

X_5= Duration of heat exposure

Where, all the factors (X_1 through X_5) values can be either +1 or -1 indicating their highest range or lowest range respectively. For concrete strength, +1 and -1 represents 6000 psi and 3500 psi respectively. For the duration of heat exposure, +1 and -1 represents 1 hour (up to 927 degrees of Celsius) and ½ hour (up to 843 degrees of Celsius) respectively. For the rebar and fireproofing, they represent their presence or absence respectively. For steel rebar, the presence can be quantified by the reinforcement ratio (ρ) value of 0.00625. For the absence of steel rebar, the reinforcement ratio is zero. Similarly, for the presence of FRP rebar, the reinforcement ratio is 0.00344, whereas the absence gives the value as zero. For any intermediate values of the factors representing numerical values at their two

levels, the respective intermediate value between -1 and +1 can be used in this equation from interpolation.

The coefficient of determination, R^2 for this equation is found as 0.948 from the software R. This means that around 94.8% of the observed variation can be explained by the model's inputs.

Chapter 5

DESTRUCTIVE TEST

The four point bending destructive test was performed to evaluate the effect of concrete strength, presence of steel rebar, presence of fireproofing, presence of FRP rebar and temperature of heat treatment on the bending capacity of the beam samples. In this chapter, the procedure and result analysis of the four point bending test will be discussed.

5.1. Test Setup

ASTM C78/C78M−18 code was followed for the four point bending test. Figure 5- 1 shows the guideline for setup illustrated in the code. The reason it is called four point bending test is that loads and reactions or boundary conditions are applied in total four points of the beam. The load is applied at an equal distribution on one third and two third point of the span. That is another reason that this test is also known as third point loading.

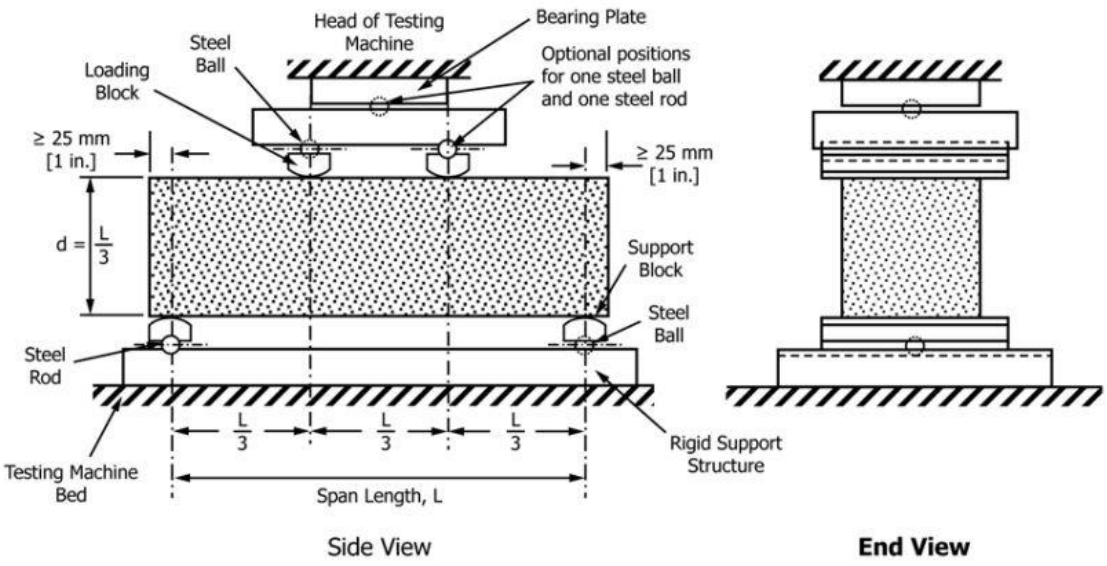

Figure 5- 1: Four point bending guideline (ASTM C78/C78M, 2018).

Test setup for the control and heat-exposed beams was done as shown in Figure 5- 2. Two strain gauges were installed on each beam before testing as shown in the figure. One strain gauge was installed in the middle by the side of the beam just an inch below from the top surface to monitor the compressive strain, and the other strain gauge was installed in the bottom mid location where the tension is highest to monitor the tensile strain. The linear variable displacement transducer (LVDT) was set at the middle bottom point of the beam to monitor displacement during load application. For the test, equally divided increasing load was applied in the one-third points of the beams until failure.

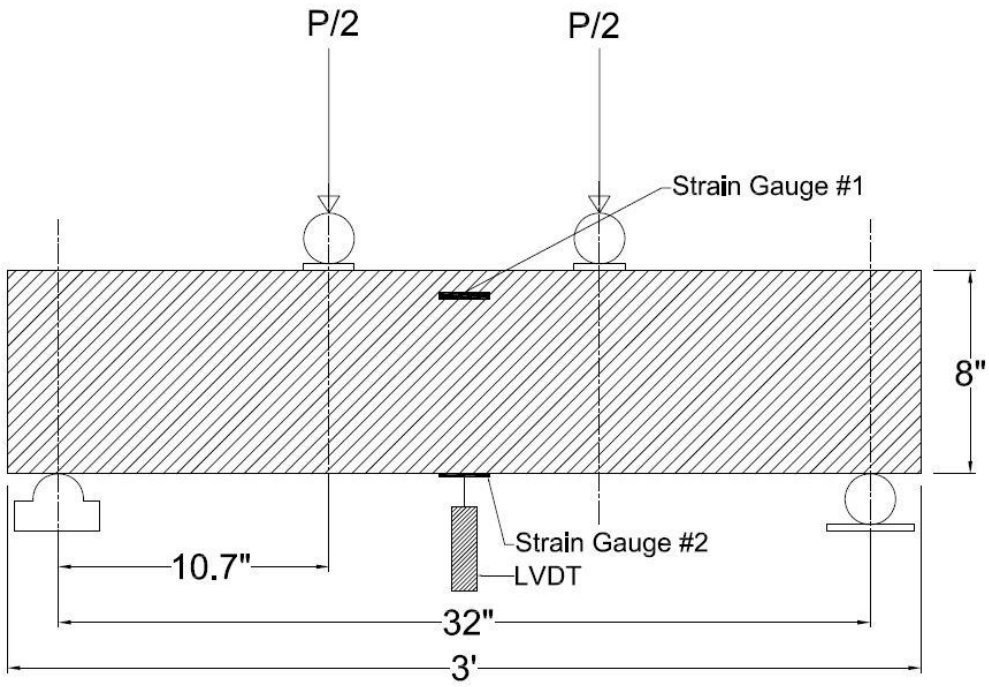

Figure 5- 2: Test setup details for four point bending.

400 kip universal testing machine was used for the four point bending in the laboratory (Figure 5- 3). One hinged and another roller support was used for the setup as per the ASTM code.

Figure 5- 3: Four point bending in laboratory.

From the test, it was observed that the control beams showed flexure failure patterns, whereas the heat-treated beams showed mostly flexure and shear combined failure modes. The probable reason for that was because the heat-treated beams' concrete lost a significant amount of strength after the heat exposure resulting in increasing probability of shear failure than control specimens.

5.2. Result Analysis of Four Point Bending Test

Figure 5- 4 represents a comparison of the bending capacities between the control, heat-treated and fireproofed beams. It can be seen that the fireproofing significantly improves the bending capacity of the beams compared to the non-fireproofed specimens. The effect of the duration of heat exposure and the type of reinforcement can also be observed. It is evident that the steel rebar specimens showed higher bending capacity than the specimens containing FRP reinforcements. In addition, it can be said that the duration of heat has a negative effect on the bending capacity unless it is fireproofed. However, the fireproofed beams could not prove to be immune against the heat exposure rather showed some amount of decrement in the bending capacity. Nevertheless, even with the reduction, the bending capacity of the fireproofed beams is higher than the usual non-fireproofed beams.

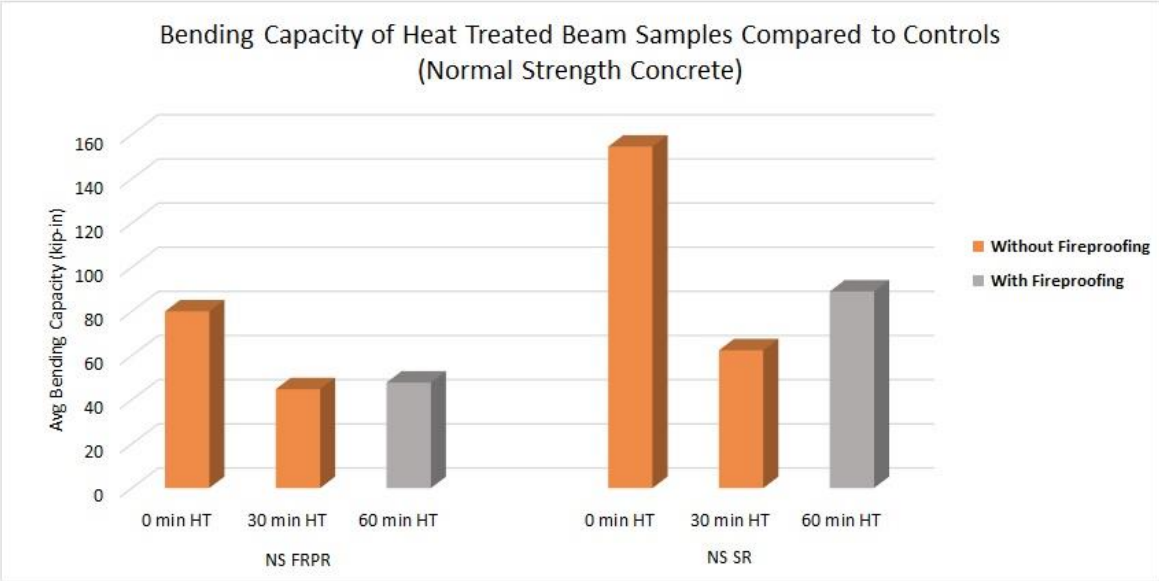

(a) Normal strength concrete samples.

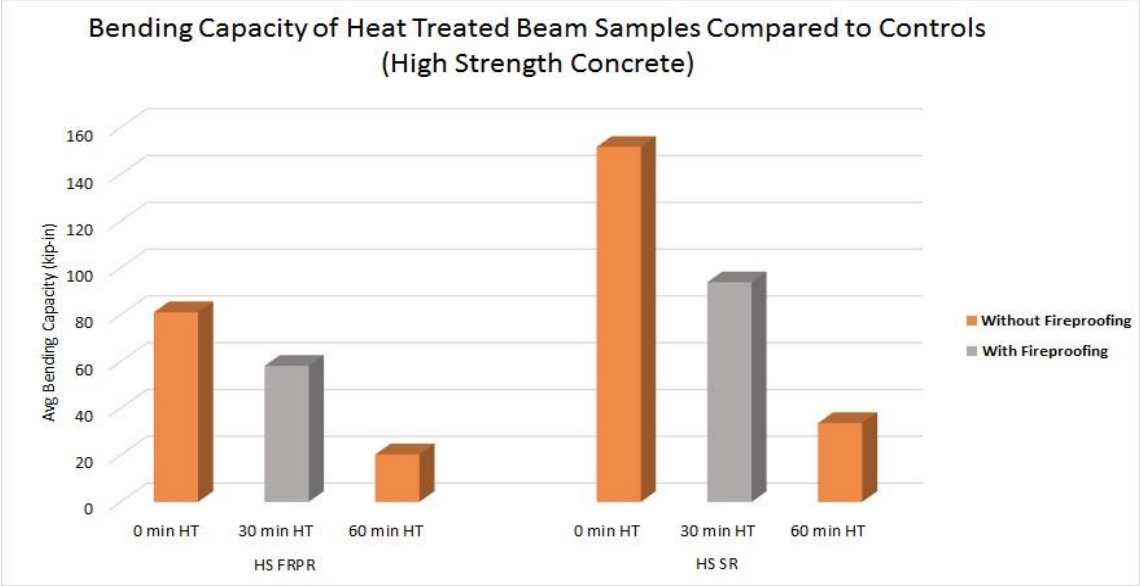

(b) High strength concrete samples.

Figure 5- 4: Comparison of the bending capacities.

The four point bending raw data were post processed and summarized. The ultimate bending capacity in kip-inch was considered for analysis. The software R was used to perform statistical analysis on the post processed data.

Figure 5- 5 shows the Residuals vs fitted values and the Normality Probability Plot (NPP) graphs from R. The distribution of the points in the Residuals vs fitted values graph implies that constant error variance is possible. In addition, the Normality Probability Plot (NPP) shows that the curve tends to follow the linear pattern. The Shapiro-Wilk normality test result from R implies with 95% confidence that the distribution of the data passes normality. Therefore, the data distribution did not need any further

modification.

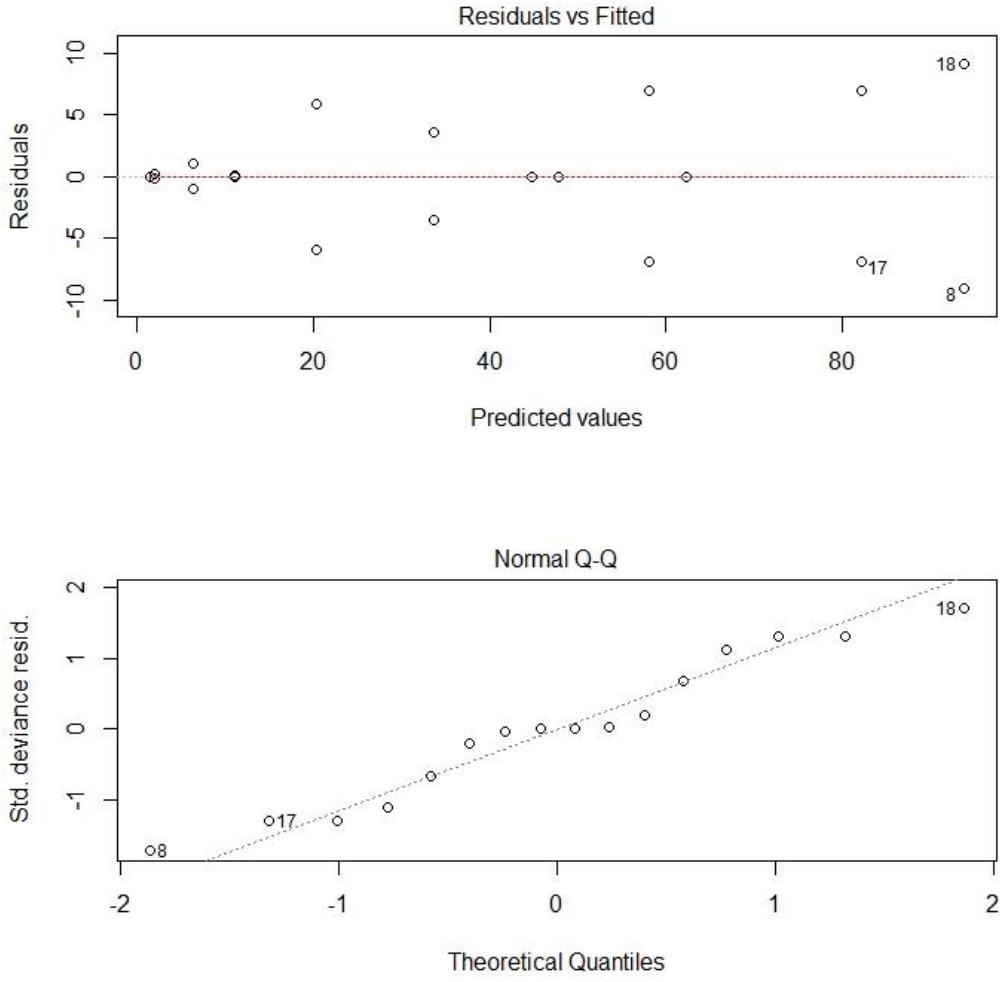

Figure 5- 5: Residual vs Fitted Values and Normality Probability Plot for four point bending.

The R output for Analysis of Variance (ANOVA) is presented in Table 5- 1. It can be concluded from the ANOVA table that the Steel rebar, CFRP

rebar, and Temperature of Heat Treatment have almost 100% significant effect on the ultimate bending capacity. Besides, fireproofing has a possible effect on bending capacity as well. Also according to the ANOVA table, on the bending capacity, the temperature of heat treatment has a significant combined effect with steel reinforcement and fireproofing and highly possible combined effect with concrete strength.

Table 5- 1: R output for ANOVA of Bending test data.

	Df	Sum Sq	Mean Sq	F value	Pr(>F)	
Concrete.Strength	1	128	128	2.262	0.171032	
Steel.Reinforcement	1	9767	9767	172.529	1.07e-06	***
Fire.Proofing	1	2027	2027	35.816	0.000329	***
FRP.Bar	1	4538	4538	80.168	1.92e-05	***
Duration.of.Heat.Treatment	1	1346	1346	23.772	0.001231	**
Concrete.Strength:Steel.Reinforcement	1	176	176	3.116	0.115542	
Concrete.Strength:Fire.Proofing	1	132	132	2.337	0.164848	
Concrete.Strength:FRP.Bar	1	144	144	2.537	0.149902	
Concrete.Strength:Duration.of.Heat.Treatment	1	1128	1128	19.923	0.002101	**
Steel.Reinforcement:Fire.Proofing	1	324	324	5.716	0.043801	*
Steel.Reinforcement:Duration.of.Heat.Treatment	1	6	6	0.100	0.760194	
Residuals	8	453	57			

Signif. codes: 0 ‘***’ 0.001 ‘**’ 0.01 ‘*’ 0.05 ‘.’ 0.1 ‘ ’ 1

The box and whisker plots of Figure 5- 6 prepared by R shows the interquartile range, possible outliers, and means of the bending test data concerning each parameter. The two lines outside the boxes, also known as whiskers, extend to the highest and lowest values of observations. The horizontal lines inside the boxes represent the medians.

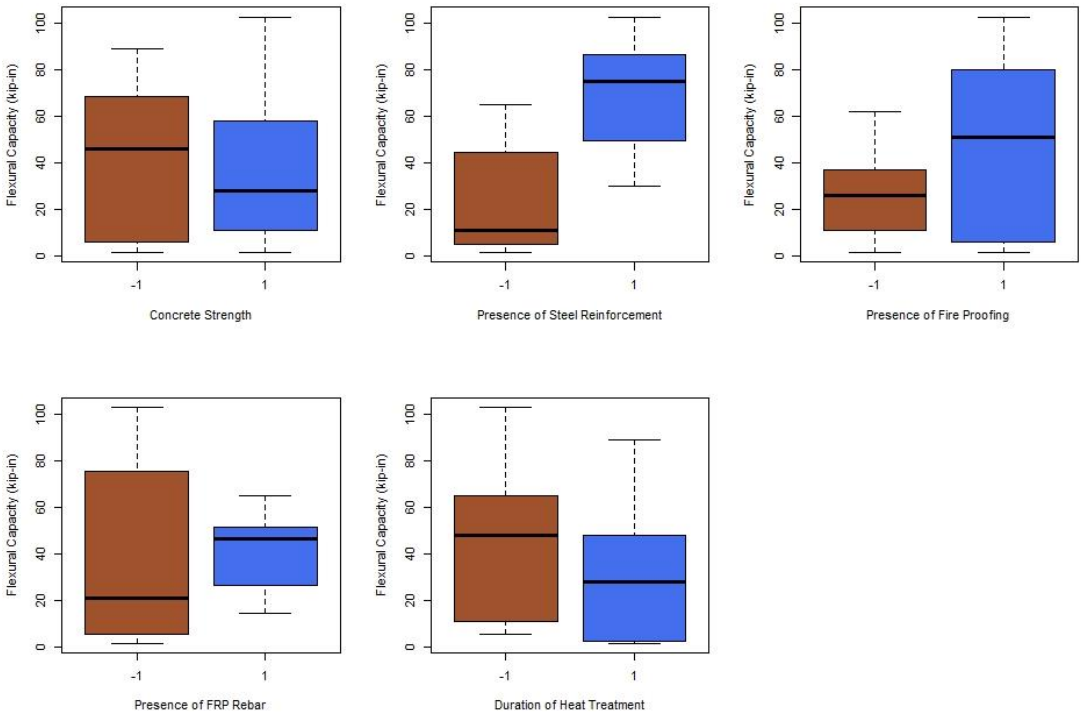

Figure 5- 6: Whisker Box plots for four point bending data.

Figure 5- 7 shows the main effects of the parameters on the bending capacity of the beams. From the main effect plots, it is evident that the steel reinforcement, fireproofing and temperature of heat treatment have a significant main effect on the bending capacity of the beam specimens.

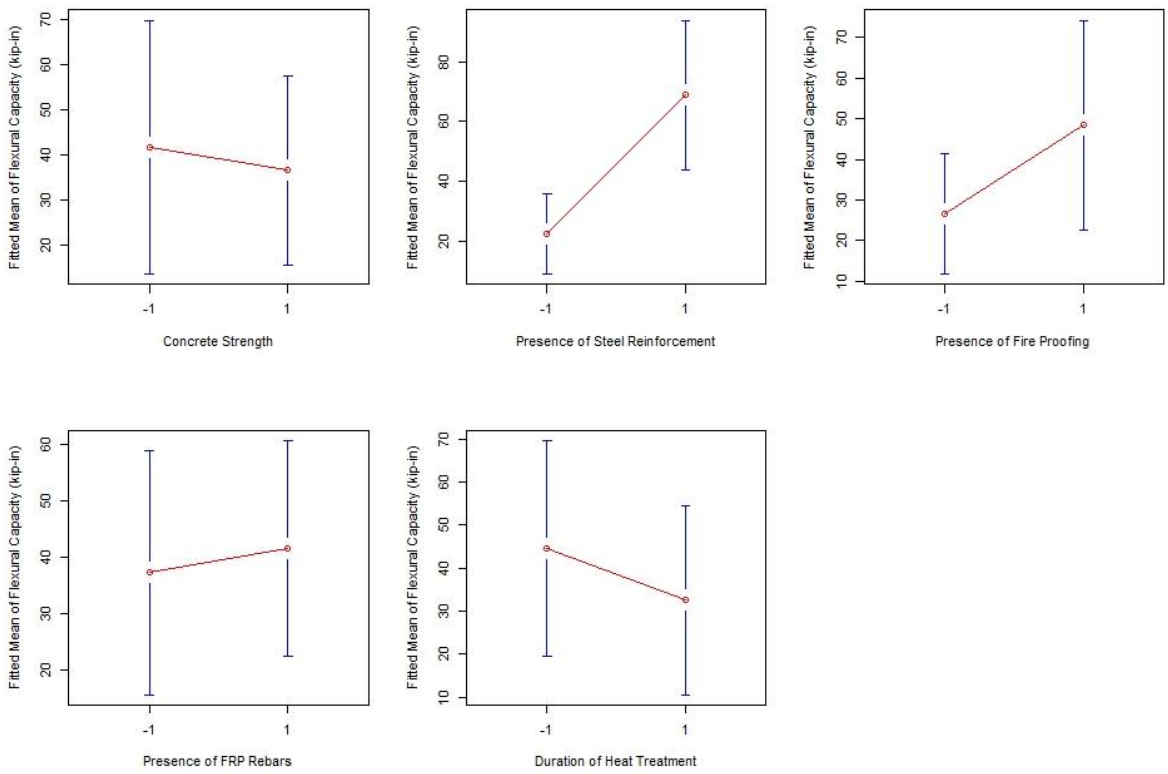

Figure 5- 7: Main effect plots for bending test data.

Figure 5- 8 shows the interaction plots for the four point bending test. The interaction plot clearly shows that there is significant interaction effect of concrete strength and temperature of heat treatment on the bending capacity. The plot shows possibility of interaction effect on bending capacity by concrete strength and fireproofing, steel reinforcement and fireproofing, lastly FRP rebar and temperature of heat treatment.

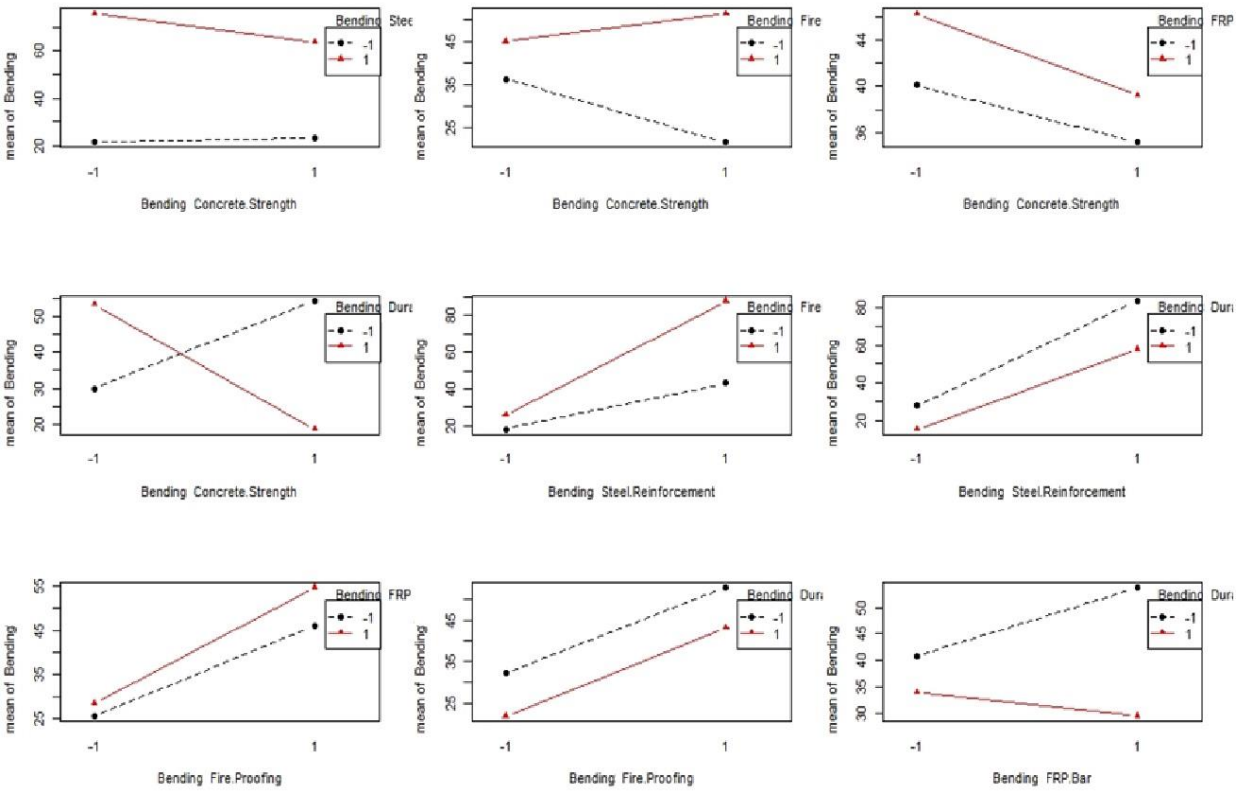

Figure 5- 8: Interaction effect plots for bending test data.

The following simplified equation no [5- 1] was achieved through the regression analysis by the software R:

$$Y = 55.39 - 3.89\,X_1 + 31.383\,X_2 + 9.443\,X_3 + 18.753\,X_4 - 6.813\,X_5$$
$$- 2.78\,X_1X_2 + 2.603\,X_1X_3 - 2.423\,X_1X_4 - 5.653\,X_1X_5 + 4.883\,X_2X_3$$

--------- [5- 1]

Here,

Y= Ultimate Bending Capacity (kip-in)

X_1= Concrete Strength

X_2= Steel Rebar

X_3= Fireproofing

X_4= FRP Rebar

X_5= Duration of heat exposure

Where, all the factors (X_1 through X_5) values can be either +1 or -1 indicating their highest range or lowest range respectively. For concrete strength, +1 and -1 represents 6000 psi and 3500 psi respectively. For the duration of heat exposure, +1 and -1 represents 1 hour (up to 927 degrees of Celsius) and ½ hour (up to 843 degrees of Celsius) respectively. For the rebar and fireproofing, they represent their presence or absence respectively. For steel rebar, the presence can be quantified by the reinforcement ratio (ρ) value of 0.00625. For the absence of steel rebar, the reinforcement ratio is zero. Similarly, for the presence of FRP rebar, the reinforcement ratio is 0.00344, whereas the absence gives the value as zero. For any intermediate values of the factors representing numerical

values at their two levels, the respective intermediate value between -1 and +1 can be used in this equation from interpolation.

The coefficient of determination, R^2 for this equation is found as 0.977 from the software R. This means that around 97.7% of the observed variation can be explained by the model's inputs.

The outcomes of the bending test discussed in this chapter were used for the Finite Element Modeling (FEM) residual strength model's calibration. The FEM or numerical model presented in the next chapter utilizes the results of the bending test to calibrate its concrete damage plasticity properties.

Chapter 6

NUMERICAL MODELING

Finite Element Model (FEM) for the main study beam sample was created using ABAQUS, a non-linear finite element software. A numerical heat transfer model was developed and calibrated for the beam samples. Afterward, a residual bending capacity model was developed and calibrated. This chapter discusses the procedure, result analysis and applicability of the developed numerical models.

6.1. Heat Transfer Model

Heat transfer is a theory, which explains the flow of thermal energy or heat, occurring due to the difference in temperature. It also describes the subsequent temperature distribution and changes. The study of heat transfer concerns the exchange of energy, mass, and momentum in the form of conduction, convection and radiation. These processes can be explained by the mathematical formulas, which can be taken care of by ABAQUS software.

For the heat transfer FEM model, multiple attempts were made to calibrate the model with the data achieved through thermocouples during

the experiments. The heat application was considered through two sets of surfaces; three surfaces directly exposed to heat through heating coil panels and the other three surfaces indirectly exposed. Two temperature profiles for these two sets of surfaces were achieved through the thermocouples data from the experiments. Figure 6- 1 shows the applied temperature profiles.

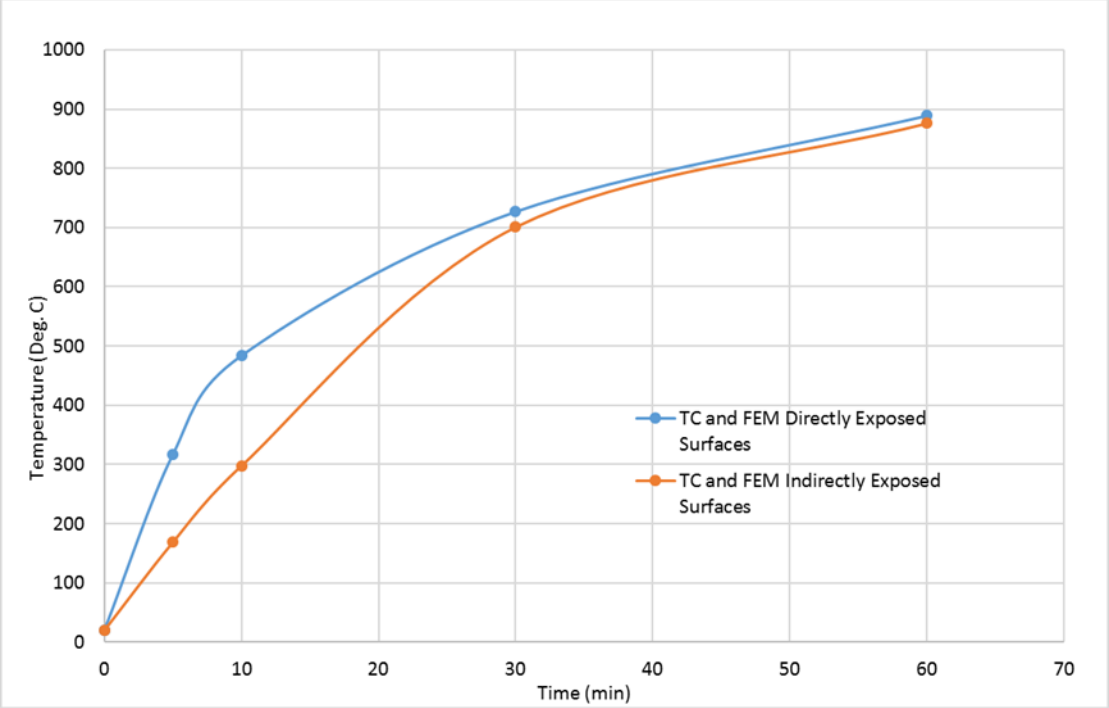

Figure 6- 1: Applied temperature profiles.

Figure 6- 2 represents the nodal temperature distribution of a steel reinforced normal strength concrete beam after one hour (up to 943^{o}C) heat

exposure. Node to node tie constraint was used to get the temperature profile of the rebar.

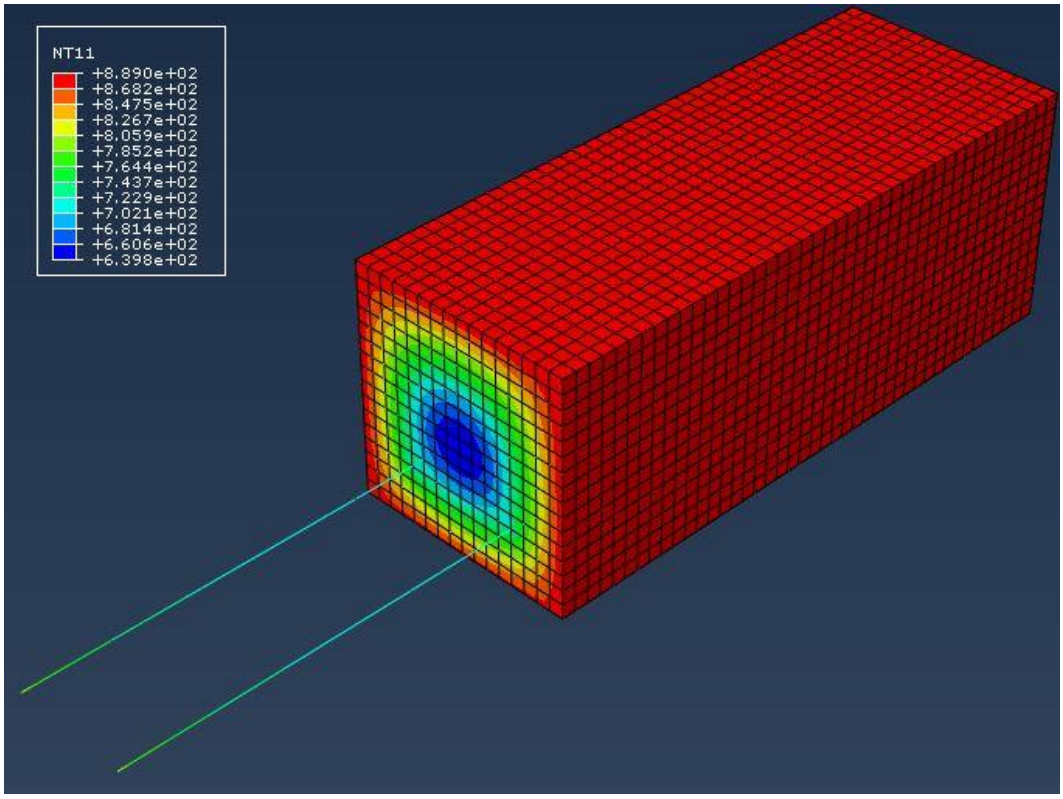

(a) Sectional view normal to Z-axis.

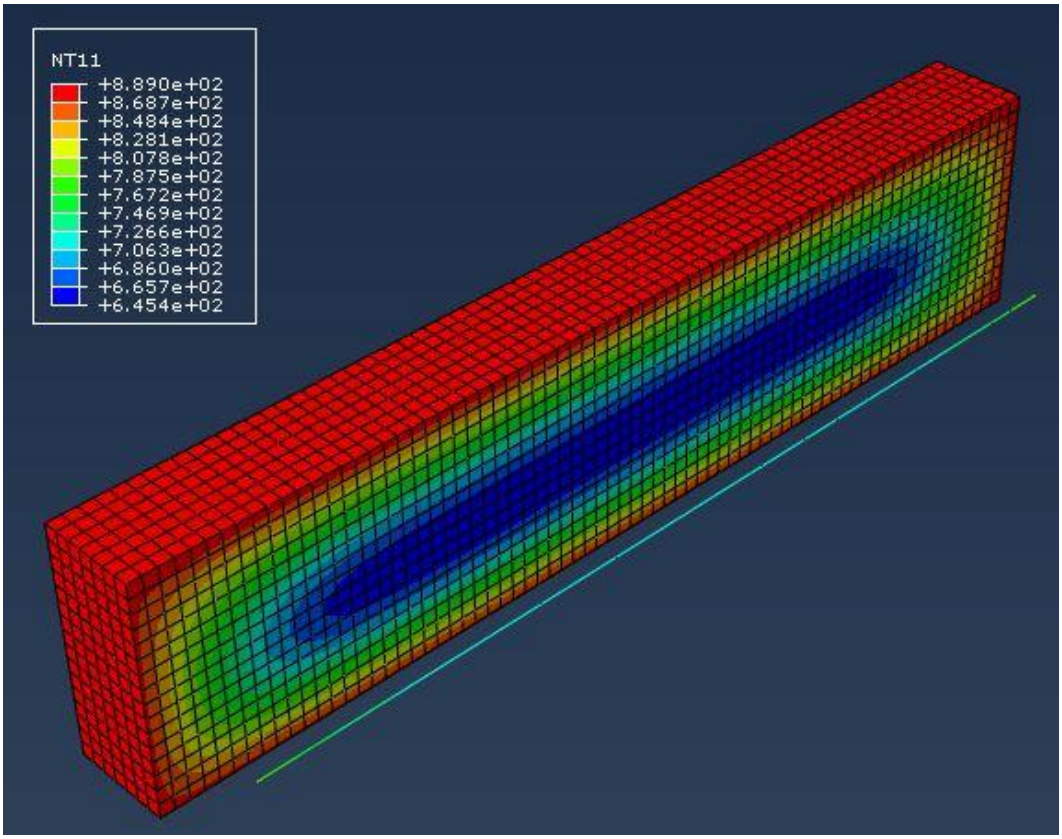

(b) Sectional view normal to X-axis.

Figure 6- 2: Nodal temperature output from the heat transfer FEM.

Eurocode 2 (2004) was followed for the high-temperature properties of concrete (Eurocode 2, 2004). The specific heat, density, thermal conductivity, and thermal strain was calculated using the equation in the code (Appendix-A). In addition to conduction, convection and radiation modes of the heat transfer were considered through interactions. The

numerical study on the simplified temperature prediction method for insulated CFRP strengthened RC beams exposed to standard fire by Hao et al. was followed for convection and radiation inputs (Hao et al. 2019). For convection, the type of interaction was considered as surface film condition having a film coefficient of 0.025 mW/(mm^2.^{o}C). The definition of the interaction was chosen as the embedded coefficient. For the radiation mode of heat transfer, the type of interaction considered was surface radiation. An emissivity of 0.8 was considered. The model was calibrated according to the temperature profile data from inside the samples (mid-level and rebar level). Figure 6- 3 shows the temperature profile comparison between FEM and thermocouple temperatures from experimental data, at two different elevations inside the sample. Though the finite element mid-height level (four inches deep from any surface) temperature profile shows a gradual increase pattern but the experimental temperature shows an initial steeper increase and then being constant at around 100^o C. This is because of the moisture trapped inside the concrete. As long as not all the moisture inside the concrete was vaporized, following the law of physics, the temperature remained at around 100^o C. The moisture at rebar level (six inches deep from the top and two inches above the bottom surface) was vaporized due to being nearer to the heat exposed surface. That is why the temperature profile did not show any pattern at mid-height level.

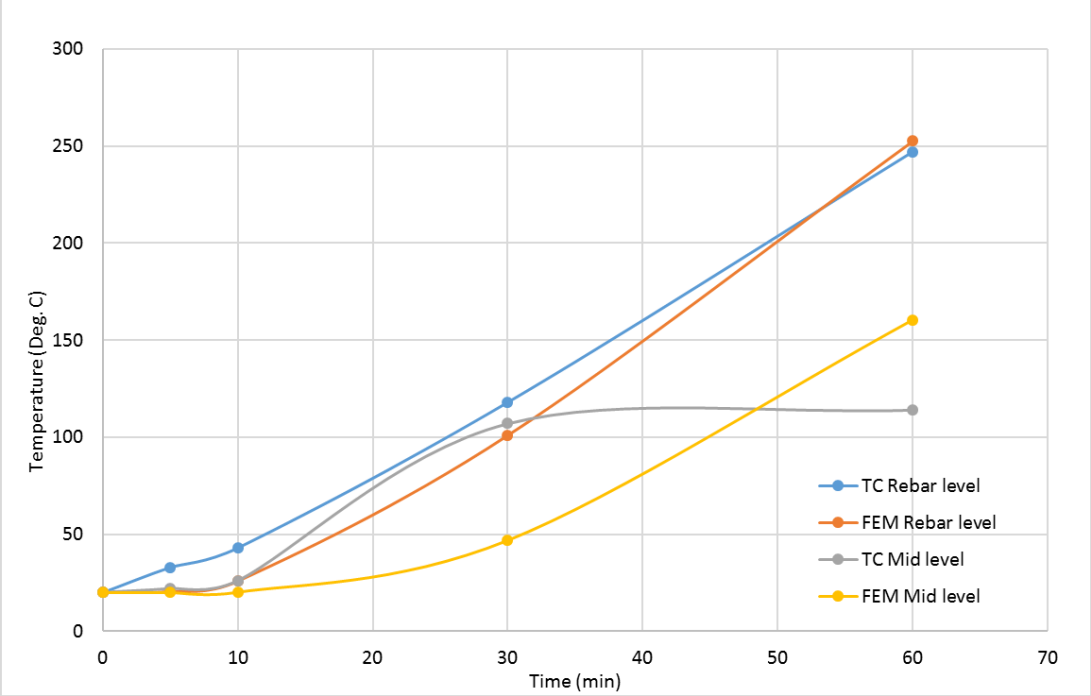

Figure 6- 3: Temperature profile comparison between FEM and experimental data.

6.2. Residual Flexural Capacity Modeling

Initially, to assess the compressive behavior of concrete, 4 inch diameter X 8 inch height (100 mm diameter X 200 mm height) cylinder samples were tested in the laboratory. To assess the behavior at room temperature, six cylinders for each concrete type were tested following the ASTM C39/C39M-18 code (ASTM C39, 2018) after 28 days (Figure 6- 4). The compressive test failure data for these cylinders are presented in Table 6- 1 .

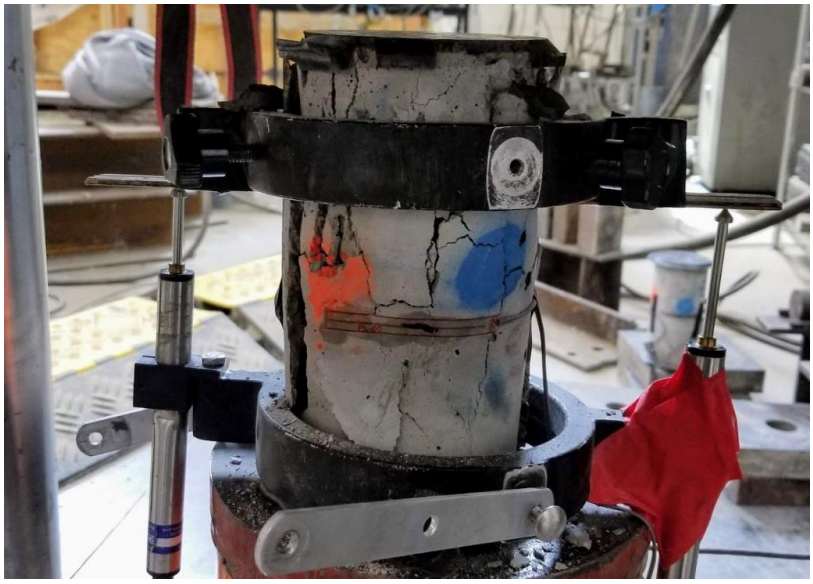

Figure 6- 4: Cylinder test for compressive behavior.

Table 6- 1: Data from the compressive test of cylinders.

Concrete Type	Cylinder No	Failure Load, lbf	Compressive Strength, Psi	Average Compressive Strength, Psi(MPa)
Normal strength	1	43000	3421.83	3376.74 (23.28)
	2	41500	3302.47	
	3	42900	3413.87	
	4	39500	3143.31	
	5	43200	3437.75	

	6	44500	3541.19	
High strength	1	78600	6254.79	6112.88 (42.15)
	2	75600	6016.06	
	3	75800	6031.97	
	4	76900	6119.51	
	5	76300	6071.76	
	6	77700	6183.17	

To figure out the compressive behavior of heat-treated concrete, cylinder samples were heat-treated in the furnace following the same fire curve used earlier for both half an hour and one hour durations. After the heat treatment, it was seen that most of the cylinder samples were damaged due to heat exposure (Figure 6- 5) and the test could not be performed for the heat-treated samples. So, to consider the compressive behavior of heat-treated concrete, a theoretical approach was adopted. It was decided to calibrate the numerical models of the heat-treated beam samples by the load vs deflection data from the bending test experiment.

(a) Placing the cylinders in the furnace for heat treatment.

(b) Heat exposed damaged concrete cylindrical samples.

Figure 6- 5: Heat treatment of concrete cylindrical samples.

Compressive and tensile behavior properties of concrete damage plasticity after heat exposure were considered according to Eurocode 2 (2004) and the study performed by Kodur et al. in 2016 (Kodur et al., 2016). The temperature at the mid-point above the neutral axis, which is around half an inch, was considered for the residual capacity analysis. This consideration was made because it seemed logical to consider the temperature at the compression zone to derive the most accurate concrete damage plasticity properties. According to the conservative research approach, the tensile behavior of concrete below the neutral axis can be ignored. In addition to that, according to Eurocode 2 (2004), the tensile property reduction factor for a temperature above 600^{o} C should be considered zero (Appendix A). According to the study by Kodur et al., the compressive strength of concrete after cooling down to room temperature can be considered ten percent less than the concrete strength at elevated temperature. Eurocode 2 provides the guideline for the compressive strength and strain at elevated temperatures (Appendix A). The total compressive strain was achieved following the stress-strain relationship provided in Eurocode 2 (Appendix A). The inelastic strain and damage parameters for the compressive behavior of concrete damaged plasticity (CDP) property input of ABAQUS was calculated following the ABAQUS CDP guideline, provided in the ABAQUS manual (ABAQUS analysis user's

manual, 2008). Figure 6- 6 shows a schematic presentation of stress vs strain behavior of concrete from the mentioned website for compressive and tensile behaviors for CDP.

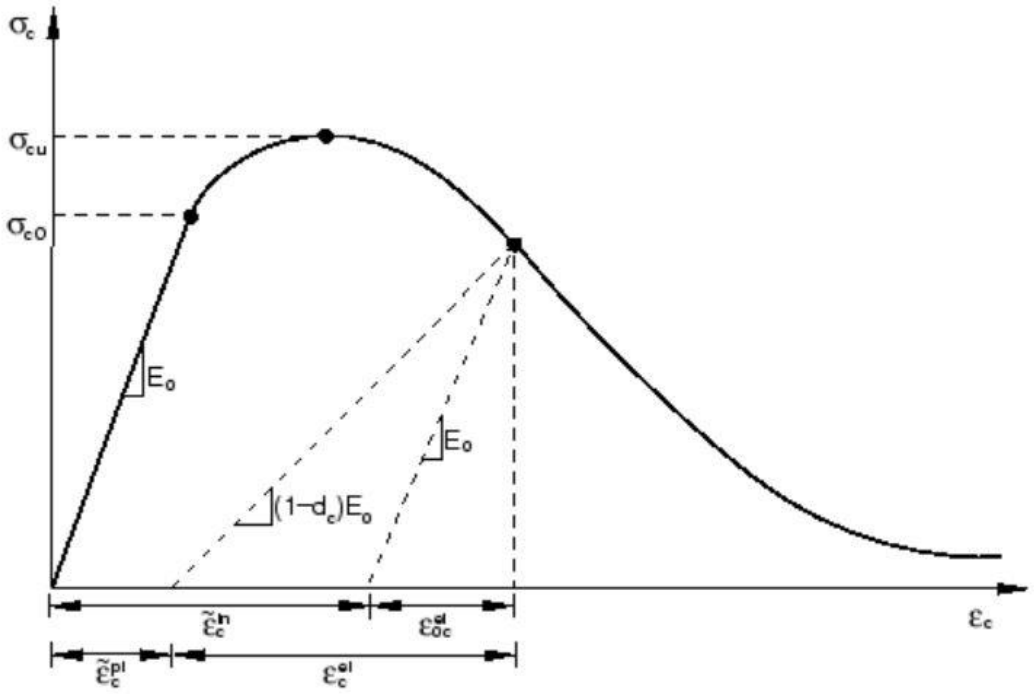

(a) Compressive behavior

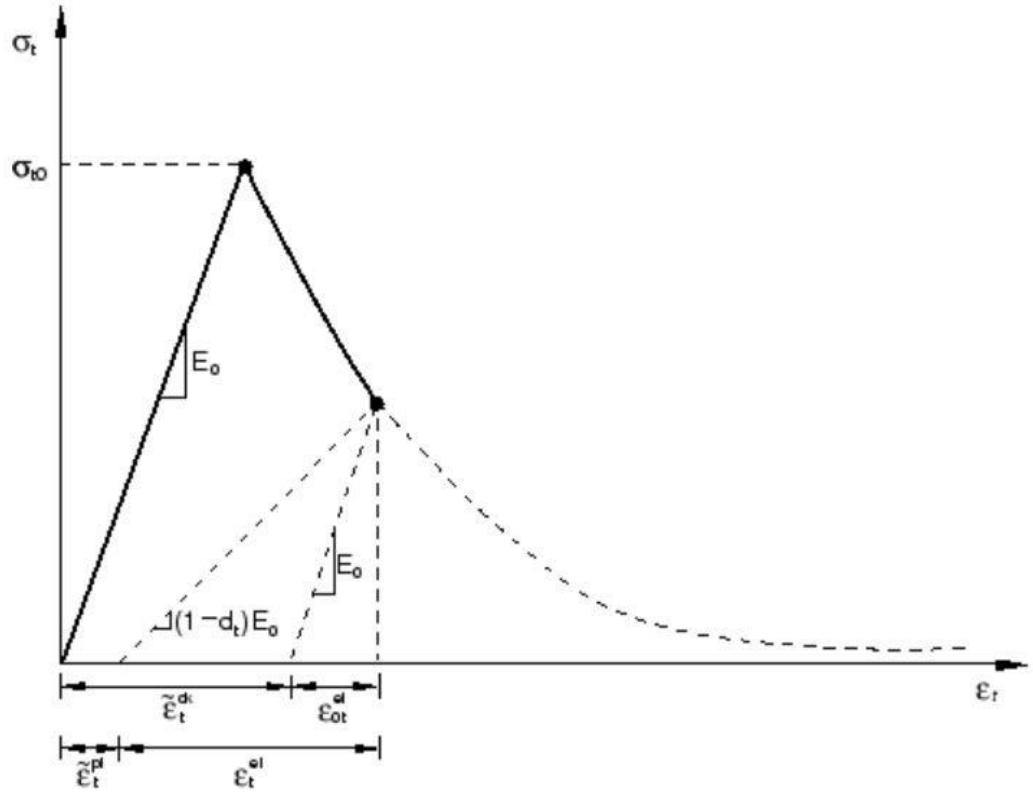

(b) Tensile behavior

Figure 6- 6: Concrete Damage Plasticity (CDP) behaviors.

As the peak temperature of the considered point at mid-level above the neutral axis (around half an inches from top surface) for all the heat exposures from the experiments (both half hour up to 843^{o} C and one hour up to 927^{o} C) is above 600^{o} C, so as per Eurocode the tension property of the concrete can be ignored. That is why the tensile plastic property of the heat-treated concrete was ignored in the model.

Afterward, the boundary condition and load were applied as per the four-point bending and the model was calibrated for the residual bending capacity. Figure 6- 7 shows the S33 stress output for a one hour heat-treated normal strength steel reinforced concrete specimen after analyzing from ABAQUS.

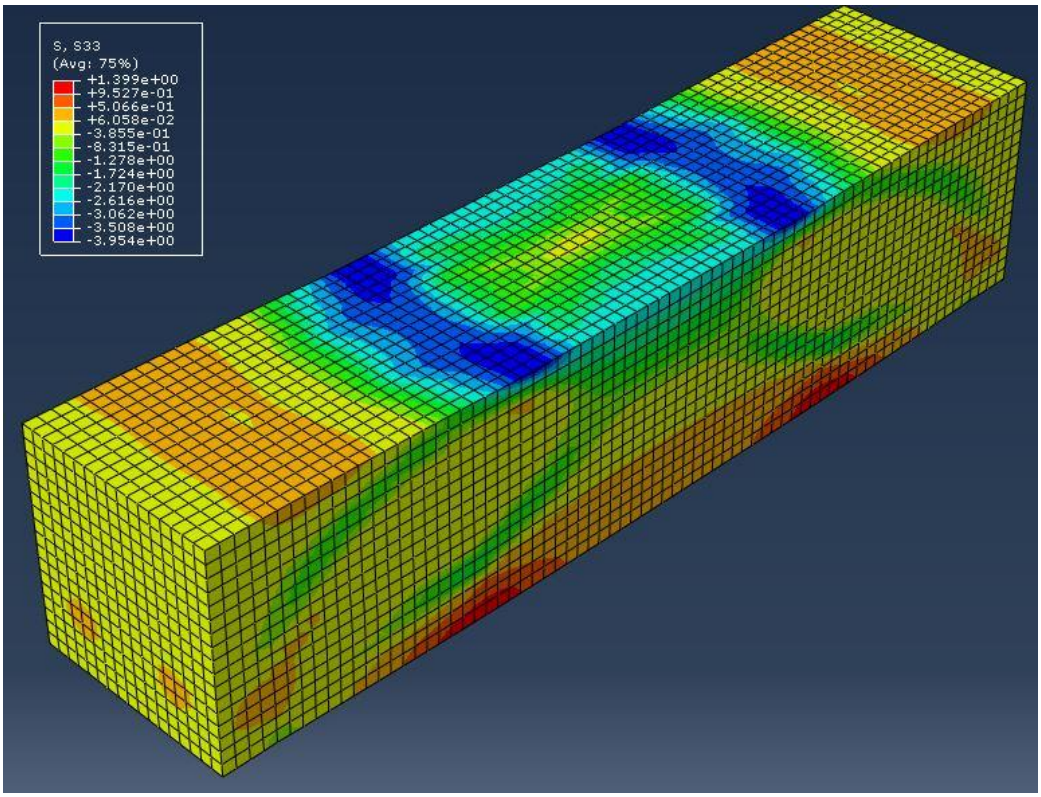

Figure 6- 7: ABAQUS S33 stress output for a one hour heat-treated normal strength steel reinforced concrete specimen.

Load vs deflection data was calculated from the experiments through the load cell and LVDT outputs. On the other hand, load vs deflection data was extracted from the ABAQUS model as well for comparison. A few load vs deflection graphs comparing the experimental and the numerical model output are shown in Figure 6- 8. It can be said that the load vs deflection relationship of the FEM is satisfactory in comparison with the experimental data.

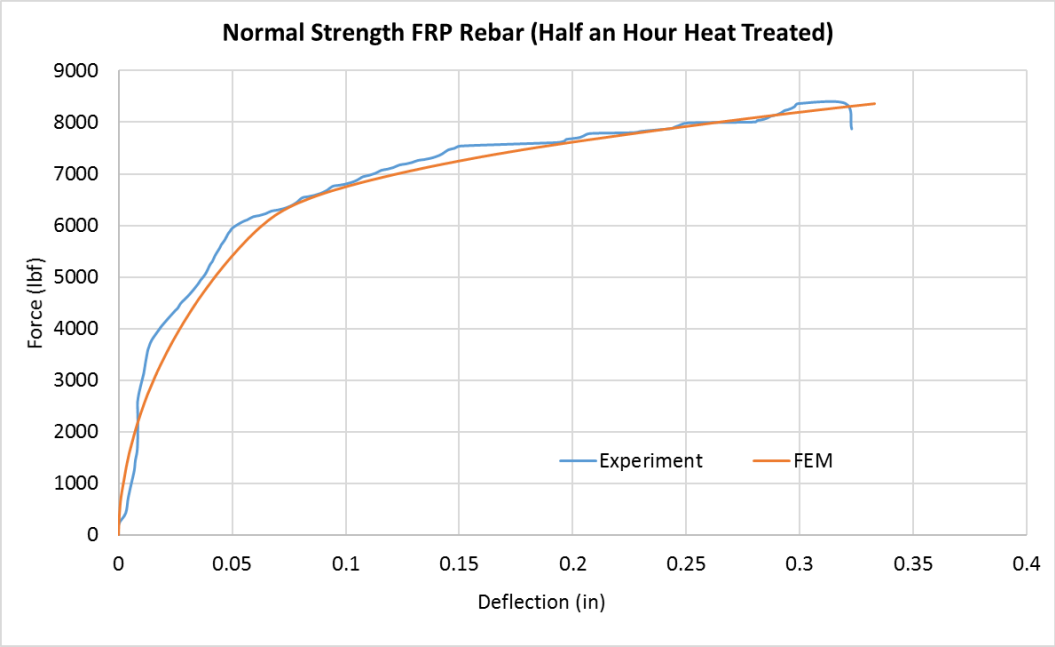

(a) Load vs Deflection curves for normal strength concrete sample with FRP rebar heat-treated for half an hour.

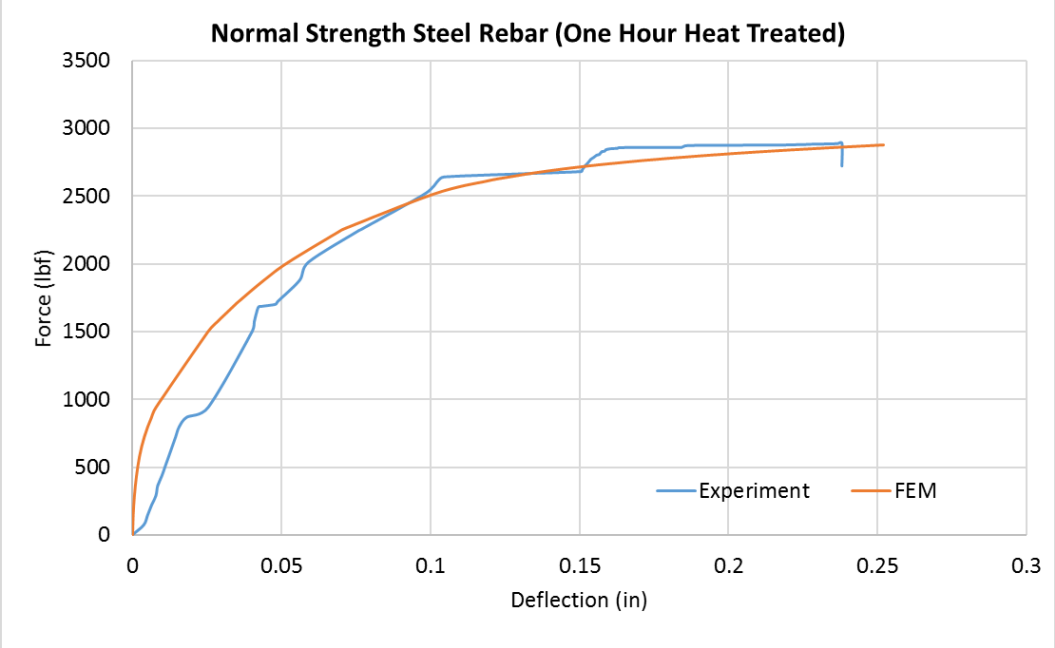

(b) Load vs Deflection curves for normal strength concrete sample with steel rebar heat-treated for one hour.

Figure 6- 8: Load vs Deflection comparison.

The developed numerical models can be used for any further parametric analysis, which was not considered in the experiment.

Chapter 7

DISCUSSION AND CONCLUSION

This chapter includes a summary of the findings of the performed NDT, bending test, and numerical modeling, which were discussed until now. This chapter also presents a proposed procedure for combined qualitative and quantitative evaluation of the bending capacity of a fire-affected concrete structure. The concluding theory of this chapter can be applied as a tool to evaluate the condition of a fire-affected concrete structure.

7.1. Summary of findings and deduction

The findings and conclusion can be summarized in the following statements:

- The study explored the ability of NDT methods like Schmidt hammer, infrared camera, ultrasound pulse, impact echo, and GPR to evaluate fire-affected concrete beams having different parameters e.g. concrete strength, presence of steel rebar, presence of FRP rebar, presence of fireproofing, and duration/temperature of heat exposure.

- All the NDT methods used in this study proved to be capable of identifying all or a partial number of considered parameters. A quantifiable method or equation was established for each of the NDT methods, which can be used to identify the parameters.
- The developed equations for the NDT methods can be used to find out the relationship between the NDT readings and the Bending capacity of the concrete structural member.
- For Schmidt hammer or rebound hammer test data of Q value, the presence or absence of reinforcement bars (steel or FRP) did not make much difference in the scanned data. It is because the Schmidt hammer test concentrates mainly on the surface hardness.
- The presence or absence of steel or FRP bars also made significantly less effect on the impact echo test frequency (Hz). It is believed that the reason is that the impact echo mainly concentrates on the integrity of the media. In other words, impact echo can identify voids, delamination, separations in a media successfully but the change of media e.g. concrete to steel or FRP creates a very less significant impact on the impact echo data.
- The ultrasound proved to be an adequately reliable NDE method in identifying the parameters.

- The GPR test can be considered highly dependable for NDE of fire-affected concrete with different parameters. Almost all the parameters have shown a significant effect on the GPR maximum amplitude value.
- The infrared camera showed that it could be used as one of the highly accurate qualitative analysis device in case of fire-related hazards on a concrete structure. It could successfully denote the subsurface voids and damages when there was still heat transmission.
- The four point bending destructive test, which was performed as the last stage of the experimental works, was the lab-based destructive test performed to co-relate the NDT data with the residual ultimate bending capacity of a concrete member. The developed equation can also be used to derive the bending capacity according to the considered parameters.
- The simulated heat in the lab furnace for the experiment was uniform which created uniform damage on the samples. In a real life fire hazard scenario the damage might not be uniform due to flame action. Still, in that scenario, the outcome of this study can be used to perform analysis based on the mostly effected area.

- The study was performed in relation to the residual positive bending capacity of the beam samples. The negative bending capacity was not considered.

7.2. Comparison of R-Squared After Simplification of Equations

As mentioned in Chapter 4 and Chapter 5, the achieved equations for NDT and bending capacity were simplified by getting rid of some terms, which bares very less effect. Table 7- 1 shows the effect on the coefficient of determination, R^2 before and after simplification of the equations. From the table, it can be deducted that the simplifications had minimal effect on R^2.

Table 7- 1: Comparison of R^2 before and after simplification of equations.

Equation for	R^2 for Original Equation	R^2 for simplified Equation	Percentage Decrease
Schmidt Hammer	0.959	0.954	0.52 %
Ultrasound array tomography	0.854	0.852	0.23 %
Impact echo (IE)	0.707	0.7	0.99 %
Ground penetrating radar (GPR)	0.957	0.948	0.94 %

Bending Capacity	0.978	0.977	0.1 %

7.3. Proposed Procedure

A procedure is proposed in order to successfully evaluating a fire-affected concrete structure with the help of discussed NDT methods and the developed equations. This proposed procedure can be followed to identify the residual bending capacity of a fire-affected concrete member. This method can help the investigators and engineers for quantifiable investigation of the residual bending capacity, based on which a decision can be made for repair or demolition.

To summarize the proposed process, a few flowcharts were prepared for the NDE of fire-affected concrete (Figure 7- 1 and Figure 7- 2). The first step of the process is to collect all the available data from design details and/or site. The information required is the details about the considered parameters. If all the parameter values are available, a cross check can be performed by NDE on the bending capacity. If the data is not available, then another thorough approach should be adopted.

In the case where all the parametric data are available, one or more of the NDT methods from Schmidt hammer, impact echo, ultrasound tomography or ground penetrating radar (GPR) should be chosen to be utilized. Initially, the NDE parameters of those methods should be

calculated from the equations showed in chapter 4. Then a qualitative scanning with the thermal camera should be done to identify a mostly affected area. Afterward, that area should be scanned using the selected method/s of NDT. After that, the scanned values should be compared with the pre-calculated expected values. If the values look similar, the bending capacity equation from chapter 5 can be used to calculate the bending capacity with the considered parameter values. If the values do not look similar, then it might mean that the area considered does not fully represent the parameters. In this case, another mostly damaged area should be identified by the thermal camera, and that area should be scanned using the selected NDT method(s). At this step, emphasis should be given to find a uniformly damaged area. Afterward, the scans should be checked if the NDE values match the expected values. If the values match, a conclusion can be drawn that the parametric values are dependable, and the residual capacity can be calculated using those parametric values.

In case if the parametric values are not available or an acceptable outcome could not be achieved from the previous approach, a detailed analysis using NDE methods should be performed. In this case, the initial step is to consider two or more NDT methods that cover three equations. The options available for selection would be Schmidt hammer (2 equations), impact echo (1 equation), ultrasound tomography (1 equation) and ground

penetrating radar (GPR) (2 equations). The fire-affected surface and design data should be observed for data on the presence of steel or FRP rebar, and fireproofing layer. This observation should also be used while selecting the NDT methods knowing that specific NDT method is sensitive towards specific parameters. Afterward, a qualitative analysis should be performed with the thermal or infrared camera and a most effected zone should be determined. Then the selected area should be scanned using the considered NDT methods. Then the NDE equations for the selected methods should be used from chapter 4 and the unknown values of the parameters should be identified. Using the achieved parametric values, the bending capacity should be calculated.

Afterward, the decision regarding the rehabilitation of the fire-affected concrete can be made based on the outcome.

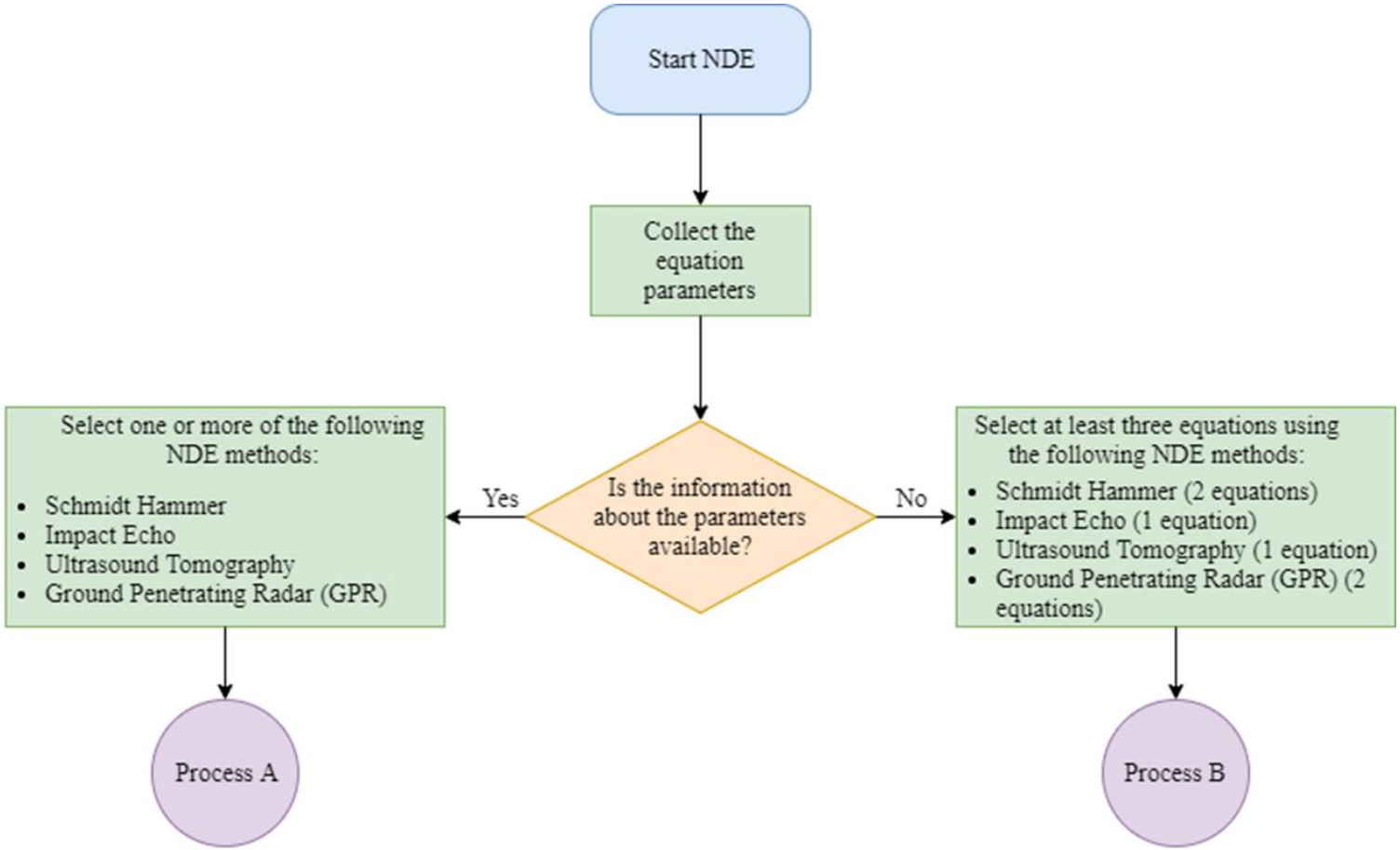

Figure 7- 1: Proposed procedure (part 1).

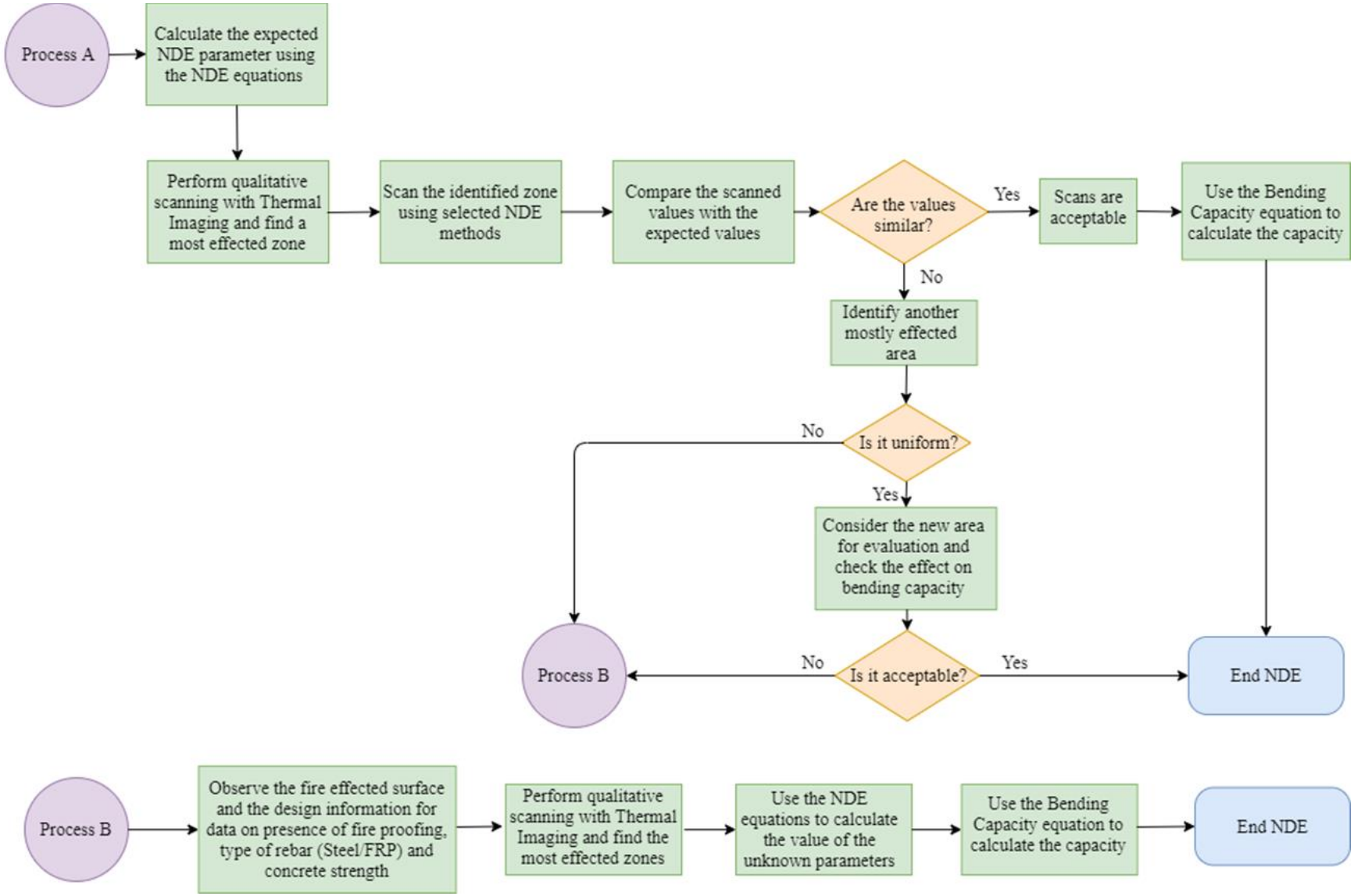

Figure 7- 2: Proposed procedure (part 2).

The mentioned procedure can be used for the structures where the positive bending moment is a key factor. For the cases where it is not the key factor, for example, near the support, some other approach can be adopted. For cases where the damage is mostly near the support and under the beam or girder, the key factor is the residual compressive strength. For this scenario, a pair of NDE methods can be used for scanning and the exposed temperature value can be determined from the equations. Afterward, a numerical model can be developed following the details mentioned in chapter 6 and a heat transfer model can be established and calibrated. From the heat transfer model, the temperature of the crucial point can be determined and using that temperature value, from Eurocode 2, the residual compressive strength can be determined. Afterward, a decision regarding the repair or demolition can be made based on the residual compressive strength near the support.

7.4. Recommendation for Future Research

The following recommendations for future studies can be made:

- This research concentrated on five parameters or variables. In the future, additional parameters can be considered for similar research. A few recommendations regarding the additional parameters can be

fiber reinforcement in concrete, rate of cooling, and ultra high strength concrete, etc.

- This study had two levels for each parameter. An investigation with additional levels of parameters can be performed which would increase the reliability of the study further.
- A full fractional factorial experimental design can be considered, instead of half-fractional factorial design, which will increase the number of samples per criterion for investigation. In this case, the number of parameters can be lowered to maintain a similar total number of samples. Though the study with the full fractional experimental design would not be able to cover a large number of factors or parameters, it would add some more reliability to the limited selected parameters by having a higher number of data per criterion.
- A fire exposure experiment, e.g. hydrocarbon pool fire test can be considered which would give an idea about the variations of flame action.
- Beam column joint samples can be considered to investigate the effect of fire near the joints.

Appendix A

High Temperature Properties of Normal Strength Concrete Per Eurocode 2 (2004)

Specific heat (J/kg°C)

$c = 900, for\ 20°C \leq T \leq 100\ °C$

$c = 900 + (T - 100), for\ 100°C \leq T \leq 200\ °C$

$c = 1000 + (T - 200)\ /\ 2, for\ 200°C \leq T \leq 400\ °C$

$c = 1100, for\ 400°C \leq T \leq 1200\ °C$

Density (kg/m3)

$\rho = \rho(20℃), for\ 20℃ \leq T \leq 100℃$

$\rho = \rho(20℃)(1-(0.02(T-115)/85)), for\ 115℃ \leq T \leq 200℃$

$\rho = \rho(20℃)(0.98-(0.03(T-200)/200)), for\ 200℃ \leq T \leq 400℃$

$\rho = \rho(20℃)(0.95-(0.07(T-400)/800)), for\ 400℃ \leq T \leq 1200℃$

$Volumetric\ specific\ heat = \rho c$

Thermal conductivity $(W/m℃)$

$All\ types$

$Upper\ limit$

$K_C = 2-0.2451(T/100)+0.0107(T/100)^2, for\ 20℃ \leq T \leq 1200℃$

$Lower\ limit$

$K_C = 1.36-0.136(T/100)+0.0057(T/100)^2, for\ 20℃ \leq T \leq 1200℃$

Thermal strain

Carbonate Aggregates:

$\varepsilon_{th} = -1.2x10{-}4 + 6x10{-}6T + 2.3x10{-}11T3, for\ 20℃ \leq T \leq 700℃$

ε_{th}= $14x10{-}3, for\ 700℃ \leq T \leq 1200℃$

Siliceous Aggregates:

$\varepsilon_{th} = -1.2x10{-}4 + 6x10{-}6T + 1.4x10{-}11T3, for\ 20℃ \leq T \leq 805℃$

ε_{th}= $12x10{-}3, for\ 805℃ \leq T \leq 1200℃$

Stress-strain relationships (MPa):

$$\sigma_c(\theta) = \frac{3\varepsilon f'_{c,\theta}}{\varepsilon_{c1,\theta}\left(2+\left(\frac{\varepsilon}{\varepsilon_{c1,\theta}}\right)^3\right)} \quad for\ \varepsilon \leq \varepsilon_{c1},$$

for numerical purposes a decending branch for $\varepsilon c1, \leq \varepsilon \leq \varepsilon cu1, \theta$ *should be adopted.Linear or non linear models are permitted. For the variables in this equation refer to the following table.*

Temperature, °C	Siliceous			Carbonate		
	$\frac{f'_{c,\theta}}{f'_{c,20}}$	$\varepsilon_{c1,\theta}$	$\varepsilon_{cu1,\theta}$	$\frac{f'_{c,\theta}}{f'_{c,20}}$	$\varepsilon_{c1,\theta}$	$\varepsilon_{cu1,\theta}$
20	1.00	0.0025	0.0200	1.00	0.0025	0.0200
100	1.00	0.004	0.0225	1.00	0.0040	0.0225
200	0.95	0.0055	0.0250	0.97	0.0055	0.0250
300	0.85	0.0070	0.0275	0.91	0.0070	0.0275
400	0.75	0.0100	0.0300	0.85	0.0100	0.0300
500	0.60	0.0150	0.0325	0.74	0.0150	0.0325
600	0.45	0.0250	0.0350	0.60	0.0250	0.0350
700	0.30	0.0250	0.0375	0.43	0.0250	0.0375
800	0.15	0.0250	0.0400	0.27	0.0250	0.0400
900	0.08	0.0250	0.0425	0.15	0.0250	0.0425
1000	0.04	0.0250	0.0450	0.06	0.0250	0.0450
1100	0.01	0.0250	0.0475	0.02	0.0250	0.0475
1200	0.00	-	-	0.00	-	-

References

- NFPA, “Fires by Occupancy or Property Type.” NFPA Report - Fires by Occupancy or Property Type, 2019, https://www.nfpa.org/News-and-Research/Data-research-and-tools/US-Fire-Problem/Fires-by-occupancy-or-property-type.
- Titman, D. J., “Applications of Thermography in Non-Destructive Testing of Structures.” NDT & E International, Volume 34, Issue 2, Pages 149-154, ISSN 0963-8695, March 2001.
- Colombo, M., and Roberto F., "New NDT Techniques for the Assessment of Fire-Damaged Concrete Structures." Fire Safety Journal 42, no. 6-7: 461-472, 2007.
- Chew, M. Y. L., “The Assessment of Fire-damaged Concrete.” Building and Environment, Volume 28, Issue 1, Pages 97-102, ISSN 0360-1323, 1993.
- Achillides, Z., and Pilakoutas, K. "Bond Behavior of Fiber Reinforced Polymer Bars under Direct Pullout Conditions." Journal of Composites for construction 8, no. 2: 173-181, 2004.
- Yaqub, M., and C. G. Bailey, C.G., "Repair of Fire-damaged Circular Reinforced Concrete Columns with FRP Composites." Construction and Building Materials 25, no. 1: 359-370, 2011.

- Williams, B., Kodur, V., Green, M. F., and Bisby, L., "Fire Endurance of Fiber-Reinforced Polymer Strengthened Concrete T-Beams." ACI structural Journal 105, no. 1: 60-67, 2008.
- Chen, L., Luo, C. and Lua, J., "FDS and Abaqus Coupling Toolkit for Fire Simulation and Thermal and Mass Flow Prediction." Fire Safety Science 10: 1465-1477, 2011.
- Hu, Y.J., Cheng, J., Liu, W., Yu, Q.Q., and Zhou, Y.L., "Degradation of the In-Plane Shear Modulus of Structural BFRP Laminates Due to High Temperature." Sensors 18, no. 10: 3361, 2018.
- Cadwallader, R. “Closed Bardin Road Bridge over Texas 360 Set for Repairs.” Star Telegram. Fort Worth Star-Telegram, December 30, 2016. https://www.star-telegram.com/news/local/arlington/article123860004.html.
- Lloyd, J., Guinyard, T., and Murphy, S., “Bridge to Be Demolished After Tanker Fire.” NBC 7 San Diego. NBC 7 San Diego, December 15, 2011. https://www.nbcsandiego.com/news/local/Tanker-Fire-60-Freeway-Bridge-Demolition--135660998.html.
- Pirani, F. “7 Things We Know Now about the I-85 Bridge Collapse.” ajc. The Atlanta Journal-Constitution, March 2, 2018. https://www.ajc.com/news/local/things-know-now-about-the-bridge-collapse/Wge6pwVF4kPJx6J0TuaTHL/.

- Crosby, R., and Munks, J., “After Fire, Crews Demolish Las Vegas Moulin Rouge Building.” Las Vegas Review Journal, October 06, 2017. https://www.reviewjournal.com/local/after-fire-crews-demolish-las-vegas-moulin-rouge-building/
- Garlock, M., Paya-Zaforteza, I., Kodur, V., and Gu, L., "Fire Hazard in Bridges: Review, Assessment and Repair Strategies." Engineering structures 35: 89-98, 2012.
- Wright, W., Lattimer, B., Woodworth, M., Nahid, M., and Sotelino, E. "Highway bridge fire hazard assesment, draft final report." Virginia polytechnic institute and state university. TRB Project 12-85 (2013).
- Alos-Moya, J., Paya-Zaforteza, I., Eugenia, M., Garlock, M., Loma-Ossorio, E., Schiffner, D., and Hospitaler, A., "Analysis of a Bridge Failure Due to Fire Using Computational Fluid Dynamics and Finite Element Models." Engineering Structures 68: 96-110, 2014.
- Quiel, Spencer E., Takayuki Yokoyama, Lynne S. Bregman, Kevin A. Mueller, and Shalva M. Marjanishvili. "A streamlined framework for calculating the response of steel-supported bridges to open-air tanker truck fires." Fire Safety Journal 73 (2015): 63-75.
- ASCE. "2017 infrastructure report card." Reston, VA: ASCE, 2017.
- McGill, Nick. “Study Says Indiana's Bridges Are the 13th Most 'Structurally Deficient' in the Country.” FOX59, 16 Feb. 2017,

https://fox59.com/2017/02/15/study-says-indianas-bridges-are-the-13th-most-structurally-deficient-in-the-country/.

- Gong, X., and Agrawal, K. A., "Numerical Simulation of Fire Damage to a Long-Span Truss Bridge." Journal of bridge Engineering 20, no. 10: 04014109, 2014.
- Chung, K., Park, S., and Choi, S. "Material effect for predicting the fire resistance of concrete-filled square steel tube column under constant axial load." Journal of Constructional Steel Research 64, no. 12: 1505-1515, 2008.
- Astaneh-Asl, A., Noble, C. R., Son, J., Wemhoff, A. P., Thomas, M. P., and McMichael, L. D. "Fire protection of steel bridges and the case of the MacArthur Maze fire collapse." In TCLEE 2009: Lifeline Earthquake Engineering in a Multihazard Environment, pp. 1-12. 2009.
- Trubey, J., Kanell, M. and Kass, A., " Costs of I-85 bridge fire to ripple across region", 2017.
- Wickert, D. "Price tag for new I-85 bridge: Up to 16.6 million." 2017.
- Sika Corporation, "State Highway 183 MacArthur Boulevard Overpass Emergency Repair" ICRI Concrete Repair Bulletin, 2006.

- Wang, Y.C., Wald, F., Vacha, J., and Hajpal, M., “Fire-damaged Structures.” Urban Habitat Constructions Under Catastrophic Events, 2010.
- Bikhiet, M. M., El-Shafey, N. F., and El-Hashimy, H. M. “Behavior of reinforced concrete short columns exposed to fire.” Alexandria Engineering Journal, 53(3), 643-653, 2014.
- Stochino, F., Mistretta, F., Meloni, P., and Carcangiu, G., "Integrated approach for post-fire reinforced concrete structures assessment." Periodica Polytechnica. Civil Engineering, 1-23, 2017.
- Pathak, R. P., Munzni, B. K., Sharma, P., Mahure, N. V., Vyas, S., and Ratnam, M., "Estimation of Fire Damage to Concrete Structure: A Case Study." International Journal of Engineering 2, no. 4: 130-136, 2013.
- Aggelis, D. G., Kordatos, E. Z., Soulioti, D. V., and Matikas, T. E., "Combined use of thermography and ultrasound for the characterization of subsurface cracks in concrete." Construction and Building Materials 24, no. 10, 1888-1897, 2010.
- Alcaíno, P., María, H. S., Cortés, M., and Alfaro, J., "Fast Assessment of Post-Fire Residual Strength of Reinforced Concrete Frame Buildings Based on Non-Destructive Tests." In

Multidisciplinary Digital Publishing Institute Proceedings, vol. 2, no. 8, p. 515. 2018.

- Daungwilailuk, T., Cao, T. N., Pansuk, W., and Pheinsusom, P., "Evaluating damaged concrete depth in reinforced concrete structures under different fire exposure times by means of NDT and DT techniques." Engineering Journal 21, no. 7, 233-249, 2017.
- Park, G. K., and Yim, H. J., "Evaluation of fire-damaged concrete: an experimental analysis based on destructive and nondestructive methods." International Journal of Concrete Structures and Materials 11, no. 3, 447-457, 2017.
- Ékes, C., “GPR: A New Tool for Structural Health Monitoring of Infrastructure.” Terraprobe Geoscience Corp., Canada, 2007.
- Talaha, N. A. A., Senin, F. S., and Hamid, R., "Determination of Defect and Deterioration of Concrete Slab in a Building after Fire Using Ground Penetrating Radar and Visual Inspection Method.” Conference: International Technical Conference, December 2016.
- Carino, N. J., Sansalone, M., and Hsu, N. N., "Flaw Detection in Concrete by Frequency Spectrum Analysis of Impact-Echo Waveforms." International advances in nondestructive testing 12: 117-146, 1986.

- Carino, N. J. "The impact-echo method: an overview." Structures 2001: A Structural Engineering Odyssey, pp. 1-18. 2001.
- Clayton, D. A., Cyrus M. S., Ferraro, C. C., Nelson, J., Khazanovich, L., Hoegh, K., Chintakunta, S., and Popovics, J., “Evaluation of ultrasonic techniques on concrete structures.” No. ORNL/TM-2013/430. Oak Ridge National Lab. (ORNL), Oak Ridge, TN (United States), 2013.
- FLIR, “The Ultimate Infrared Handbook for R&D Professionals” Academic, 2009.
- Brencich, A., Cassini, G., Pera, D., and Riotto, G., "Calibration and Reliability of the Rebound (Schmidt) Hammer Test." Civil Engineering and Architecture 1, no. 3: 66-78, 2013.
- ASTM International. E119-18ce1, “Standard Test Methods for Fire Tests of Building Construction and Materials.” West Conshohocken, PA; ASTM International, 2018.
- National Fire Protection Association. NFPA 502, Standard for road tunnels, bridges, and other limited access highways. NFPA, 2011.
- Beneberu, E. S. "Hydrocarbon pool fire performance of fiber reinforced polymer (FRP) strengthened and thermally insulated bridge girders." PhD diss., 2016.

- Federal Highway Administration, “Impact Echo (IE).” NDE Technology. Accessed November 2, 2019. https://fhwaapps.fhwa.dot.gov/ndep/DisplayTechnology.aspx?tech_id=13.
- Riad, M. "Quantitative Non-destructive Evaluation (NDE) of FRP Laminate-Concrete Bond Strength." PhD diss., 2017.
- GSSI, “GSSI Handbook for RADAR Inspection of Concrete.” Geophysical Survey Systems, Inc, 2005.
- ASTM International. C78/C78M-18 “Standard Test Method for Flexural Strength of Concrete (Using Simple Beam with Third-Point Loading).” West Conshohocken, PA; ASTM International, 2018.
- Committee for European Normalisation (CEN), “Eurocode 2: design of concrete Structures-Part 1-2: general rules – structural fire design.” Brussels, Belgium, EN 1991-1-2, 2004.
- Hao, Jianwen, Kun Dong, Wei Liu, and Jitong Jiang. "Simplified Temperature Prediction Method for Insulated CFRP-Strengthened RC Beams Exposed to Standard Fire." In IOP Conference Series: Earth and Environmental Science, vol. 242, no. 6, p. 062054. IOP Publishing, 2019.

- ASTM International. C39/C39M-18 “Standard Test Method for Compressive Strength of Cylindrical Concrete Specimens.” West Conshohocken, PA; ASTM International, 2018.
- Kodur, V. K. R., and Ankit Agrawal. "An approach for evaluating residual capacity of reinforced concrete beams exposed to fire." Engineering Structures 110 (2016): 293-306.
- Simulia, “Concrete damaged plasticity.” ABAQUS Analysis User’s Manual Version 6.8, Section 19. 6. 3, 2008. http://130.149.89.49:2080/v6.8/books/usb/default.htm?startat=pt05ch19s06abm38.html

Biographical Information

Upal Mohammad Towfiqul Quadir completed his Master's degree in Structural Engineering at The University of New South Wales (UNSW) in Sydney, Australia in November 2013. He completed his Bachelor's degree in Civil Engineering from the Military Institute of Science and Technology (MIST) in Dhaka, Bangladesh in November 2011. Previously he worked as a faculty member in the North South University, International University of Business Agriculture and Technology and also in the Military Institute of Science and Technology (MIST), Dhaka. He also worked as a Structural Design Engineer in a composite structure design and erection company named Buildtrade Engineering from Dhaka in 2012. During his tenure at MIST, he also worked in several Detailed Engineering Assessment (DEA) projects of garments factories around Dhaka. He has worked in several research projects such as Behavior analysis of Carbon Fiber Reinforced Polymer (CFRP) jacketed RC slender columns and Development of sustainable green concrete using industrial wastes or by-products starting from 2014. His research interest includes Fiber Reinforced Polymer (FRP) for structural strengthening, building construction, sustainable concrete, mechanical and micro structural properties of concrete, structural property and behavior analysis, fire effect on structures, Non-destructive Evaluation (NDE), Non-destructive Testing (NDT), and retrofitting.